Performance of top-quark and *W*-boson tagging with ATLAS in Run 2 of the LHC

The ATLAS Collaboration

The performance of taggers for hadronically decaying top quarks and *W* bosons in *pp* collisions at $\sqrt{s}$ = 13 TeV recorded by the ATLAS experiment at the Large Hadron Collider is presented. A set of techniques based on jet shape observables are studied to determine a set of optimal cut-based taggers for use in physics analyses. The studies are extended to assess the utility of combinations of substructure observables as a multivariate tagger using boosted decision trees or deep neural networks in comparison with taggers based on two-variable combinations. In addition, for highly boosted top-quark tagging, a deep neural network based on jet constituent inputs as well as a re-optimisation of the shower deconstruction technique is presented. The performance of these taggers is studied in data collected during 2015 and 2016 corresponding to 36.1 fb^{-1} for the $t\bar{t}$ and γ + jet and 36.7 fb^{-1} for the dijet event topologies.

Contents

1 Introduction

With the increase of the Large Hadron Collider (LHC) [1] centre-of-mass energy to 13 TeV in Run 2, it is increasingly important for searches for physics phenomena beyond the Standard Model to probe processes involving highly boosted massive particles, such as W and Z bosons and top quarks [2–5]. To fully exploit these final states, it is important to reconstruct and accurately identify the hadronic decay modes of these massive particles which serve as an effective tool to reject events produced by background processes and improve the sensitivity in searches for physics beyond the Standard Model. Techniques to achieve this aim were studied by both the ATLAS and CMS collaborations during the course of Run 1 of the LHC [6–9]. In this paper, these studies are performed with Run 2 data with particular attention to the investigation of multivariate techniques based on both jet shape observables and an approach using the jet constituents as input observables in addition to the optimisation of the shower deconstruction technique for highly boosted top-quark tagging.

In Section 2 the ATLAS detector is briefly described, followed by a description of the Monte Carlo and data samples used in the analysis in Section 3. The set of jet reconstruction and tagging techniques investigated in this work is described in Section 4. The optimisation procedure for each tagger, as well as a comprehensive comparison of the tagging techniques using Monte Carlo simulation are presented in Section 5. In Section 6, the pp collision data recorded in 2015 and 2016 are used to evaluate the performance of these tagging techniques, with the measurement of signal and background efficiencies using boosted lepton+jet $t\bar{t}$, dijet and γ + jet topologies and the robustness of the various techniques when confronted with varying levels of event pile-up. Finally, concluding remarks are given in Section 7.

2 ATLAS detector

The ATLAS detector [10, 11] at the LHC covers nearly the entire solid angle around the collision point.[1] It consists of an inner tracking detector (ID) surrounded by a thin superconducting solenoid, electromagnetic and hadronic calorimeters, and a muon spectrometer composed of three large superconducting toroid magnets and precision tracking chambers. For this study, the most important subsystems are the calorimeters, which cover the pseudorapidity range $|\eta| < 4.9$. Within the region $|\eta| < 3.2$, electromagnetic calorimetry is provided by barrel and endcap high-granularity lead/liquid-argon (LAr) sampling calorimeters, with an additional thin LAr presampler covering $|\eta| < 1.8$ to correct for energy loss in material upstream of the calorimeters. Hadronic calorimetry is provided by a steel/scintillator-tile calorimeter, segmented into three barrel structures within $|\eta| < 1.7$, and two copper/LAr hadronic endcap calorimeters which instrument the region $1.5 < |\eta| < 3.2$. The forward region $3.1 < |\eta| < 4.9$ is instrumented with copper/LAr and tungsten/LAr calorimeter modules.

Inside the calorimeters, the inner tracking detector measures charged-particle trajectories in a 2 T axial magnetic field produced by the superconducting solenoid. It covers a pseudorapidity range $|\eta| < 2.5$ with pixel and silicon microstrip detectors, and the region $|\eta| < 2.0$ with a straw-tube transition radiation tracker.

---

[1] ATLAS uses a right-handed coordinate system with its origin at the nominal interaction point (IP) in the centre of the detector and the z-axis along the beam pipe. The x-axis points from the IP to the centre of the LHC ring, and the y-axis points upwards. Cylindrical coordinates (r, ϕ) are used in the transverse plane, ϕ being the azimuthal angle around the z-axis. The pseudorapidity is defined in terms of the polar angle θ as $\eta = -\ln \tan(\theta/2)$. Angular distance is measured in units of $\Delta R \equiv \sqrt{(\Delta \eta)^2 + (\Delta \phi)^2}$.

The muon spectrometer (MS) comprises separate trigger and high-precision tracking chambers measuring the deflection of muons in a magnetic field generated by superconducting air-core toroid magnets. The precision chamber system covers the region $|\eta| < 2.7$ with three layers of monitored drift tubes, complemented by cathode strip chambers in the forward region where the background is highest. The muon trigger system covers the range $|\eta| < 2.4$ with resistive plate chambers in the barrel and thin gap chambers in the endcap regions.

A two-level trigger system is used to select events for offline analysis [12]. The first step, named the level-1 trigger, is implemented in hardware and uses a subset of detector information to reduce the event rate from 40 MHz to 100 kHz. This is followed by a software-based high-level trigger which reduces the final event rate to an average of 1 kHz.

3 Data and simulated samples

The taggers described in this article were initially designed, as described in Section 5, using Monte Carlo (MC) simulated samples for two signal processes and one background process. The dijet process was used to simulate jets from gluons and non-top quarks. It was modelled using the leading-order Pythia8 (v8.186) [13] generator with the NNPDF2.3LO [14] parton distribution function (PDF) set and a set of tuned parameters called the A14 tune [15]. Events were generated in slices of jet transverse momentum (p_T) to sufficiently populate the kinematic region of interest (between 200 and 2500 GeV). Event-by-event weights were applied to correct for this generation methodology and to produce the expected smoothly falling jet p_T distribution of the multijet background. The signal samples containing either high-p_T top-quark or W-boson jets were obtained from two physics processes modelling phenomena beyond the Standard Model. For the W-boson sample, high-mass sequential standard model [16] $W' \rightarrow WZ \rightarrow q\bar{q}q\bar{q}$ events were used. For the top-quark sample, high-mass sequential standard model $Z' \rightarrow t\bar{t}$ events were used as a source of signal jets. Both the W bosons and top quarks were required to decay hadronically. The two signal processes were simulated using the Pythia8 [13] generator with the NNPDF2.3LO PDF set and A14 tune for multiple values of the resonance (W' or Z' boson) mass between 400 and 5000 GeV in order to populate the entire jet p_T range[2] from 200 to 2500 GeV and to reduce the impact of MC statistical uncertainties on the calculated signal efficiencies.

For the study of W-boson and top-quark jets in data, described in Section 6, a number of MC samples are needed to model both the $t\bar{t}$ signal and backgrounds. The Powheg-Box v2 generator [17–19] was used to simulate $t\bar{t}$ and single-top-quark production in the Wt- and s-channels at next-to-leading order (NLO), while for the single-top-quark t-channel process, the NLO Powheg-Box v1 generator and the CT10 [20] NLO PDF set was used. For all processes involving top quarks, the parton shower, fragmentation, and the underlying event were simulated using Pythia6 (v6.428) [21] with the CTEQ6L1 [22] PDF set and the corresponding Perugia 2012 tune (P2012) [23]. The top-quark mass was set to 172.5 GeV. The h_{damp} parameter, which controls the matching of the matrix element to the parton shower, was set to the mass of the top quark. The $t\bar{t}$ process is normalised to the cross-sections predicted to next-to-next-to-leading order (NNLO) in α_S and next-to-next-to-leading logarithm (NNLL) in soft-gluon terms while the single-top-quark processes are normalised to the NNLO cross-section predictions [24].

---

[2] As the combination of these signal samples with different generated heavy resonance masses results in irregular top-quark and W-boson p_T distributions, the events are reweighted at the generator level to either a constant or a falling jet p_T distribution, as is typical for light jets.

Several additional variations of the $t\bar{t}$ generator are used for the estimation of modelling uncertainties. Estimates of the parton showering, hadronisation modelling and underlying-event uncertainty are derived by comparing results obtained with the POWHEG-BOX v2 generator interfaced to HERWIG++ (v2.7.1) [25] instead of PYTHIA6. To estimate the hard-scattering modelling uncertainty, the NLO MADGRAPH5_AMC@NLO (v2.2.1) generator [26] (hereafter referred to as MC@NLO) is used with PYTHIA6. To estimate the uncertainty in the modelling of additional radiation, the POWHEG-BOX v2 generator with PYTHIA6 is used with modified renormalisation and factorisation scales ($\times 2$ or $\times 0.5$) and a simultaneously modified h_{damp} parameter value ($h_{\mathrm{damp}} = m_{\mathrm{top}}$ or $h_{\mathrm{damp}} = 2 \times m_{\mathrm{top}}$) as described in Ref. [27].

Samples of W/Z+jets and Standard Model diboson ($WW/WZ/ZZ$) production were generated with final states that include either one or two charged leptons. The SHERPA [28] generator version 2.1.1 and version 2.2.1 were used to simulate these processes at NLO with the CT10 PDF set to simulate the diboson and W/Z+jets production processes, respectively. The W/Z+jets events are normalised to the NNLO cross-sections [29].

For the study of γ + jet events in data, events containing a photon with associated jets were simulated using the SHERPA 2.1.1 generator, requiring a photon transverse momentum above 140 GeV. Matrix elements were calculated with up to four partons at LO and merged with the SHERPA parton shower [30] using the ME+PS@LO prescription [31]. The CT10 PDF set was used in conjunction with the dedicated parton shower tune developed by the SHERPA authors.

The MC samples were processed through the full ATLAS detector simulation [32] based on GEANT4 [33]. Additional simulated proton–proton collisions generated using PYTHIA8 (v8.186) with the A2M [15] tune and MSTW2008LO PDF set [34] were overlaid to simulate the effects of additional collisions from the same and nearby bunch crossings (pile-up), with a mean number of 24 collisions per bunch crossing. All simulated events were then processed using the same reconstruction algorithms and analysis chain as is used for the data.

Data were collected in three broad categories to study the signal efficiency and background rejection. For the signal, a set of observed top-quark and W-boson jet candidates is obtained from a sample of $t\bar{t}$ candidate events in which one top quark decays semileptonically and the other decays hadronically, the lepton-plus-jets decay signature. The background is studied using data samples enriched in dijet events and γ + jet events. In addition to covering different p_{T} regions, the dijet and γ + jet samples differ in what partons initiated the jets under study. In the γ + jet topology the jets are mostly initiated by quarks over the full p_{T} range studied, while for the dijet topology the fraction of quarks initiating jets is slightly smaller than the gluon fraction at low p_{T} and becomes large at high p_{T}. The data for the $t\bar{t}$ and γ + jet studies were collected during normal operations of the detector and correspond to an integrated luminosity of $36.1\,\mathrm{fb}^{-1}$. For the dijet analysis, additional data where the toroid magnet was turned off are used. This adds an additional $0.6\,\mathrm{fb}^{-1}$. For both datasets, only data collected while all relevant detector subsystems were fully functional and in which at least one primary vertex was reconstructed with at least five associated ID tracks consistent with the LHC beam spot are used [35].

The lepton-plus-jets events were collected with a set of single-electron and single-muon triggers that became fully efficient for p_{T} of the reconstructed lepton greater than 28 GeV. The dijet events were collected with a single large-R jet trigger, where the jet was reconstructed using the same algorithm described in Section 4.1 and with a radius parameter of $R = 1.0$. This trigger became fully efficient for an offline jet p_{T} of approximately 450 GeV. The γ + jet jet events were collected with a single-photon trigger that became fully efficient for an offline photon p_{T} of approximately 155 GeV.

4 Jet substructure techniques

The identification of hadronic jets originating from the decay of boosted W and Z bosons and top quarks can broadly, and somewhat arbitrarily, be divided into two stages: jet reconstruction and jet tagging. In the first, the hadronic energy flow of the event is exclusively divided into a number of jets, composed of constituents, with the primary goal being to most accurately reconstruct the interesting energy flows in the case of true signal jets while suppressing contributions from event pile-up. In the second, the information about the jet constituents is distilled into a single observable by different means to obtain a criterion by which to identify a jet as originating from a hadronically decaying massive particle, such as a W boson or a top quark. A number of techniques and observables pertaining to these two categories have been described and investigated extensively in previous work [6, 7] with only a short summary of the relevant techniques presented here. In the case of the identification of W bosons, the techniques and conclusions are more broadly applicable to both W and Z bosons, with dedicated studies concerning the separation of W-boson jets from Z-boson jets performed in Ref. [36].

4.1 Jet reconstruction

In this work, jets are reconstructed with the intention of capturing the full energy flow resulting from the decay of a massive particle. This reconstruction primarily uses inputs in the form of noise-suppressed topological clusters of calorimeter cells [37] that are individually calibrated to correct for effects such as the non-compensating response of the calorimeter and inactive material, and which are assumed to be massless [38]. These topoclusters are then used as inputs to build two different types of jets. The first uses the anti-k_t algorithm [39] with a radius parameter of $R = 1.0$ to form jets which are further trimmed[3] to remove the effects of pile-up and the underlying event. Trimming [42] is a grooming technique in which the original constituents of the jets are reclustered using the k_t algorithm [43] with a radius parameter R_{sub} to produce a collection of subjets. These subjets are then discarded if they have less than a specific fraction (f_{cut}) of the p_T of the original jet. The trimming parameters used here are $R_{sub} = 0.2$ and $f_{cut} = 0.05$. These large-R jets are then calibrated in a two-step procedure that first corrects the jet energy scale and then the jet mass scale [38, 44]. The resulting set of constituents forms the basis from which further observables are calculated. The second type of jet clustering, needed for the HEPTopTagger algorithm [45, 46], makes use of the Cambridge/Aachen (C/A) jet algorithm [47, 48] with a radius of $R = 1.5$ which aims to identify top-quark jets across a broad p_T range, in particular reaching low p_T. These jets, used in conjunction with the HEPTopTagger algorithm described in Section 4.3.4, are also groomed to mitigate the effects of pile-up. Trimming with subjet radius of $R_{sub} = 0.2$ and momentum fraction $f_{cut} = 0.05$, the same as those used in the trimming of the anti-k_t $R = 1.0$ jet collection, is found to produce jet reconstruction and identification performance independent of the average number of interactions per bunch crossing.

In simulation, in addition to jets reconstructed from detector-level observables, a set of jets based on generator-level information is also used to characterise the performance of a given tagging algorithm. These jets are reconstructed with the anti-k_t algorithm with a radius parameter $R = 1.0$, using stable particles from the hard scatter with lifetimes greater than 10 ps, excluding muons and neutrinos, as constituents. These jets, to which no trimming algorithm is applied, are referred to as *truth jets*, and the related observables are denoted by the superscript "true".

---

[3] When using topoclusters [37] as jet inputs, the trimming algorithm, as opposed to pruning [40] or split-filtering [41] was found to be optimal in terms of accurately reconstructing the important aspects of the energy flow as shown in Ref. [6].

4.2 Jet labelling

As the aim of this study is the evaluation of the performance of jet tagging algorithms, the labelling of the particle that initiated the jet is of particular importance. For signal jets, this labelling is based on the partonic decay products of the particle of interest (W boson or top quark) in a three-step process. First, reconstructed jets are matched to truth jets with a matching criterion of $\Delta R(j_{\text{true}}, j_{\text{reco}}) < 0.75$. Next, those truth jets are matched to truth W bosons and top quarks (W, t) with a matching criterion of $\Delta R(j_{\text{true}}, \text{particle}) < 0.75$. Finally, the partonic decay products of the parent W boson or top quark (two quarks for hadronically decaying W bosons and an additional b-quark) are matched to the reconstructed jet. A reconstructed jet is labelled as a W-boson or top-quark jet if the parent particle and all of its direct decay products are contained within a region in (η,ϕ) with $\Delta R < 0.75 \times R_{\text{jet}}$, where R_{jet} is the jet radius. In the case of W bosons, this means that both of the daughter partons from the $W \to q\bar{q}'$ decay are contained within the jet. For jets matched to the parent W boson, at $p_{\text{T}} \sim 200$ GeV only 50% of the jets are fully contained when using this criterion while for $p_{\text{T}} > 500$ GeV the containment rises to nearly 100%. In the case of top-quark jets, the possible final-state topologies for the jet are more complex, including the possibility of the large-R jet containing only the b-quark from the top decay, only the two quarks from the W-boson decay, or a pairing of a b-quark and one of the daughter W-boson quarks within $\Delta R < 0.75 \times R_{\text{jet}}$ around the jet axis. As seen in Figure 1, the fraction of large-R jets falling into each category depends strongly on the p_{T} of the parent particle with only 60% of jets being fully contained at 600 GeV and with 100% containment not being reached even at 1500 GeV. This variation in containment, particularly in the case of top-quark tagging in which a top-quark jet is labelled as such only when the top parton, the b-quark from its decay as well as the two light quarks from the subsequent W-boson decay are contained within the region $\Delta R < 0.75 \times R_{\text{jet}}$ around the jet axis, serves as a strong motivation for the various optimisation strategies described in Section 5.
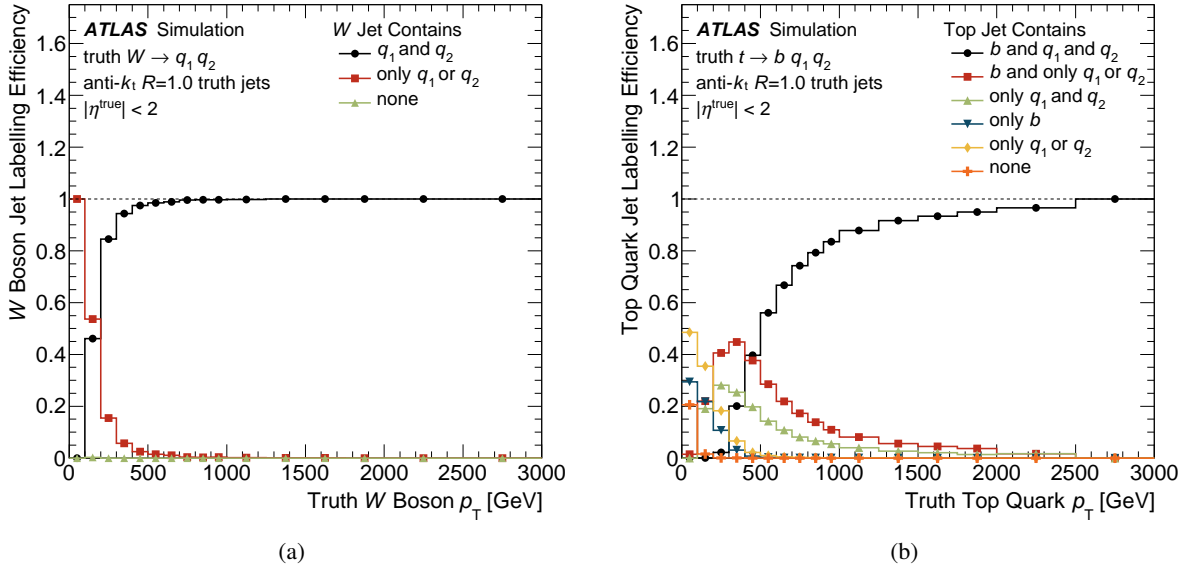

Figure 1: Containment of the W-boson (a) and top-quark (b)decay products in a single truth-level anti-k_t $R = 1.0$ jet as a function of the particle's transverse momentum.

4.3 Tagging techniques

After reconstructing the jet as a collection of constituents, a number of methods can be used to classify a jet as originating from a heavy particle (W boson or top quark) decay as opposed to a light jet originating from gluons and quarks of all flavours other than top quarks. The motivation behind the various techniques differs, but they all attempt to form a decision criterion by which to identify a jet as originating from a W boson or top quark.

4.3.1 Jet moments

The first broad class of observables studied for classification are directly based on the constituents of the trimmed jet and attempt to quantify a particular feature of the jet in an analytic way. Of these features, the most powerful is the jet mass, which for a jet formed from the decay of a heavy particle has a scale associated with the mass of the particle, whereas for light jets high masses are less likely as they need to be generated through QCD emissions. Traditionally, the jet mass was calculated as the invariant mass of the collection of topoclusters of the trimmed jet (m^{calo}) [6]. However, at very high p_{T}, the resolution of this observable decreases when energy depositions from individual particles begin to merge in clusters. To mitigate this effect, the fine spatial granularity of the inner detector is used to calculate the jet mass as the invariant mass of the ghost-associated [49] charged-particle tracks scaled by the ratio of the transverse momenta of the trimmed jet and the associated tracks to form the track-assisted mass (m^{TA}). To achieve good performance across a broad range of jet transverse momenta, an average of m^{calo} and m^{TA}, weighted by the inverse of their resolutions is calculated to form the combined mass (m^{comb}) [44].

In addition to the jet mass, a number of other observables quantify the extent to which the jet constituents are clustered or uniformly dispersed and can be used to augment the discrimination power from the jet mass alone. This can be done by explicitly using a set of axes (e.g. N-subjettiness, τ_{21} and τ_{32}), declustering the jet (e.g. splitting measures, $\sqrt{d_{12}}$ and $\sqrt{d_{23}}$), or using all jet constituents to quantify the dispersion of the jet constituents in an axis-independent way (e.g. planar flow or energy correlation functions). In previous ATLAS studies [6, 7], it was found that for W boson tagging, energy correlation variables, in particular D_2, were the best-performing tagging observables while for top-quark tagging the N-subjettiness ratio, τ_{32}, was found to be optimal. This can be understood from an analytical point of view in the context of W-boson tagging [50] and is attributed to additional wide-angle radiation present in parton jets originating from W-boson decays, which is more fully exploited in the energy correlation functions than in the N-subjettiness moments.

The full set of jet moments studied in this work is summarised in Table 1 while a more complete description of the observables under study can be found in Ref. [6]. These moments are studied individually when paired with the jet mass (m^{comb}) as well as in multivariate combinations, similar to those studied in Refs. [8, 51, 52], with the intention of exploiting correlations between the observables and creating a more powerful single discriminant across a broad p_{T} range from 200 to 2000 GeV, the range commonly probed in searches.

4.3.2 Topocluster-based Tagger

All of the jet moments presented in Section 4.3.1 and summarised in Table 1 make use of a specific physical motivation to distil the individual jet constituent measurements into a single observable. However, recent

Table 1: Summary of jet moments studied along with an indication of the tagger topology to which the observable is applicable. In the case of the energy correlation observables, the angular exponent β is set to 1.0 and for the N-subjettiness observables, the winner-take-all [53] configuration is used. A concise description of each jet moment can be found in Ref. [6].

Observable	Variable	Used for	References
Calibrated jet kinematics	p_{T}, m^{comb}	top,W	[44]
Energy correlation ratios	e_3,C_2,D_2	top,W	[50, 54]
N-subjettiness	τ_1,τ_2,τ_{21}	top, W	[55, 56]
	τ_3,τ_{32}	top	
Fox–Wolfram moment	R_2^{FW}	W	[57, 58]
Splitting measures	z_{cut}	W	[59, 60]
	$\sqrt{d_{12}}$	top, W	
	$\sqrt{d_{23}}$	top	
Planar flow	$\mathcal{P}$	W	[61]
Angularity	a_3	W	[62]
Aplanarity	A	W	[58]
KtDR	$KtDR$	W	[63]
Qw	Q_w	top	[59]

simulation-based studies have found that the more direct use of the jet constituents [64–67] as inputs to a machine-learning algorithm can lead to significant improvements in discriminating power as compared to more traditional, jet-moment-based discriminants. Therefore, in this work, a classifier that makes use of lower-level input observables is investigated which focuses specifically on the identification of high-p_{T} top quarks with $p_{\mathrm{T}} > 450$ GeV where traditional prong-based moments begin to fail due to subjet merging. This classifier is referred to as "TopoDNN" throughout the work.

4.3.3 Shower deconstruction

Shower deconstruction (SD) [68] is an approach which attempts to classify jets according to the compatibility of the radiation pattern of the jet with a predefined set of parton shower hypotheses in a manner similar to the matrix element method [69]. For a set of input subjets, intended to be representative of the partonic decay products of the top quark, loose compatibility with the decay of a top quark is ensured by requiring that the jet has at least three subjets, that two or more subjets have a mass in a window centred around the W-boson mass (Δm_W), and that at least one more subjet can be added to obtain a total mass in a window centred around the top-quark mass (Δm_{top}). If the jet passes these requirements, then a set of potential shower histories is constructed for the signal and background models. Each shower history represents a possible means by which the chosen model could have resulted in the given subjet configuration. A probability is assigned to each shower history based on the parton shower model from which the χ variable is defined as the likelihood ratio of the signal and background hypotheses. The logarithm of this likelihood ratio log χ is used as the final discriminant.

4.3.4 HEPTopTagger

An alternative approach to top-quark tagging is the HEPTopTagger (HTT) algorithm [45, 46]. Unlike the previous observables that are calculated from the constituents of the $R = 1.0$ trimmed jets, this technique relies on reconstructing jets using the C/A algorithm with $R = 1.5$ to allow the tagging of fully contained boosted top quarks to be effective at lower values of p_T (> 200 GeV) and to take advantage of the C/A clustering sequence which attempts to reverse the decay structure of the top-quark decay. The first step of this process is to trim the $R = 1.5$ jet, as described in Section 4.1. The resulting set of jet constituents are then analysed with the HEPTopTagger algorithm, which identifies the hard jet substructure and tests it for compatibility with the 3-prong pattern of hadronic top-quark decays using an algorithm which is designed to mitigate the effects of pile-up by removing low-p_T portions of the jet. The HEPTopTagger studied in this paper is the original algorithm, from Ref. [45], not the extended HEPTopTagger2 algorithm [70] and is executed with $m_{cut} = 50$ GeV, $R_{filt}^{max} = 0.25$, $N_{filt} = 5$, $f_W = 15\%$, settings found to be optimal in Ref. [7]. The result of the algorithm is a top-quark-candidate four-vector. The jet is considered to be tagged if the mass of this resultant top-quark-candidate four-vector is between 140 and 210 GeV and its p_T is larger than 200 GeV.

5 Tagger optimisation

A wide variety of techniques, described in Section 4, exist for identifying W-boson and top-quark jets. In this section, each of these techniques is explored and optimised and an inclusive comparison of the performance of each technique is made based on the W-boson or top-quark (signal) efficiency and light-jet (background) rejection, defined as the inverse of the background efficiency. This performance is quantified in exclusive kinematic regimes based on the p_T of the associated anti-k_t $R = 1.0$ truth jet (p_T^{true}) to more closely resemble the kinematics of the parent particle and allow comparison of taggers employing different jet clustering algorithms. Finally, to mitigate any bias in the tagging performance due to differences between the p_T spectra of the signal and background jet samples, the simulated signal samples described in Section 3 are combined and weighted (separately for W bosons and top quarks) such that the truth p_T distribution of the ensemble of signal jets matches that of the light-jet background.

5.1 Cut-based optimisation

The first approach to tagging is based on selection cuts on jet shape observables. This approach was studied in preparation for Run 2 [71, 72] to provide a set of guiding techniques that were used extensively in searches. The primary goal of these taggers is to provide a simple set of selections on jet moments that yield a constant signal efficiency as a function of the transverse momentum of the jet across a broad p_T range, thus being widely applicable. In the case of W-boson tagging, one of these observables is taken to be m^{comb} and the discrimination power is augmented by a selection on another jet moment defined in Table 1, while in the case of top tagging, a more inclusive strategy is explored where all pairwise combinations of jet moments are investigated. This optimisation is performed as a function of the p_T of the associated anti-k_t $R = 1.0$ truth jet for both W-boson and top-quark tagging. The tagging strategy resulting from this optimisation provides a benchmark in terms of tagging performance to which other tagging strategies can be compared.

This simple tagger is optimised using a sample of signal W-boson or top-quark jets as well as background light jets extracted from the samples described in Section 3. In each event the two reco jets matched to the two highest-p_T truth jets within $|\eta| < 2$ are studied. In the case of signal, W-boson (top-quark) jets are retained if they are truth labelled as such according to the procedure in Section 4.2 and have a transverse momentum greater than 200 GeV (350 GeV). In the case of background, no labelling procedure is applied and the two highest-p_T jets from the dijet sample are retained.

For this study, the general optimisation procedure to determine the two-variable selection criteria is the same for both W-boson and top-quark jet tagging. For each pair of observables, the selection criteria which give the chosen signal efficiency and the largest background rejection are considered optimal and taken as the selection criteria in that region of jet p_T. In the case of m^{comb}, the selection region is two-sided for W-boson tagging, selecting a region near m_W, and one-sided in the case of top-quark tagging, selecting an inclusive region of high jet mass. In the case of the other jet moments, the selection criteria are always one-sided, the direction of which depends on the particular observable in question. This procedure is repeated for exclusive bins of jet p_T and a sequence of selection criteria for each of the jet moment observables is derived. Finally, this sequence of selection criteria is parameterised by a smooth function dependent on the jet p_T. All single-sided cuts are parameterised as a function of p_T with a polynomial function to describe features which occur due to correlation of the combined-tagger variable. In the case of the W-boson tagging, the m^{comb} selection is fit using a four-parameter (p_i) function of the form $\sqrt{(p_0/p_T + p_1)^2 + (p_2 \cdot p_T + p_3)^2}$ chosen to encapsulate the dominant effects on the jet mass resolution. Throughout this work, the targeted signal efficiencies are taken to be constant with respect to jet p_T with values of 50% for W-boson tagging and 80% for top-quark tagging. These signal efficiency working points are largely based on those commonly used in searches for physics beyond the Standard Model. In the case of top-quark tagging, a working point with higher efficiency is commonly used because the dominant backgrounds involve processes including real top quarks [2, 73] while in the case of searches for signals involving W-boson jets, the backgrounds are largely dominated by processes involving light-quark jets [74, 75] thereby requiring a selection that more effectively rejects background at the expense of signal efficiency.

In Figure 2, the resulting background rejections as a function of the jet p_T^{true} are shown for a selection of the most powerful two-variable combinations. Based on this study, in the case of W tagging, the combination of m^{comb} and D_2 is most powerful in the kinematic range of interest and is taken as the baseline pairing for W tagging. However, at higher jet p_T^{true}, where the power of D_2 decreases, $\sqrt{d_{12}}$ retains constant discrimination power. In the case of top-quark jet tagging, the behaviour of the most powerful taggers provide a large background rejection at low p_T^{true}, plateauing at a lower value for high jet p_T^{true} due to the wider top-quark mass peak. The two-variable combinations that do not involve mass perform marginally better than those with mass across the entire kinematic range studied. As a consequence, the specific cut-based top-quark jet tagger used in an analysis may depend on the context of the analysis and not on the performance alone. Therefore, the baseline two-variable cut-based top-quark jet tagger is selected to be the one composed of one-sided selections on m^{comb} and τ_{32}, as it has been commonly used in ATLAS.

5.2 Jet-moment-based multivariate taggers

Some of the moments presented in Section 4.3.1 contain complementary information and it has been shown that combining these observables by creating a multivariate W-boson or top-quark classifier provides higher discrimination, albeit to differing degrees [8, 76, 77]. In this work boosted decision tree (BDT) and deep neural network (DNN) algorithms are investigated following a procedure similar to the
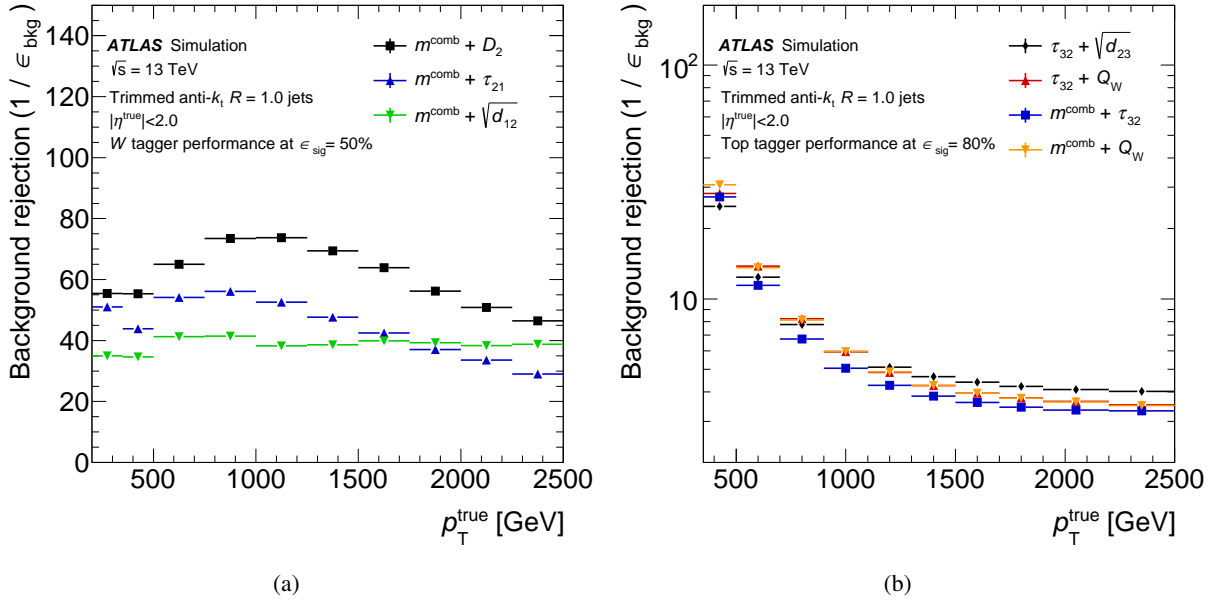
Figure 2: The W-boson (a) and top-quark tagging (b) background rejection as a function of jet p_T^{true} for the best performing two-variable combinations at fixed signal efficiency.

one in Ref. [77]. The goal is to discriminate W-boson and top-quark jets from light jets and to provide a single jet-tagging discriminant that is widely applicable in place of the single jet moment, described in Section 5.1, to augment the discrimination of m^{comb} alone across a broad p_T range, providing another widely applicable and more powerful tagger.

The two algorithmic classes used here, BDTs and DNNs, are explored in parallel to determine if one of the architectures is better suited to exploit differences between the input observables and their correlations among high-level variables in signal and background. The internal settings, so called hyper-parameters, used for the BDTs and DNNs are summarized in Appendix A. For the design of all multivariate discriminants, exclusive subsamples of signal and background jets are derived from the more inclusive sample selected as in Section 5.1 to be used separately for the training and testing of the discriminant. To ensure that all jet substructure features are well-defined for the training, two additional selection criteria are applied to the jet mass ($m^{comb} > 40$ GeV) and number of constituents ($N^{const} \geq 3$). The jets which fail to meet these criteria are not used in the training. However, in the evaluation of the performance of the tagger, such jets are classified as background jets only if they fail the m^{comb} requirement, taking this auxiliary selection into account in the calculation of the signal efficiency and background rejection. The chosen input observables used for either W-boson or top-quark tagging are the full set of observables summarised in Table 1, noting that both the jet mass (m^{comb}) and transverse momentum are directly used as inputs. Therefore, when defining a final working point for this tagger, unlike in the case of the cut-based taggers in Section 5.1, no additional direct selection beyond the $m^{comb} > 40$ GeV requirement is imposed on the mass. Finally, in the design of the classifiers, all studies are performed in a wide p_T^{true} bin and jets are given weights to create a constant p_T^{true} spectra so as to not bias the training. However, the performance comparison of these taggers with the cut-based ones, as well as the full comparison of all tagging techniques in Section 5.5, is made with p_T^{true} distributions for signal jets weighted to match that of the multijet background sample.

The set of observables used in the BDT classifiers is determined using a procedure in which the observables applicable to each topology, specified in Table 1, which give the largest increase in relative performance are sequentially added to the network. For each successive observable that is to be added to the classifier, the BDT classifier is trained with jets from the training set and the relative performance is evaluated using jets from the testing sample and the variable which gives the greatest increase in relative background rejection at a fixed relative signal efficiency of 50% (W-boson tagging) and 80% (top-quark tagging) is retained. *Relative signal efficiency* and *relative background rejection* take into account only the jets that satisfy the training criteria, where *relative signal efficiency* is defined as

$$\epsilon_{\text{sig}}^{\text{rel}} = (N_{\text{signal},m^{\text{comb}}>40 \text{ GeV},N^{\text{const}}>2}^{\text{tagged}})/(N_{\text{signal},m^{\text{comb}}>40 \text{ GeV},N^{\text{const}}>2}^{\text{tagged\&untagged}})$$

and in a similar manner, *relative background rejection* is defined as $1/\epsilon_{\text{bkg}}^{\text{rel}}$. The smallest set of variables which reaches the highest relative background rejection within statistical uncertainties is selected. The minimum number of selected variables is 11 for W-boson tagging and 10 for top-quark tagging. The relative background rejection achieved at each stage for both classifiers is shown in Figure 3.
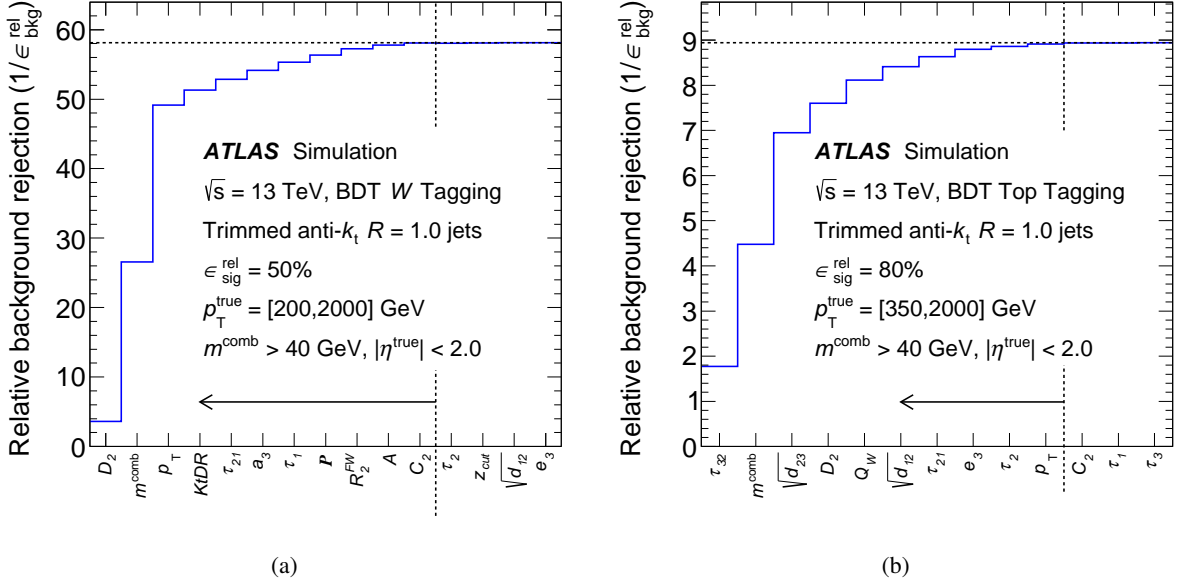

Figure 3: The relative background rejection of the jet-shape-based BDT discriminant for different sets of variables, with more variables added successively at the 50% (W-boson tagging) and 80% (top-quark tagging) relative signal efficiency working point for W-boson (a) and top-quark (b) tagging. Only jets which satisfy the training criteria are considered when calculating the relative signal efficiency and relative background rejection. The performance is evaluated with constant $p_{\text{T}}^{\text{true}}$ spectra. Uncertainties are not presented. The horizontal dashed lines indicate the level of performance saturation, while the vertical dashed lines and solid arrow represent the set of jet moments used in the final construction of the discriminant.

In a similar manner, the observables used in the DNN classifier are chosen by comparing the performance when using different sets of input variables to find the set of observables which gives the largest relative background rejection at a fixed relative signal efficiency. In this case, variables are not added in succession due to the time requirements to train the large number of networks. Instead, groups of observables are chosen by selecting variables according to their dependence on the momentum scale of the jet substructure objects, what features of the substructure they describe and their dependence on other substructure

variables. A summary of all the variables tested for the DNN is shown in Table 2. For each group, the DNN classifier is constructed using the training set of jets and the relative performance is evaluated using the jets in a testing set. The relative background rejection achieved inclusively in jet p_T^{true} is shown in Figure 4. The performance of the DNN tagger depends on both the number of variables and the information content in the group. The chosen groups of inputs for W-boson tagging and top-quark tagging are listed in Table 2. Within statistical uncertainties, the number of variables necessary for maximum rejection at a fixed relative signal efficiency of 50% (W-boson tagging) and 80% (top-quark tagging) is found to be 12 variables for W-boson tagging (Group 8 in Table 2) and 13 variables for top-quark tagging (Group 9 in Table 2).

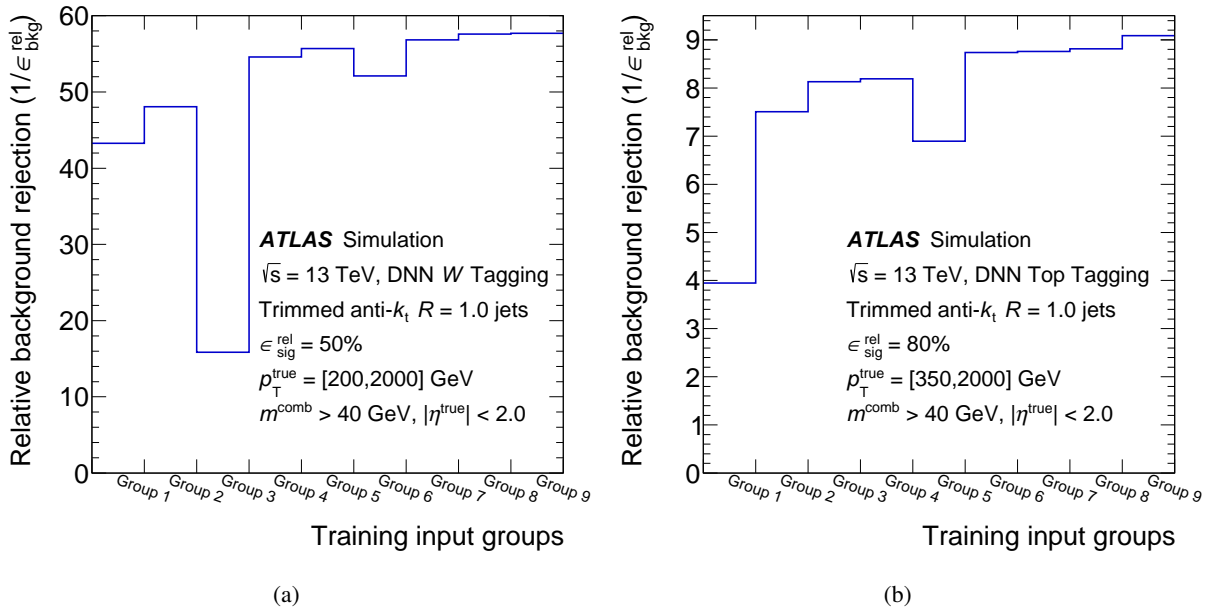(a)   (b)

Figure 4: Distributions showing the training with different set of variables and relative improvement in performance for the DNN W-boson (a) and top-quark (b) taggers at the 50% and 80% relative signal efficiency working point, respectively. Only jets which satisfy the training criteria are considered when calculating the relative signal efficiency and relative background rejection. The performance is evaluated with constant p_T^{true} spectra. Uncertainties are not presented.

Similarly to the cut-based two-variable optimised taggers, for the chosen BDT and DNN taggers the working points are defined as a function of the reconstructed jet p_T so that they yield constant signal efficiencies versus p_T. In both cases, the target signal efficiency working point is obtained by the fixed jet mass requirement of $m^{\text{comb}} > 40$ GeV, relevant N^{const} criteria and a single-sided selection on the relevant discriminant. The performance of the resulting BDT and DNN discriminants is characterised by the background rejection, evaluated as a function of jet p_T^{true}, for a fixed signal efficiency of 50% (W-boson tagging) and 80% (top-quark tagging). It can be seen in Figure 5 that in the case of W-boson tagging, the performance improvements beyond the cut-based taggers are highest at low jet p_T and decrease at higher p_T^{true}, presumably due to the merging of calorimeter energy depositions and subsequent loss of granularity in discerning substructure information. However, in the case of top-quark tagging, the improvements in performance are more sizeable, showing increases in background rejection of roughly a factor of two over the entire kinematic range studied. This is attributed to the greater complexity of the top-quark decay in contrast to that of the isolated W boson, indicating that a single observable does not adequately capture

the full discrimination power and that there are richer correlations between the observables that are being exploited by the classifier algorithms. A common feature of both tagging topologies is that the particular algorithm (i.e. BDT and DNN) used to construct the discriminant does not influence the performance that can be obtained. This is somewhat expected due to the relatively small number of inputs found to be useful for the DNN and helps to put a ceiling on the performance achievable using the combination of jet moments alone [65].
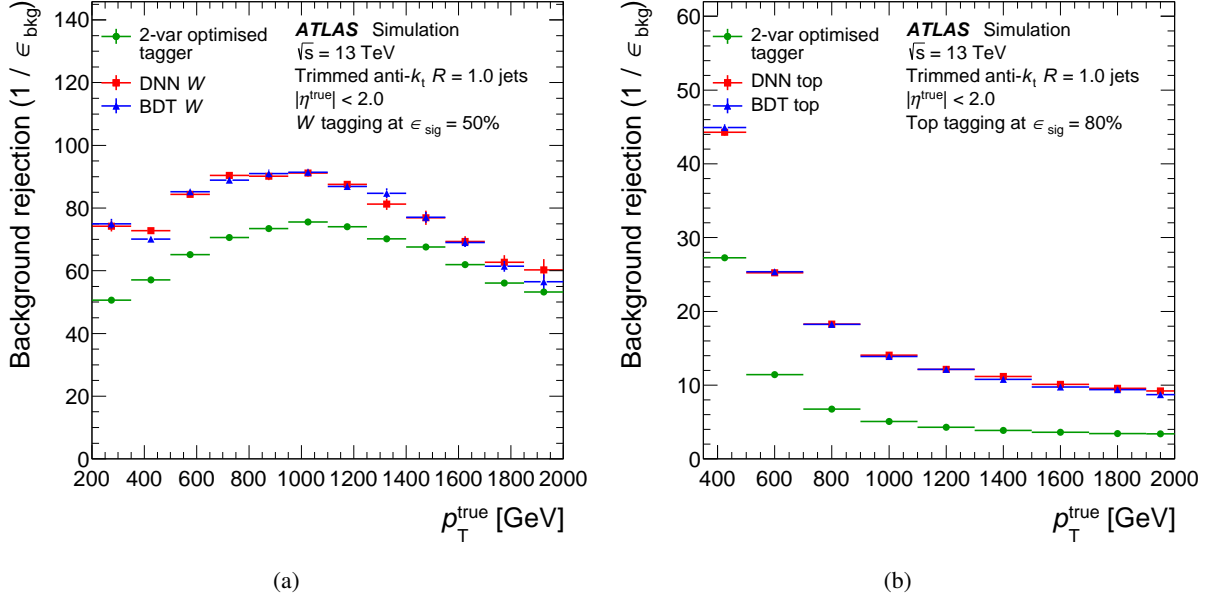

(a)   (b)

Figure 5: The background rejection comparison of W-boson taggers at fixed 50% signal efficiency working point (a) and top-quark taggers at fixed 80% signal efficiency working point (b) for the multivariate jet-shape-based taggers as well as the two-variable optimised taggers, which are composed of a selection on m^{comb} and D_2 in the case of W-boson jet tagging and m^{comb} and τ_{32} for top-quark jet tagging. The performance is evaluated with the $p_{\mathrm{T}}^{\mathrm{true}}$ distribution of the signal jets weighted to match that of the multijet background samples. Statistical uncertainties of the background rejection are presented.

Table 2: A summary of the set of observables that were tested for *W*-boson and top-quark tagging for the various DNN input observable groups as well as the final set of DNN and BDT input observables as chosen using Figures 3 and 4.

| | W Boson Tagging | | | | | | | | | | | Top Quark Tagging | | | | | | | | | | |
| | DNN Test Groups | | | | | | | | | Chosen Inputs | | DNN Test Groups | | | | | | | | | Chosen Inputs | |
Observable	1	2	3	4	5	6	7	8	9	BDT	DNN	1	2	3	4	5	6	7	8	9	BDT	DNN
m^{comb}	○	○		○	○	○	○	○	○	○	○		○	○	○		○	○	○	○	○	○
p_{T}	○	○			○	○		○	○	○	○			○	○			○	○	○	○	○
e_3	○	○				○			○		○			○				○		○	○	○
C_2			○	○	○		○	○	○		○	○	○	○		○	○		○	○		○
D_2			○	○	○		○	○	○	○	○	○	○	○		○	○		○	○		○
τ_1	○	○				○			○	○					○			○		○		○
τ_2	○	○				○			○						○			○		○	○	○
τ_3															○			○		○		○
τ_{21}			○	○	○		○	○	○	○	○	○	○	○		○	○		○	○	○	○
τ_{32}												○	○	○		○	○		○	○	○	○
R_2^{FW}			○	○	○	○	○	○	○	○	○											
$\mathcal{P}$			○	○	○	○	○	○	○	○	○											
a_3			○	○	○	○	○	○	○	○	○											
A			○	○	○	○	○	○	○	○	○											
z_{cut}			○	○	○		○	○	○		○											
$\sqrt{d_{12}}$		○				○	○	○	○	○	○					○	○	○	○	○	○	○
$\sqrt{d_{23}}$																○	○	○	○	○	○	○
$KtDR$		○				○	○	○	○	○	○											
Q_w																○	○	○	○	○	○	○

5.3 Topocluster-based deep neural network tagger

Recently, a number of jet phenomenology studies have found that using lower-level information more directly pertaining to the jet energy flow can lead to further improvements in the ability to distinguish signal W-boson and top-quark jets from light jets [64–67]. Furthermore, it was seen in Figure 5 that the performance gains for the high-level variables BDT and DNN combination are significantly larger for top-quark tagging than for W-boson tagging. Consequently, a top-quark jet tagger based directly on the jet constituents, focusing on the high-p_T top quarks with $p_T > 450$ GeV where cluster merging decreases the power of the axis-based observables (e.g. N-subjettiness), is designed.

The jet tagger based on low-level jet input information studied in this work closely follows that described in Ref. [66] and the reader is referred there for a more in-depth review of the optimisation of the techniques used; only a brief summary is provided in the following. The first aspect of note which sets this tagger apart from those studied in Refs. [64, 65, 67] is that there is no use of pixelation in this tagger. Instead, the input features used in this tagger are the four-vectors of the topoclusters in the large-R anti-k_t trimmed jet in the (p_T, η, ϕ) representation, noting that topoclusters are taken as massless by convention. As a preprocessing step, the p_T of each constituent four-vector is normalised by $1/1700$ to bring the scale of the input network features within the same magnitude between approximately 0 and 1. The (η, ϕ) location of the set of constituents is then transformed by a process that involves a translation, a rotation, and a flip based on the assumed three-subjet topology of a top-quark decay. Of the full set of constituents, only the 10 highest-p_T constituents are used as input to the neural network. This was found to provide optimal background rejection for this network architecture as compared to using more or fewer clusters and can be qualitatively understood by examining the fraction of the jet p_T carried by each of the clusters, shown in Figure 6 where the distribution of the p_T-fraction for the 10 highest-p_T clusters is shown along with the mean value of each of these cluster distributions. It is seen that the first 10 clusters, on average carry more than 99% of the p_T of the jet. Therefore, including further clusters saturates the information for the network to disentangle when discriminating signal from background. If a jet has fewer than 10 constituents, the remaining inputs to the neural network are taken to be null vectors. The three components of each four-vector are used as input to a fully connected neural network with four hidden layers composed of 300, 102, 12 and 6 nodes, respectively. This network architecture was determined through manual hyper-parameter tuning, exploring a space between 4-6 and 40-1000 nodes per layer. The network is trained on jets where only the initial top parton is required to be matched to the reconstructed jet obtained from the Z' (signal) and light jets (background) in the high-p_T region from 450 GeV to 2400 GeV in p_T. To remove bias in the training due to the difference in kinematics between the signal and background samples, a subset of the background ensemble of jets is selected in a random fashion such that the jet p_T distribution is the same in both signal and background, as opposed to the BDT and DNN taggers described in Section 5.2, which use event-by-event reweighting.

5.4 Shower deconstruction tagger

The shower deconstruction tagging method was studied extensively in Run 1 [7]. The aim of the method, described in Section 4.3.3, is to determine whether the subjet pattern is compatible with a parton shower profile typical of a top-quark decay. In previous ATLAS studies, the subjets were defined by forming C/A subjets with $R = 0.2$ using the ungroomed large-R jet constituents as inputs. However, in Run 2, shower deconstruction was recommissioned in the context of the search for a heavy W' boson decaying to a top quark and a bottom quark where the mass-splitting between the W' and the top quark was large
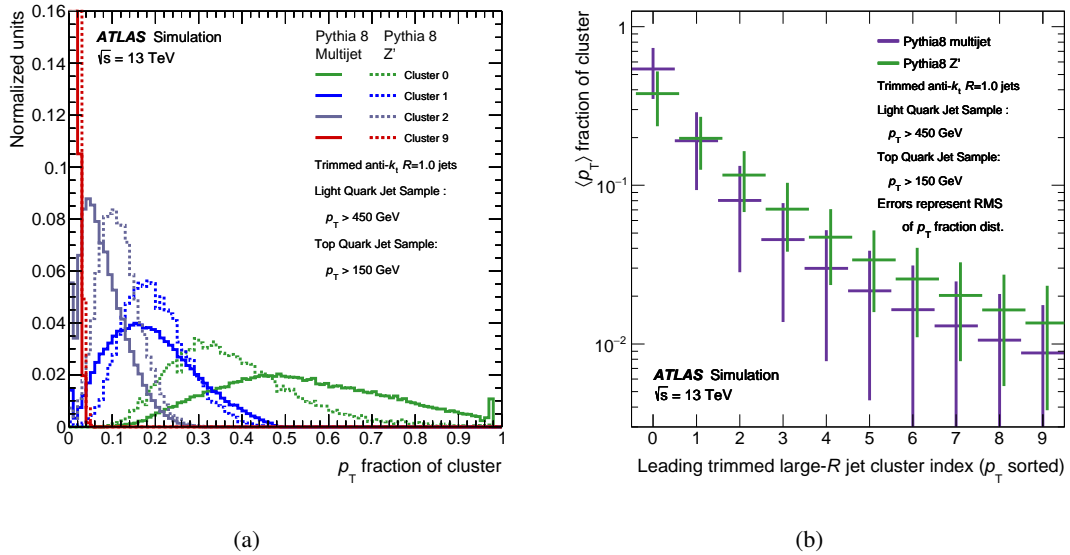
(a)

(b)

Figure 6: The distribution of the fraction of p_T carried by the highest-p_T cluster (Cluster 0) along with the next-highest (Cluster 1), third-highest (Cluster 2), and tenth-highest-p_T (Cluster 9) clusters (a) along with the average value of the ratio of the cluster p_T to the jet p_T for the 10 highest-p_T clusters (b). The dashed lines in (a) show distributions for signal jets, and the full lines show distributions for background jets. The vertical lines on each point in (b) represent the RMS of the corresponding distribution of the fraction of p_T of a given cluster in (a). In (a), the distribution for the tenth-highest-p_T cluster (Cluster 9) extends beyond the maximum value of the vertical axis. The light-quark jet sample is taken from jets that pass the multijet selection as described in Section 6.2.1 while the top-quark jet sample is taken from jets that pass the semileptonic selection as described in Section 6.1.1.

enough to produce top quarks with momenta of roughly 1 TeV and above [78]. The approach taken in Run 1 to reconstruct the subjet inputs to the shower deconstruction algorithm was found to have a low signal efficiency, largely due to the subjet multiplicity falling below three and therefore producing a set of subjets that are unable to fulfil the initial consistency checks between the subjet pairings and triplets with W-boson and top-quark masses, respectively. This drop in efficiency was recovered by altering the manner in which subjets are constructed to instead use the exclusive-k_t jet clustering algorithm, run on the constituents of the trimmed large-R jet. Since splitting scales are less dependent on the large-R jet p_T than the geometric distance between the jet and its constituents, a stopping criterion is imposed to halt clustering if k_t splitting scales larger than 15 GeV are found. At that stage, the resulting set of subjets are used as subjet inputs to shower deconstruction. Because the computation time of shower deconstruction scales exponentially with the number of input subjets, the total number of subjets is limited to at most the six highest-p_T subjets, compared to a limit of nine in Run 1, with no loss in performance. Finally, the parameters controlling the top-quark topology check using subjet pairings and triplets, m_W and m_{top} respectively, were fixed to 20 GeV and 40 GeV, the same as in Run 1.

5.5 Summary of tagger performance studies in simulation

A direct comparison of the performance of all of the tagging techniques, described in Section 4 and individually optimised in Section 5, is important in providing guidance as to which technique can be most beneficial when applied in an analysis. The primary metric used to assess the performance of the

18

taggers is the background rejection as a function of the signal efficiency, characterised in the form of a receiver operating characteristic (ROC) curve, shown in Figures 7 and 8 for W-boson and top-quark tagging, respectively, for both a low- and high-p_T kinematic region. For comparison, two relatively simple cut-based taggers composed of selections on m^{comb} and a single substructure observable are shown. In the case of W-boson tagging, a fixed mass window requirement of $60 < m^{comb} < 100$ GeV is applied and a cut on the D_2 observable is used for the ROC curve. In the case of top-quark tagging, the mass selection is one-sided, requiring $m^{comb} > 60$ GeV, and a requirement on τ_{32} is varied to obtain the ROC curve. These simple taggers, along with the specific working points tuned to give constant signal efficiency and maximal background rejection, are provided as a point of reference for subsequent optimisations that were performed for studies of the more advanced techniques.

When examining Figures 7 and 8, it can be seen that a careful tuning of the simple two-variable cut-based taggers can lead to sizeable gains due to taking into consideration the correlation between m^{comb} and the auxiliary jet moment observable. The gains are significantly larger in the case of the BDT- and DNN-based high-level observable discriminants, and lead to larger improvements for top-quark tagging than for W-boson tagging. However, the BDT and DNN algorithms perform similarly to each other for all signal efficiencies, indicating that they are leveraging the correlations of the input jet moment observables equally well. Therefore, when studying the performance of these tagging techniques in data in Section 6, only the DNN-based taggers are included. The performance of the BDT-based taggers was studied and found to be similar. Finally, in the case of top-quark tagging, where more dedicated tagging techniques are studied, the conclusion is similar. Dedicated approaches, including shower deconstruction and HEPTopTagger, are more performant than a simple cut-based approach on m^{comb} and τ_{32}, but the combination of many jet-moment observables in a BDT or DNN yields the best overall performance. Of particular note, however, is the comparison of the BDT and DNN taggers using high-level observables and those using lower-level inputs, namely the jet constituents, here taken to be topoclusters. The performance of these two approaches is similar, with the TopoDNN tagger having slightly higher background rejection at high jet p_T, resulting in conclusions qualitatively similar to those found in Ref. [67], particularly at high jet p_T where the details of the signal sample used for training are less relevant.
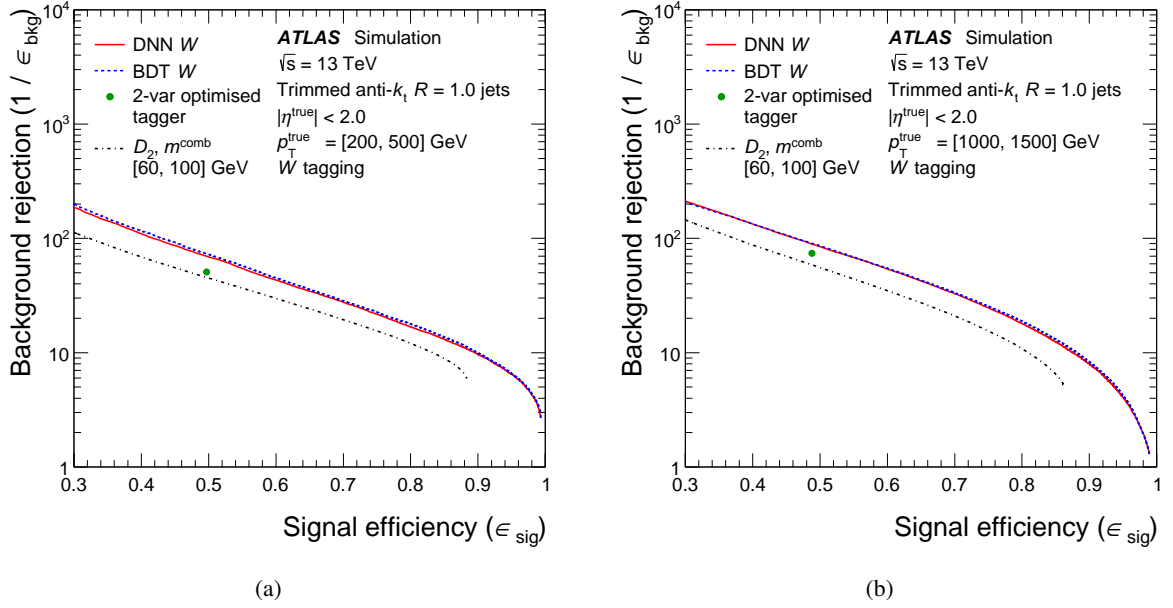
Figure 7: The performance comparison of the W-boson taggers in a low-p_T^{true} (a) and high-p_T^{true} (b) bin. The performance is evaluated with the p_T^{true} distribution of the signal jets weighted to match that of the dijet background samples.
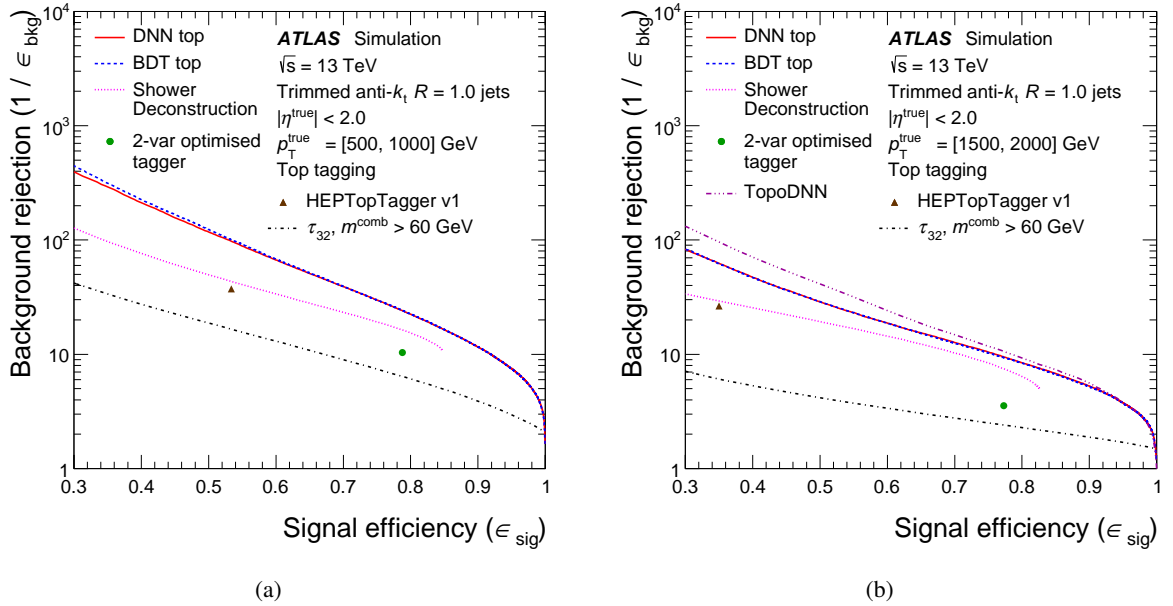

Figure 8: The performance comparison of the top-quark taggers in a low-p_T^{true} (a) and high-p_T^{true} (b) bin. The performance is evaluated with the p_T^{true} distribution of the signal jets weighted to match that of the dijet background samples.

6 Performance in data

The taggers studied in the previous sections are validated using signal and background-enriched data samples collected during 2015 and 2016 at a centre-of-mass energy of $\sqrt{s} = 13$ TeV and corresponding to an integrated luminosity of 36.1 fb^{-1}. In the case of W-boson and top-quark jets, the lepton-plus-jets $t\bar{t}$ signature is used, which provides a sample of signal jets in a p_T range of approximately 200 GeV to 1000 GeV. In the case of background light jets, two topologies are studied: a γ + jet sample enriched in light-quark jets and spanning a p_T range of approximately 200 GeV to 2000 GeV and a multijet sample which probes a mixture of light-quark and gluon jets in a p_T range of approximately 500 GeV to 3500 GeV. The primary aim of these studies is to validate the modelling of the Monte Carlo simulation in data for the techniques studied in Section 4. This is achieved by directly studying the full spectrum of a subset of important observables used in the tagging as well as directly measuring both the signal efficiency and background efficiency of the various techniques in the phase space accessible in this data sample. In the case of the measured signal efficiency and background rejection, the performance is evaluated differentially as a function of the jet transverse momentum as well as the average number of interactions per bunch crossing (μ).

6.1 Signal efficiency in boosted $t\bar{t}$ events

To study the modelling of signal W-boson and top-quark large-R jet tagging, a sample of data enriched in $t\bar{t}$ events where one top quark decays hadronically and the other semileptonically in both the electron and the muon decay channel is selected in a similar manner to Refs. [6, 7]. The inclusive sample of events is decomposed into two exclusive subsamples, enriched in W-boson jets and top-quark jets, based on the proximity of a b-jet to the large-R jet. The inclusive distributions of the key observables used in each tagging method are examined and the signal efficiency is measured for a set of fixed signal efficiency working points, for which systematic uncertainties can be derived and associated with a particular tagging method.

6.1.1 Analysis and selection

To select the inclusive set of lepton-plus-jets $t\bar{t}$ events, both the data and Monte Carlo simulated events are required to pass either an inclusive electron trigger or an inclusive muon trigger, where the thresholds were varied between the 2015 and 2016 datasets due to increases in instantaneous luminosity. In the electron channel, events from the 2015 data-taking period are required to pass at least one of three triggers: one isolated electron with $p_T > 24$ GeV, one electron with $p_T > 60$ GeV without any isolation requirement, or one electron with $p_T > 120$ GeV without any isolation requirement and relaxed identification criteria. In the 2016 data-taking period, the thresholds of these electron triggers required $p_T > 26$ GeV, $p_T > 60$ GeV and $p_T > 140$ GeV, respectively. In the muon channel, events from the 2015 data-taking period are required to pass at least one of two muon triggers: one isolated muon with $p_T > 20$ GeV or one muon with $p_T > 50$ GeV and no isolation requirement. In the 2016 data-taking period, the thresholds of these triggers required $p_T > 26$ GeV and $p_T > 50$ GeV, respectively.

Events are then required to contain exactly one electron or muon candidate with $p_T > 30$ GeV that is matched to the trigger-level counterpart associated with the appropriate trigger. Electron candidates are reconstructed as ID tracks that are matched to a cluster of energy in the electromagnetic calorimeter.

Electron candidates are required to be within $|\eta| < 2.47$, excluding the calorimeter transition region from $1.37 < |\eta| < 1.52$, and satisfy the "tight" likelihood-based identification criterion based on shower shape and track selection requirements [79, 80]. Muons are reconstructed as tracks found in the ID that are matched to tracks reconstructed in the muon spectrometer. They are required to be within $|\eta| < 2.5$ and are required to satisfy the "medium" muon identification quality criteria defined in Ref. [81]. For both electrons and muons, the reconstructed lepton candidate is required to be isolated from additional activity in the event by imposing isolation criterion defined by a sum of p_T of tracks in an isolation cone with variable radius depending on the lepton p_T [81, 82].

In addition to identified leptons, small-radius jets are used to reconstruct the missing transverse momentum and identify the signal topology. These jets are reconstructed from topoclusters calibrated to the electromagnetic scale using the anti-k_t algorithm with a radius parameter of $R = 0.4$. The energy of these jets is corrected for the effects of pile-up by using a technique based on jet area [49] and the jet energy is further corrected using a jet energy scale calibration based on both Monte Carlo simulation and data [38]. To ensure that the reconstructed jets are well-measured, they are required to have $p_T > 20$ GeV, $|\eta| < 2.5$ and to satisfy "loose" quality criteria to prevent mismeasurements due to calorimeter noise spikes and non-collision backgrounds [83]. For jets with $p_T < 60$ GeV and $|\eta| < 2.4$, a requirement that the jets arise from the primary vertex, using the ID tracks associated with the jet, is imposed to suppress pile-up jets [84].

For the identification of b-quark candidate jets, jets reconstructed from ID tracks with the anti-k_t algorithm with radius parameter $R = 0.2$ are used. These jets are b-tagged using a multivariate discriminant based on impact parameter and secondary vertex information [85]. The 70% signal efficiency point selection is used. Event-by-event scale factors, evaluated in $t\bar{t}$ events [86], are applied to account for mismodelling of the selection efficiency.

The missing transverse momentum is reconstructed as the negative vectorial sum of the momenta of all reconstructed physics objects in the plane transverse to the beamline [87]. In this case, the sum consists of the single identified lepton and the full set of reconstructed and fully calibrated small-R calorimeter jets as well as ID tracks not associated with the lepton or jets. These ID tracks are included to account for the soft hadronic energy flow in the event. In the following the magnitude of the missing transverse momentum vector is denoted by E_T^{miss}.

First, events containing a leptonically decaying W boson are preselected by requiring one electron or muon candidate with $p_T > 30$ GeV and rejecting events that contain additional electrons or muons with $p_T > 25$ GeV. The missing transverse momentum is required to be greater than 20 GeV and the scalar sum of E_T^{miss} and the transverse mass of the leptonically decaying W boson candidate[4] must satisfy $E_T^{\mathrm{miss}} + m_T^W > 60$ GeV. To ensure the topology is consistent with a $t\bar{t}$ event, at least one small-R jet is required to have $p_T > 25$ GeV and to be close to the lepton ($\Delta R(\text{lepton, jet}) < 1.5$). To study W-boson and top-quark tagging, the highest-p_T large-R jet is studied, which is either a trimmed anti-k_t $R = 1.0$ jet or a C/A $R = 1.5$ jet in the case of HEPTopTagger, with $p_T > 200$ GeV and $|\eta| < 2.0$. The signal top-quark jet candidate is required to be well-separated from the semileptonic top-quark decay by requiring $\Delta R > 1.5$ between the large-R jet and the small-R jet close to lepton. Additionally, the angular separation in the transverse plane between the lepton and the large-R jet is required to be $\Delta\phi > 2.3$.

---

[4] $m_T^W = \sqrt{2p_T^\ell E_T^{\mathrm{miss}}(1 - \cos\Delta\phi)}$ is calculated from the transverse momentum of the lepton, p_T^ℓ, and E_T^{miss} in the event. $\Delta\phi$ is the azimuthal angle between the lepton momentum and the E_T^{miss} direction.

Finally, the sample preselected as above is divided into two subsamples, intended to be representative of a fully contained top-quark decay or an isolated and fully contained W-boson decay based on the proximity of a b-tagged track jet to the highest-p_T large-R jet. The track jets are clustered from at least two tracks using the anti-k_t algorithm with a radius parameter of $R = 0.2$. All tracks must fulfil $|\eta| < 2.5$ and $p_T > 10$ GeV. The sample enriched in top quarks ("top-quark selection") is defined by requiring a b-tagged track jet to have an angular separation of $\Delta R(b$-jet, large-R jet$) < 1.0$ ($\Delta R(b$-jet, large-R jet$) < 1.5$) from the large-R anti-k_t trimmed jet (C/A jet). In order to enhance the fraction of fully contained top quarks, an additional requirement of $p_T > 350$ GeV ($p_T > 200$ GeV) is also applied. The sample enriched in W-boson jets ("W-boson selection") is defined by requiring a b-tagged track jet to have angular separation $\Delta R(b$-jet, large-R jet$) > 1.0$ from the large-R anti-k_t trimmed jet. Because the geometrical separation of the daughter b-quark and the top parton decreases with increasing p_T, this requirement limits the efficiency of the W-boson selection at high jet p_T, which limits the kinematic reach to approximately 600 GeV. These requirements result in relatively pure samples of W-boson and top-quark jets as shown in Figure 9 for the anti-k_t $R = 1.0$ trimmed jet mass, including the full set of systematic uncertainties summarised in Section 6.3, while Figure 10 shows the C/A $R = 1.5$ trimmed jet mass. The disagreement between the peak positions in Monte Carlo simulation and data observed near m_W and m_{top} is attributed to a mismodelling of the jet mass scale as studied in Ref. [88]. In this paper, the $t\bar{t}$ and single-top Monte Carlo samples are divided into three subsamples based on the jet labelling criteria outlined in Section 4.2 to highlight the fraction of events in each sample of interest ("$t\bar{t}$ (top)" and "$t\bar{t}$ (W)"), with all other events in these samples being grouped together in a single subsample ("$t\bar{t}$ (other)"). The backgrounds are derived from the Monte Carlo simulations described in Section 3, with the exception of the multijet background, which is estimated using a data-driven method based on looser lepton selection criteria with a dedicated evaluation of the probability of prompt lepton reconstruction and the probability of fake/non-prompt lepton reconstruction, as was performed in Ref. [2]. The event yield in the simulation is normalised to that in the data at this stage of the selection throughout Section 6.1.1.

The primary tagging observables used by the other tagging techniques described in Section 4 are examined in Figures 11–15. For these spectra, the full set of systematic uncertainties described in Section 6.3 are included for the D_2 and τ_{32} observables, whereas for the other spectra, no dedicated experimental systematic uncertainty in the scale or resolution of the observable itself is included. Instead, the mismodelling of the simulation relative to data is taken into account as a derived uncertainty in the *in situ* measurement of the signal efficiency of the tagger itself, in a manner similar to that commonly used to evaluate mismodelling in the detector response in the context of the identification of heavy-flavour jets [89]. However, for nearly all regions of phase space, the overall relative yield of data is well-described by the Monte Carlo prediction within the theoretical uncertainties, derived from the comparison of various $t\bar{t}$ Monte Carlo generators.
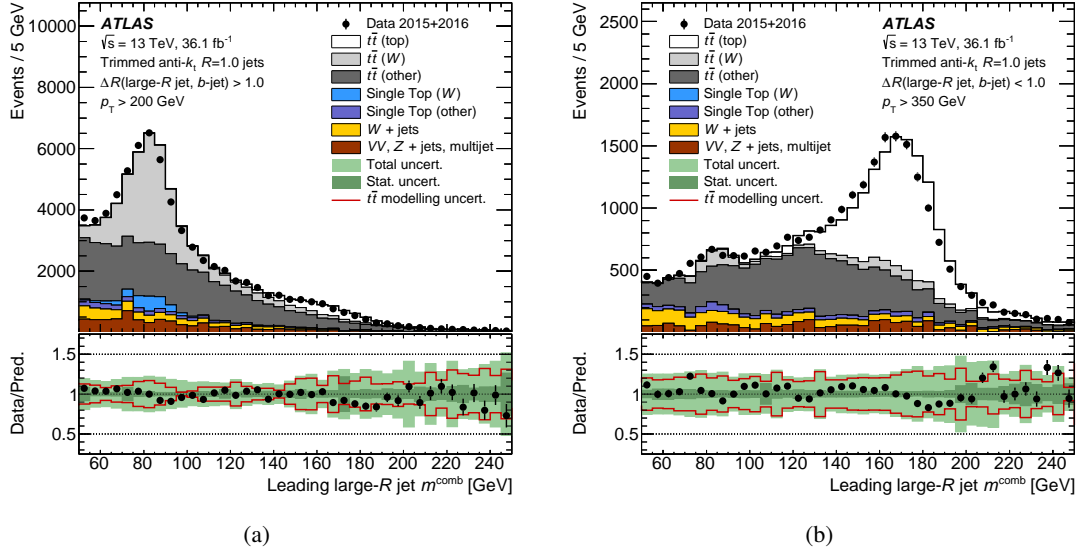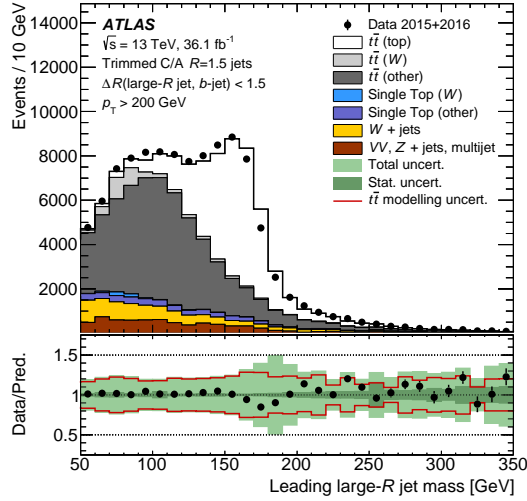
(a)   (b)

Figure 9: A comparison of the observed data and predicted MC distributions of the mass of the leading p_T anti-k_t trimmed jet in the event for the W boson (a) and top quark (b) selections in a sample enriched in lepton+jets $t\bar{t}$ events. Simulated distributions are normalised to data. The $t\bar{t}$ sample is divided into a set of subsamples (e.g. $t\bar{t}$ (top)) based on criteria described in Section 4.2. The statistical uncertainty of the background prediction (Stat. uncert.) results from limited Monte Carlo statistics as well as the limited size of the data sample used in the data-driven estimation of the multijet background.
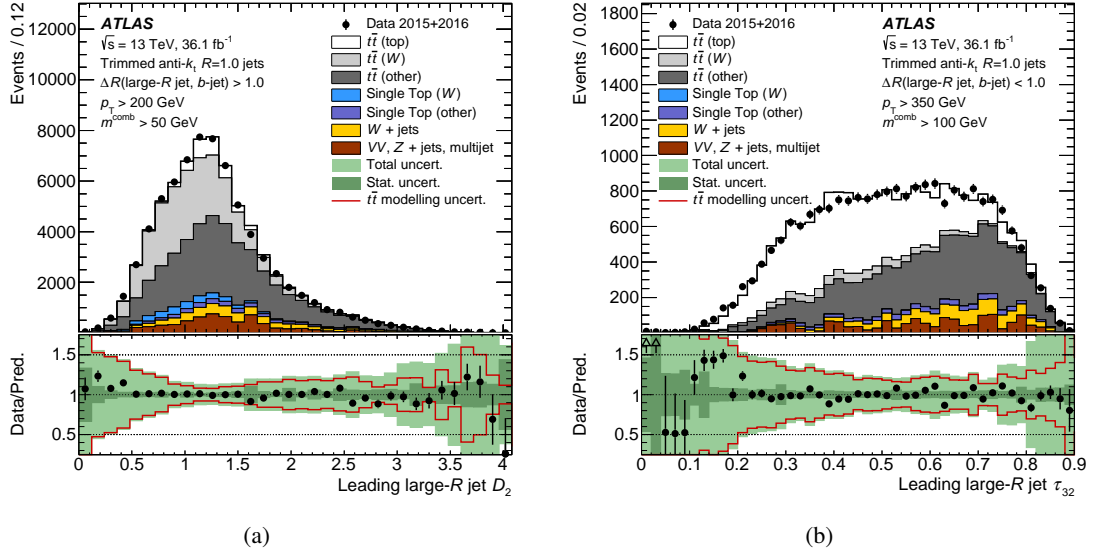

Figure 10: A comparison of the observed data and predicted MC distributions of the mass of the leading p_T C/A $R = 1.5$ trimmed jet in events passing the top-quark selection in a sample enriched in lepton+jets $t\bar{t}$ events. Simulated distributions are normalised to data. The $t\bar{t}$ sample is divided into a set of subsamples (e.g. $t\bar{t}$ (top)) based on criteria described in Section 4.2. The statistical uncertainty of the background prediction (Stat. uncert.) results from limited Monte Carlo statistics as well as the limited size of the data sample used in the data-driven estimation of the multijet background.
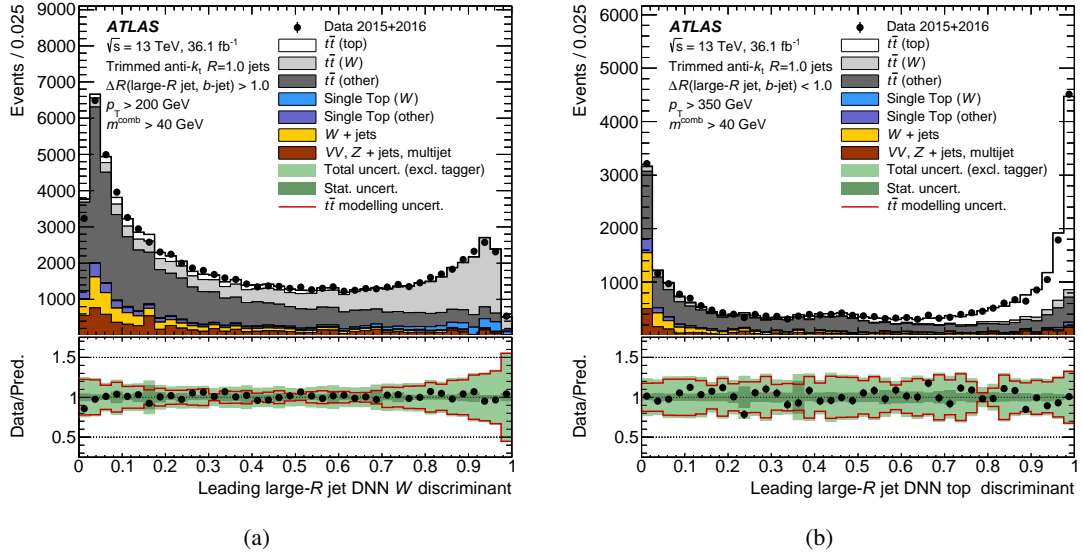
24

Figure 11: A comparison of the observed data and predicted MC distributions of the anti-k_t $R = 1.0$ trimmed jet D_2 (a) and τ_{32} (b) for the W-boson and top-quark selections, respectively, in a sample enriched in lepton+jets $t\bar{t}$ events. Simulated distributions are normalised to data. The $t\bar{t}$ sample is divided into a set of subsamples (e.g. $t\bar{t}$ (top)) based on criteria described in Section 4.2. The statistical uncertainty of the background prediction (Stat. uncert.) results from limited Monte Carlo statistics as well as the limited size of the data sample used in the data-driven estimation of the multijet background.

Figure 12: A comparison of the observed data and predicted MC distributions of the anti-k_t $R = 1.0$ trimmed jet DNN discriminant for W boson (a) and top quark (b) tagging for the respective event selections in a sample enriched in lepton+jets $t\bar{t}$ events. Simulated distributions are normalised to data. The $t\bar{t}$ sample is divided into a set of subsamples (e.g. $t\bar{t}$ (top)) based on criteria described in Section 4.2. The statistical uncertainty of the background prediction (Stat. uncert.) results from limited Monte Carlo statistics as well as the limited size of the data sample used in the data-driven estimation of the multijet background.
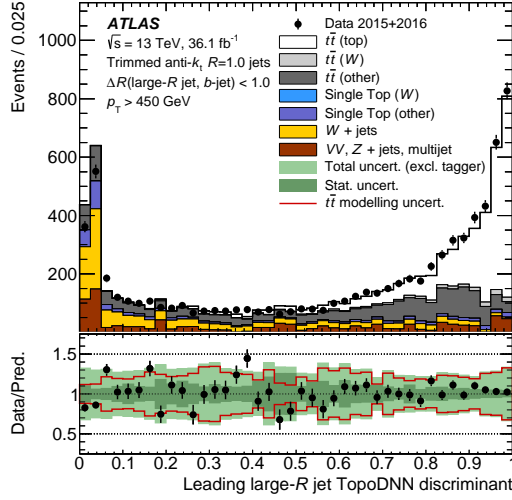
Figure 13: A comparison of the observed data and predicted MC distributions of the TopoDNN top tagger discriminant for the top-quark event selection in a sample enriched in lepton+jets $t\bar{t}$ events. Simulated distributions are normalised to data. The $t\bar{t}$ sample is divided into a set of subsamples (e.g. $t\bar{t}$ (top)) based on criteria described in Section 4.2. In this case, a $p_T > 450$ GeV selection is applied to the large-R jet to specifically focus on the kinematic region of interest for which this tagging algorithm was designed, as described in Section 5.3. The statistical uncertainty of the background prediction (Stat. uncert.) results from limited Monte Carlo statistics as well as the limited size of the data sample used in the data-driven estimation of the multijet background.
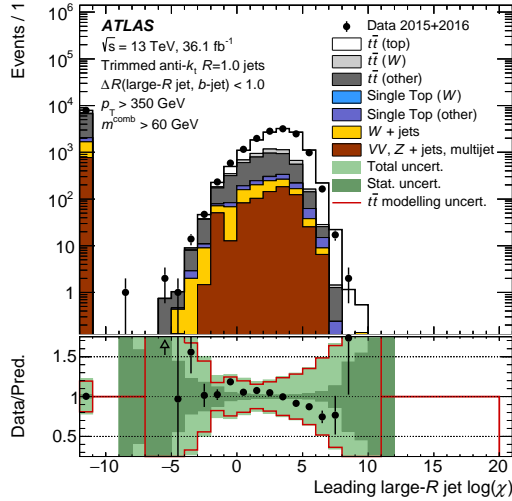

Figure 14: A comparison of the observed data and predicted MC distributions of the log χ shower deconstruction discriminant for the top-quark event selection in a sample enriched in lepton+jets $t\bar{t}$ events. Simulated distributions are normalised to data. The $t\bar{t}$ sample is divided into a set of subsamples (e.g. $t\bar{t}$ (top)) based on criteria described in Section 4.2. The ensemble of jets with a large negative log χ value correspond to the set of jets where no subjet configuration is roughly consistent with a top-quark jet topology, as described in Section 5.4. The statistical uncertainty of the background prediction (Stat. uncert.) results from limited Monte Carlo statistics as well as the limited size of the data sample used in the data-driven estimation of the multijet background.
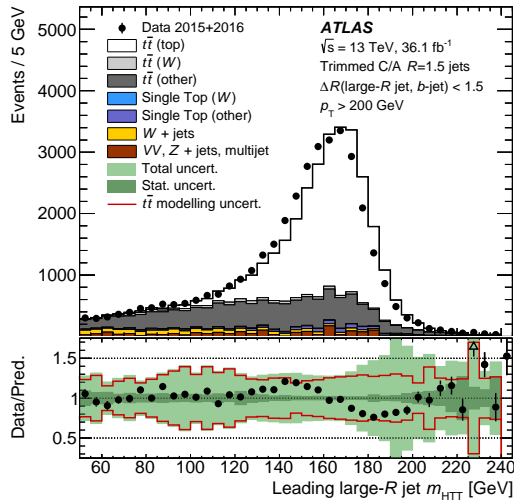
26

Figure 15: A comparison of the observed data and predicted MC distributions of the HEPTopTagger mass for the top-quark event selection in a sample enriched in lepton-plus-jets $t\bar{t}$ events. Simulated distributions are normalised to data. The $t\bar{t}$ sample is divided into a set of subsamples (e.g. $t\bar{t}$ (top)) based on criteria described in Section 4.2. The statistical uncertainty of the background prediction (Stat. uncert.) results from limited Monte Carlo statistics as well as the limited size of the data sample used in the data-driven estimation of the multijet background.

6.1.2 Signal efficiencies

Due to the relatively high purity of the samples of W-boson and top-quark jets that result from the selection described in Section 6.1.1, it is possible to measure the signal efficiency in data. This measurement, when compared with the Monte Carlo prediction, can be used to estimate the systematic uncertainty of a particular tagging method when applied in the context of an independent analysis. It can also be used to provide an *in situ* correction in the form of a jet-by-jet efficiency scale factor [86, 89]. Because the aim is to provide an efficiency measurement for a particular tagging method, it is necessary to define selection criteria based on the particular tagging discriminants described in Section 4 for which the comparison of the Monte Carlo prediction to data was shown in a rather inclusive selection of signal-like events in Section 6.1.1. In particular, the seven tagger working points for which the signal efficiency is measured here are:

- $D_2 + m^{comb}$ (W boson): A pair of selections on m^{comb} and D_2, tuned as a function of p_T, that give the largest background rejection for a fixed 50% signal efficiency for fully contained W-boson jets;

- $m^{comb} + \tau_{32}$ (top quark): A pair of selections on m^{comb} and τ_{32}, tuned as a function of p_T, that give the largest background rejection for a fixed 80% signal efficiency for fully contained top-quark jets;

- DNN (W boson): A single-sided selection of $m^{comb} > 40$ GeV and a selection on the DNN discriminant, tuned to give a fixed 50% signal efficiency as a function of p_T for fully contained W-boson jets;

- DNN (top quark): A single-sided selection of $m^{comb} > 40$ GeV and a selection on the DNN discriminant, tuned to give a fixed 80% signal efficiency as a function of p_T for fully contained top-quark jets;

- TopoDNN (top quark): A selection on the DNN discriminant, tuned to give a fixed 80% signal efficiency as a function of p_T for fully contained top-quark jets;

- Shower Deconstruction (top quark): A single-sided selection of $m^{comb} > 60$ GeV and a selection on $\log \chi$, tuned to give a fixed 80% signal efficiency as a function of p_T for fully contained top-quark jets;

- HEPTopTagger (top quark): A requirement on the HEPTopTagger candidate trimmed jet kinematics to have a mass between 140 and 210 GeV and a p_T larger than 200 GeV.

The numbers of signal-like events in data that pass and fail each of these requirements are obtained from a chi-square template fit of "signal" and "background" distributions predicted by Monte Carlo simulations to the data to correct for mismodelling of the cross-section of the various processes contributing to the phase space of interest. The labelling of "signal" events follows Section 4.2 and is based on Monte Carlo simulations of $t\bar{t}$ and single-top-quark events. To increase the stability of the fit, background templates whose shapes are similar are merged. This procedure results in a signal ($t\bar{t}(W)$ and single top(W)) and background ($t\bar{t}(top)+t\bar{t}(other)+$single top(other)+non-$t\bar{t}$) component template in the case of W-boson tagging and a signal ($t\bar{t}(top)$) and two background ($t\bar{t}(W)+t\bar{t}(other)$ and non-$t\bar{t}$) component templates in the top-quark efficiency measurement, and the normalisation of each template is allowed to float freely in the fit. The fit is performed using distributions of the mass of the leading anti-k_t trimmed jet, thus separating signal and background events, as demonstrated in Figure 16 in the case of the simple $m^{comb} + \tau_{32}$ top-quark tagger. For the measurement of the HEPTopTagger signal efficiency, the fit is performed using distributions of the mass of the leading C/A trimmed jet instead. Distributions of events that either pass

or fail the tagger under study are fit simultaneously. The total normalisation of each grouped background component is allowed to float and is extracted in the fit, while the efficiency of the tagger on background events is fixed to the value in Monte Carlo simulation. Normalisations of signal distributions in the pass and fail categories ($N_{\text{fitted signal}}^{\text{tagged}}$ and $N_{\text{fitted signal}}^{\text{not tagged}}$) are extracted from the fit. Therefore, the tagger efficiency for signal events in data can be extracted as

$$\epsilon_{\text{data}} = \frac{N_{\text{fitted signal}}^{\text{tagged}}}{N_{\text{fitted signal}}^{\text{tagged}} + N_{\text{fitted signal}}^{\text{not tagged}}}.$$

This can be compared to the tagger efficiency in Monte Carlo simulation, which is based on the numbers of predicted signal events that pass, $N_{\text{signal}}^{\text{tagged}}$, and fail, $N_{\text{signal}}^{\text{not tagged}}$, the tagger under study:

$$\epsilon_{\text{MC}} = \frac{N_{\text{signal}}^{\text{tagged}}}{N_{\text{signal}}^{\text{tagged}} + N_{\text{signal}}^{\text{not tagged}}}.$$
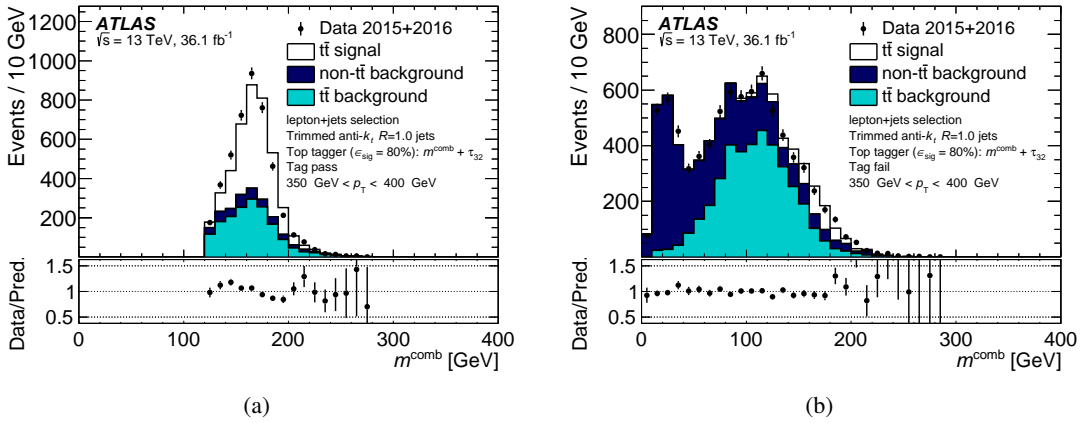

(a) (b)

Figure 16: The anti-k_t trimmed jet mass distribution in the pass (a) and fail (b) categories for the $m^{\text{comb}} + \tau_{32}$ top-quark tagger working point after the chi-square fit has been performed. The templates shown here are those used in the chi-square fit for the extraction of the three normalisation factors. The first, $t\bar{t}$ *signal*, includes only the $t\bar{t}$(top) contribution, while $t\bar{t}$ *background* includes contributions from $t\bar{t}$(W) and $t\bar{t}$(other) and the *non-$t\bar{t}$ background* component includes all other backgrounds. Only statistical uncertainties are shown.

The signal efficiency is measured in data and obtained in simulations as a function of the p_{T} of the large-R jet as well as the average number of interactions per bunch crossing (μ). The results are shown in Figures 17 and 18 for the W-boson taggers and in Figures 19–23 for the top-quark taggers.

The signal efficiency for the W-boson and top-quark taggers in Monte Carlo simulation is compatible with the measured efficiency in data within uncertainties. In the case of the W-boson tagger working points, there is a systematic difference between the target 50% signal efficiency and that measured in data due to event topology differences between W-boson jets from these two samples, as was investigated in Ref. [6]. The total uncertainty of the measured signal efficiency is typically about 50% and 15% for the W-boson and top-quark tagger efficiencies, respectively, and is largely dominated by the subtraction of the non-contained top-quark contribution. In most of the kinematic phase space, these uncertainties are dominated by systematic uncertainties, described in Section 6.3, specifically by the theoretical uncertainties in $t\bar{t}$

modelling, largely coming from the subtraction of the component of the $t\bar{t}$ Monte Carlo prediction that consists of either non-W-boson jets or non-contained top-quark jets.

When examining the measured signal efficiency as a function of the average number of interactions per bunch crossing, it is found to be quite robust against increasing levels of event pile-up, even when considering only the statistical uncertainties due to the size of the data sample, noting that the systematic uncertainties are correlated between bins.
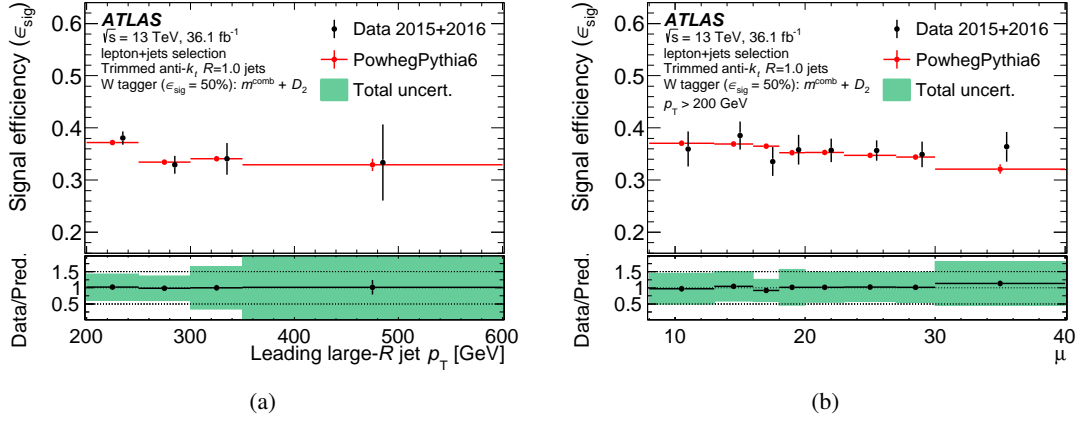

(a)   (b)

Figure 17: The signal efficiency on contained W-boson jets for the two-variable $m^{\mathrm{comb}} + D_2$ W-boson tagger as a function of the large-R jet p_T (a) and the average number of interactions per bunch crossing μ (b) in data and simulation. Statistical uncertainties of the signal efficiency measurement in data and simulation are shown as error bars in the top panel. In the bottom panel, the ratio of the measured signal efficiency in data to that estimated in Monte Carlo simulation is shown with statistical uncertainties as error bars on the data points and the sum in quadrature of statistical and systematic uncertainties as a shaded band. When considering experimental uncertainties arising from the large-R jet, only those coming from the jet energy scale and resolution are considered.

Figure 18: The signal efficiency on contained W-boson jets for the jet shape-based DNN W-boson tagger as a function of the large-R jet p_T (a) and the average number of interactions per bunch crossing μ (b) in data and simulation. Statistical uncertainties of the signal efficiency measurement in data and simulation are shown as error bars in the top panel. In the bottom panel, the ratio of the measured signal efficiency in data to that estimated in Monte Carlo is shown with statistical uncertainties as error bars on the data points and the sum in quadrature of statistical and systematic uncertainties as a shaded band. When considering experimental uncertainties arising from the large-R jet, only those coming from the jet energy scale and resolution are considered.
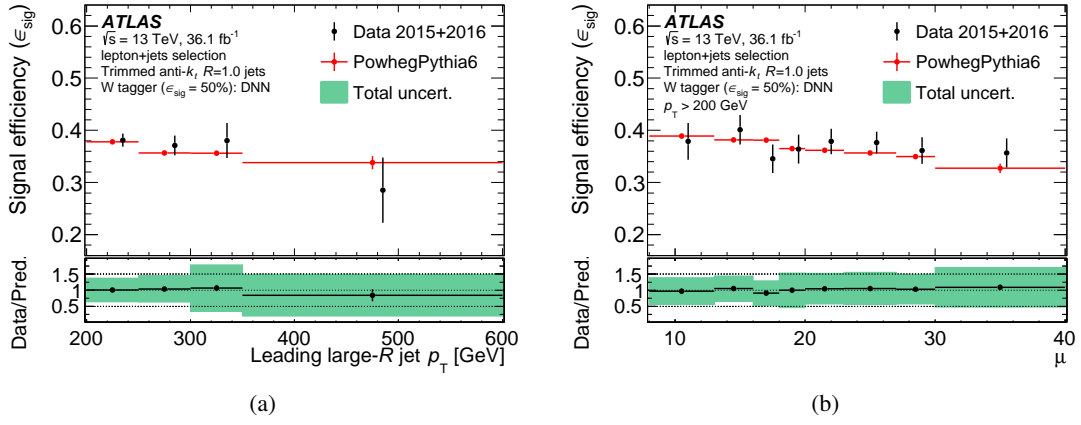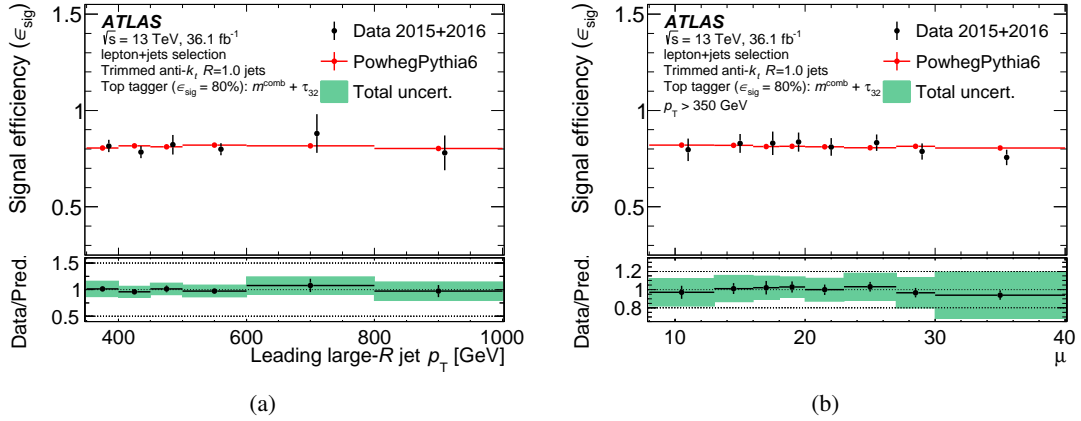

Figure 19: The signal efficiency on contained top-quark jets for the two-variable $m^{\text{comb}} + \tau_{32}$ top-quark tagger as a function of the large-R jet p_T (a) and the average number of interactions per bunch crossing μ (b) in data and simulation. Statistical uncertainties of the signal efficiency measurement in data and simulation are shown as error bars in the top panel. In the bottom panel, the ratio of the measured signal efficiency in data to that estimated in Monte Carlo is shown with statistical uncertainties as error bars on the data points and the sum in quadratre of statistical and systematic uncertainties as a shaded band. When considering experimental uncertainties arising from the large-R jet, only those coming from the jet energy scale and resolution are considered.

Figure 20: The signal efficiency on contained top-quark jets for the jet shape-based DNN top-quark tagger as a function of the large-R jet p_T (a) and the average number of interactions per bunch crossing μ (b) in data and simulation. Statistical uncertainties of the signal efficiency measurement in data and simulation are shown as error bars in the top panel. In the bottom panel, the ratio of the measured signal efficiency in data to that estimated in Monte Carlo is shown with statistical uncertainties as error bars on the data points and the sum in quadrature of statistical and systematic uncertainties as a shaded band. When considering experimental uncertainties arising from the large-R jet, only those coming from the jet energy scale and resolution are considered.
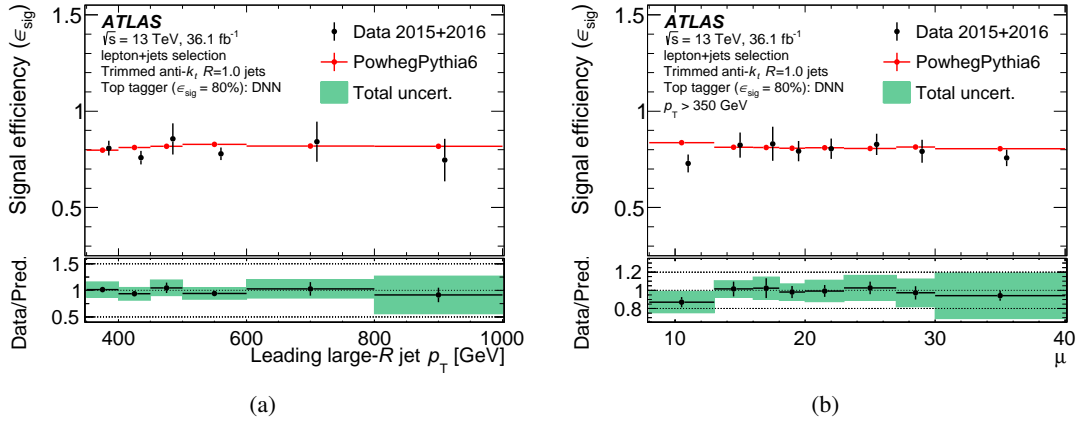

Figure 21: The signal efficiency on contained top-quark jets for the TopoDNN top-quark tagger as a function of the large-R jet p_T (a) and the average number of interactions per bunch crossing μ (b) in data and simulation. Statistical uncertainties of the signal efficiency measurement in data and simulation are shown as error bars in the top panel. In the bottom panel, the ratio of the measured signal efficiency in data to that estimated in Monte Carlo is shown with statistical uncertainties as error bars on the data points and the sum in quadrature of statistical and systematic uncertainties as a shaded band. When considering experimental uncertainties arising from the large-R jet, only those coming from the jet energy scale and resolution are considered.
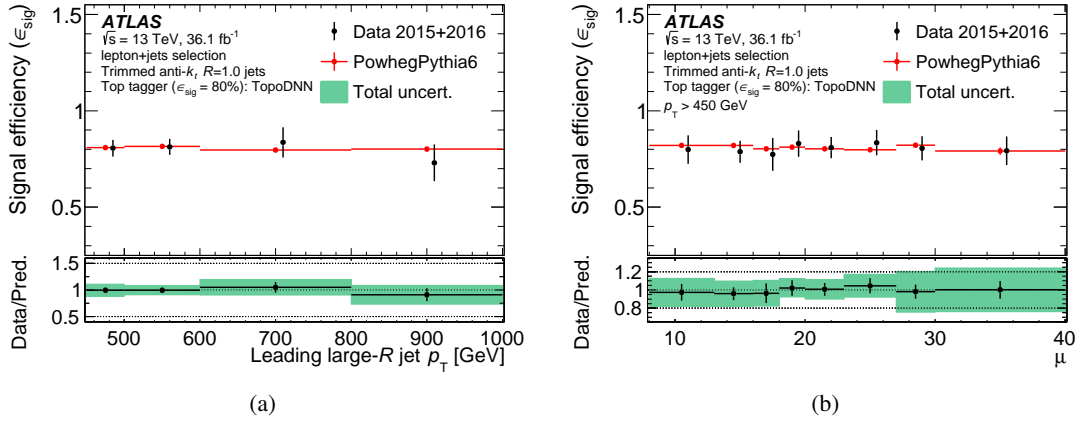
Figure 22: The signal efficiency on contained top-quark jets for the Shower Deconstruction top-quark tagger as a function of the large-R jet p_T (a) and the average interactions per bunch crossing μ (b) in data and simulation. Statistical uncertainties of the signal efficiency measurement in data and simulation are shown as error bars in the top panel. In the bottom panel, the ratio of the measured signal efficiency in data to that estimated in Monte Carlo is shown with statistical uncertainties as error bars on the data points and the sum in quadrature of statistical and systematic uncertainties as a shaded band. When considering experimental uncertainties arising from the large-R jet, only those coming from the jet energy scale and resolution are considered.
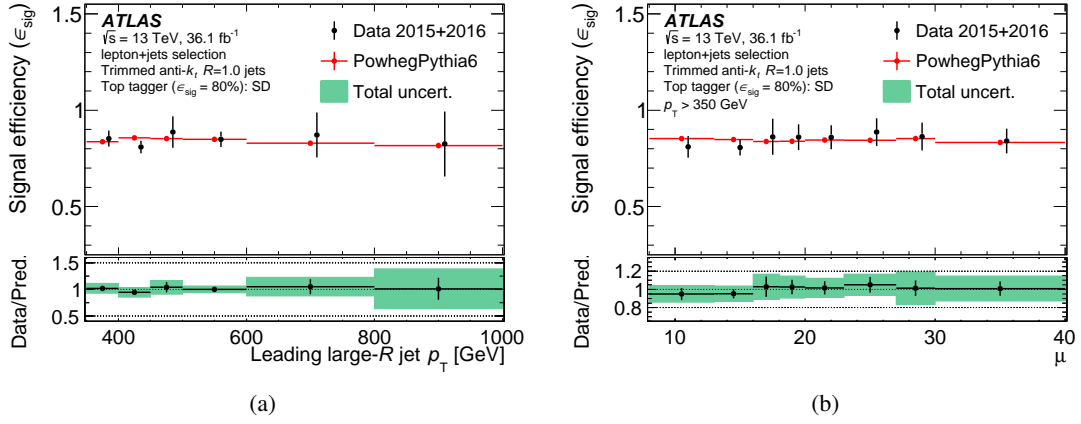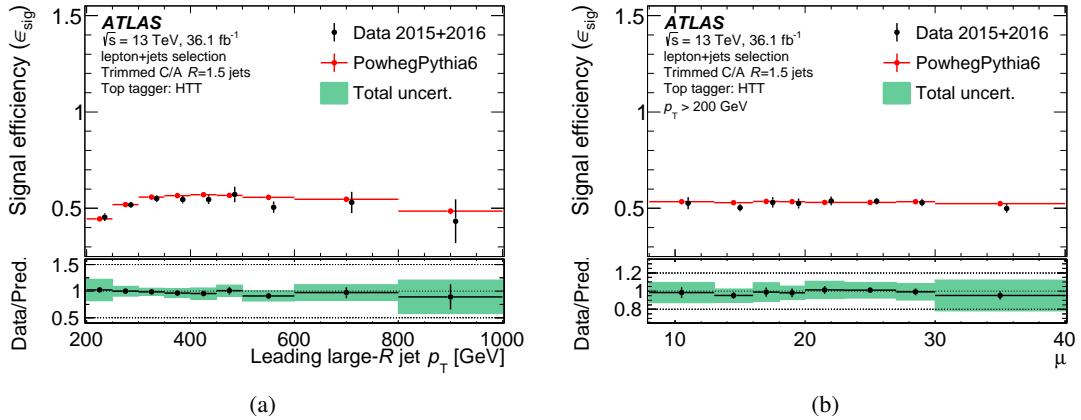

Figure 23: The signal efficiency on contained top-quark jets for the HEPTopTagger top-quark tagger as a function of the large-R jet p_T (a) and the average number of interactions per bunch crossing μ (b) in data and simulation. Statistical uncertainties of the signal efficiency measurement in data and simulation are shown as error bars in the top panel. In the bottom panel, the ratio of the measured signal efficiency in data to that estimated in Monte Carlo is shown with statistical uncertainties as error bars on the data points and the sum in quadrature of statistical and systematic uncertainties as a shaded band. When considering experimental uncertainties arising from the large-R jet, only those coming from the jet energy scale and resolution are considered. The signal efficiency on contained top-quark jets for the HEPTopTagger is not constant with respect to jet p_T as the tagger was not re-optimised after the Run-1 analysis [7].

6.2 Background rejection from multijet and γ + jet events

In addition to studying the modelling of signal W-boson and top-quark jets using a sample of $t\bar{t}$ events, the behaviour of background light jets is studied in two sets of events (enriched in multijet and γ + jet processes) to cover a broad kinematic range and probe the behaviour of quark- and gluon-enriched regions of phase space separately [90]. The first sample, multijet events, provides a means to study a mixture of light-quark and gluon jets in the kinematic range from p_T of approximately 450 GeV to 3000 GeV while the γ + jet sample is greatly enhanced in the fraction of quark jets produced and provides a means to study jets with p_T from $\sim$ 200 GeV to 2000 GeV. As in the case of the study of signal W-boson and top-quark jets in Section 6.1, the distributions of important tagging observables are examined and the background rejection is quantified in both data and Monte Carlo simulation.

6.2.1 Analysis and selection

To select the multijet sample, events are selected in both data and Monte Carlo simulation using a single-jet trigger based on a single large-R anti-k_t trimmed jet with $R = 1.0$ with an online requirement of E_T > 360 GeV during 2015 data taking and 420 GeV in 2016. Events are then required to have at least one fully-calibrated large-R anti-k_t trimmed jet with radius 1.0 with p_T > 450 GeV so that the trigger is fully efficient. After this selection, the modelling of the highest-p_T large-R jet (both anti-k_t R =1.0 trimmed and C/A R = 1.5) in the event is examined with respect to both the PYTHIA and HERWIG++ generators described in Section 3.

In the case of the γ + jet sample, events are selected in both data and Monte Carlo simulation with a single-photon trigger which selects photons satisfying "loose" quality criteria and which pass an online requirement of E_T > 120 GeV in 2015 and 140 GeV in 2016. Photon candidates are required to be within $|\eta|$ < 2.5 and satisfy a likelihood-based identification criterion based on shower shape observables in the electromagnetic calorimeter as well as the relative amount of energy in the hadronic and electromagnetic calorimeters, and are required to be isolated from other activity in the event. Both the identification and isolation criteria are required to satisfy the "tight" working point described in Ref. [91]. In addition, large-R jets are required to have p_T > 200 GeV, $|\eta|$ < 2.0 and to be well-separated from the reconstructed photon with $\Delta\phi(\text{jet}, \gamma) > \frac{\pi}{2}$. Finally, events with at least one photon with E_T > 155 GeV are selected to ensure that the trigger is fully efficient.

In both selections, the normalisation of the simulated multijet and γ + jet predictions is derived directly from data after the initial inclusive selection, taking into account the small contribution from hadronically decaying W-boson, Z-boson and $t\bar{t}$ events. First the predicted contribution from processes containing real hadronically decaying W bosons and top quarks is subtracted from data. The remaining Monte Carlo samples are then normalised to reproduce the same yield as the background-subtracted data.

Figures 24 and 25 show a comparison of the distributions of the leading anti-k_t R =1.0 and C/A R =1.5 jet mass in the inclusive multijet and γ + jet selections. In addition, the primary tagging observables used to perform W-boson and top-quark tagging described in Section 4 are shown in Figures 26–30. In general, the modelling of the shape of the tagging discriminants in data by the Monte Carlo simulation agrees at the 20% level, with non-negligible differences observed when comparing PYTHIA8 to HERWIG Monte Carlo predictions. Finally, the jet mass distribution for jets that are positively tagged using the jet-shape-based DNN discriminant optimised in Section 5.2 is shown in Figures 31 and 32 for the multijet and γ + jet topologies. Good agreement between data and Monte Carlo simulation is observed within uncertainties,

which are dominated by Monte Carlo modelling. It is further observed that the jet mass distribution is strongly distorted after the application of the tagger, a feature which is shared by all tagging techniques described in Section 4.

Figure 24: A comparison of the observed data and predicted MC distributions of the mass of the leading p_T anti-k_t trimmed jet in events for the multijet (a) and γ + jet (b) selections. The data-driven normalisation correction, described in Section 6.2.1, is shown in the legend beside the specific sample to which it applies. Systematic uncertainties are indicated as a band in the lower panel and include all experimental uncertainties related to the selection of events, as well as the reconstruction and calibration of the large-R jet.
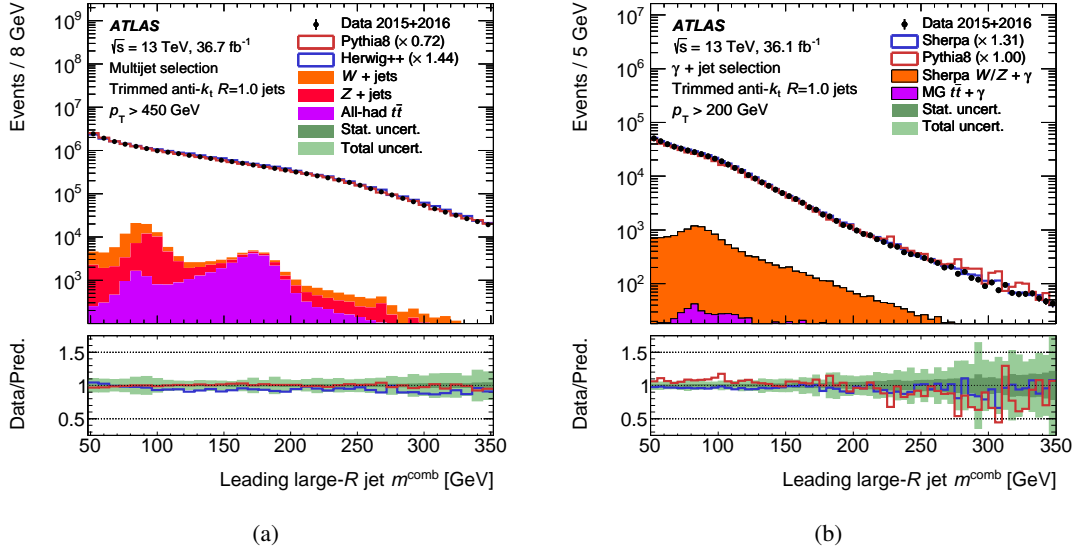
Figure 25: A comparison of the observed data and predicted MC distributions of the mass of the leading p_T C/A R =1.5 trimmed jet in events for the multijet (a) and γ + jet (b) selections. The data-driven normalisation correction, described in Section 6.2.1, is shown in the legend beside the specific sample to which it applies. Systematic uncertainties are indicated as a band in the lower panel and include all experimental uncertainties related to the selection of events, as well as the reconstruction and calibration of the large-R jet.

Figure 26: A comparison of the observed data and MC predictions in the multijet and γ + jet event samples for the anti-k_t R = 1.0 trimmed jet D_2 (a)(c) and τ_{32} (b)(d) spectra. The data-driven normalisation correction, described in Section 6.2.1, is shown in the legend beside the specific sample to which it applies. Systematic uncertainties are indicated as a band in the lower panel and include all experimental uncertainties related to the selection of events, as well as the reconstruction and calibration of the large-R jet.
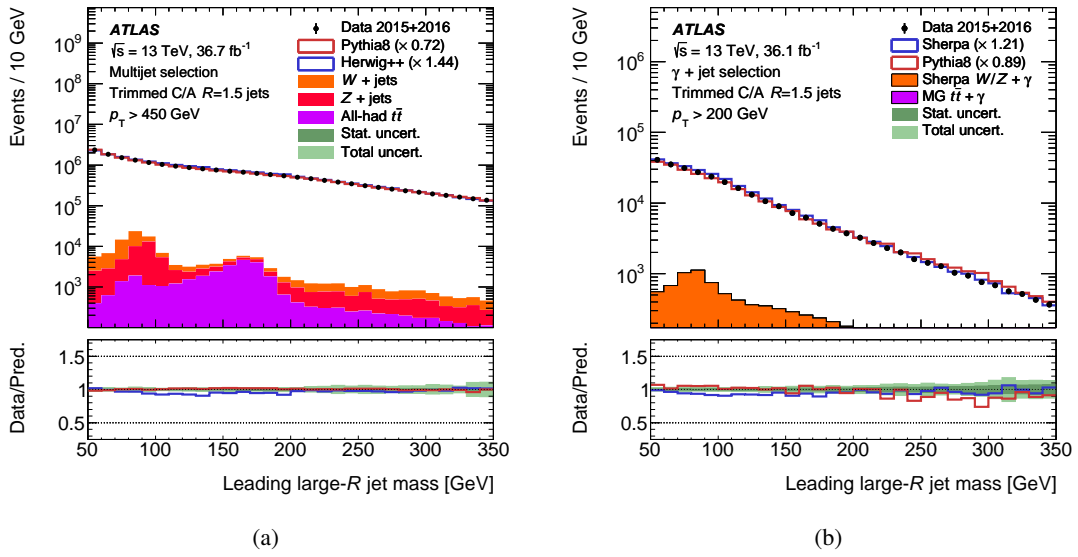
Figure 27: A comparison of the observed data and MC predictions in the multijet and γ + jet event samples for the anti-k_t R =1.0 trimmed jet spectra of the W-boson (a)(c) and top-quark (b)(d) DNN discriminants. The data-driven normalisation correction, described in Section 6.2.1, is shown in the legend beside the specific sample to which it applies. Systematic uncertainties are indicated as a band in the lower panel and include all experimental uncertainties related to the selection of events, as well as the reconstruction and calibration of the large-R jet.
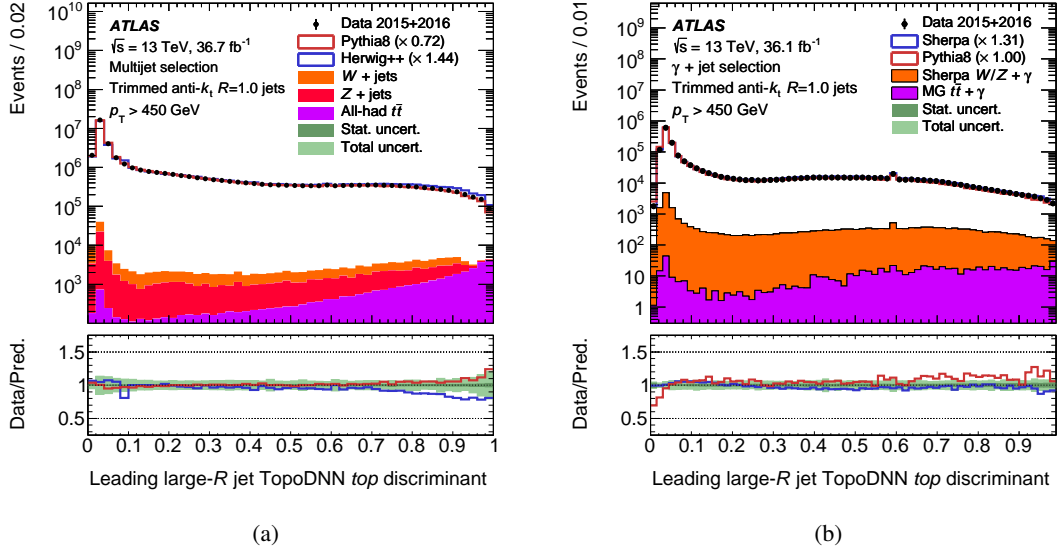
Figure 28: A comparison of the observed data and MC predictions in the multijet (a) and γ + jet (b) event samples for the anti-k_t R =1.0 trimmed jet spectra of the TopoDNN top tagger discriminant. The data-driven normalisation correction, described in Section 6.2.1, is shown in the legend beside the specific sample to which it applies. Systematic uncertainties are indicated as a band in the lower panel and include all experimental uncertainties related to the selection of events, as well as the reconstruction and calibration of the large-R jet.
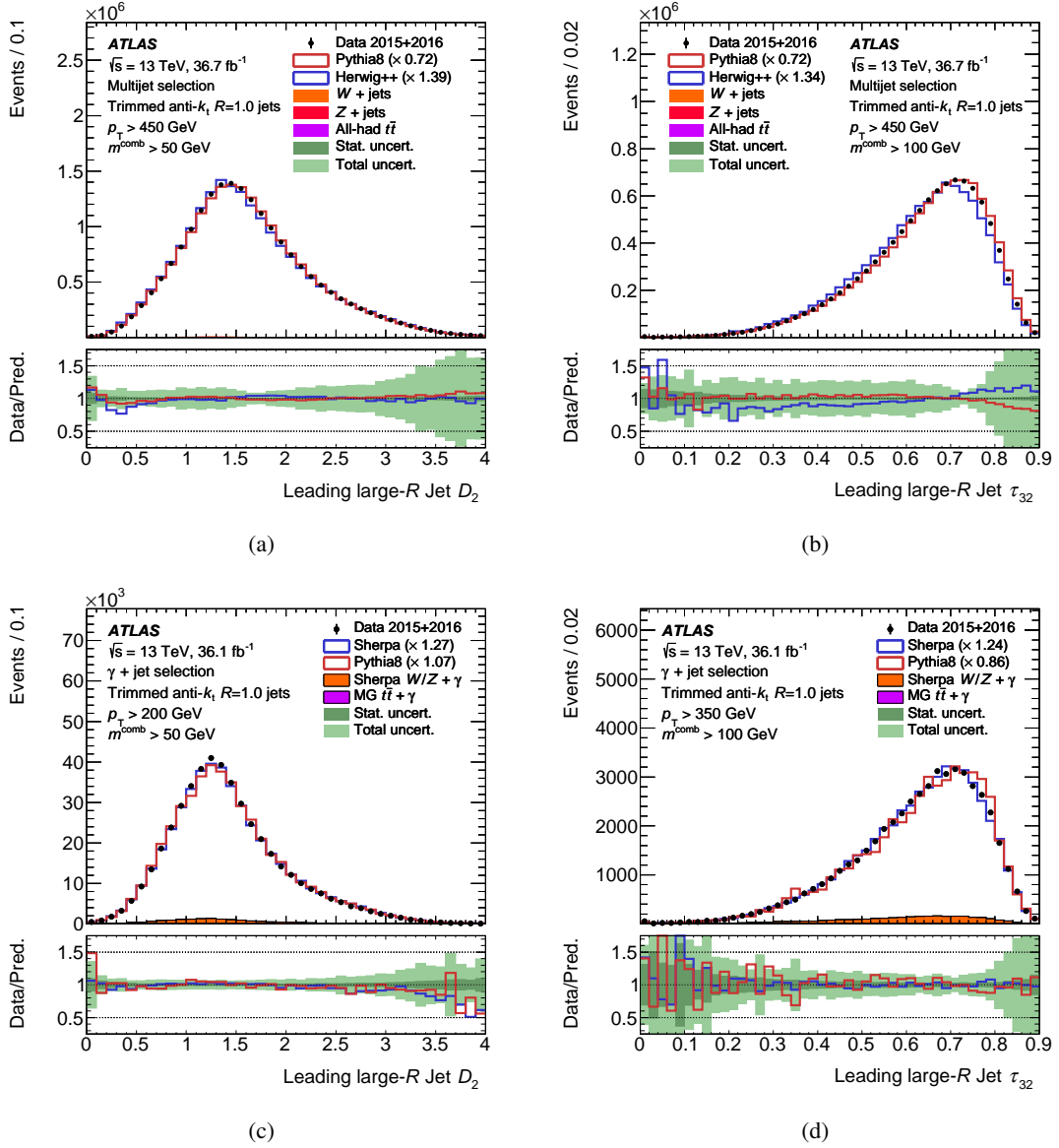

Figure 29: A comparison of the observed data and MC predictions in the multijet (a) and γ + jet (b) event samples for the anti-k_t R =1.0 trimmed jet spectra of the log χ shower deconstruction discriminant. The data-driven normalisation correction, described in Section 6.2.1, is shown in the legend beside the specific sample to which it applies. Systematic uncertainties are indicated as a band in the lower panel and include all experimental uncertainties related to the selection of events, as well as the reconstruction and calibration of the large-R jet.
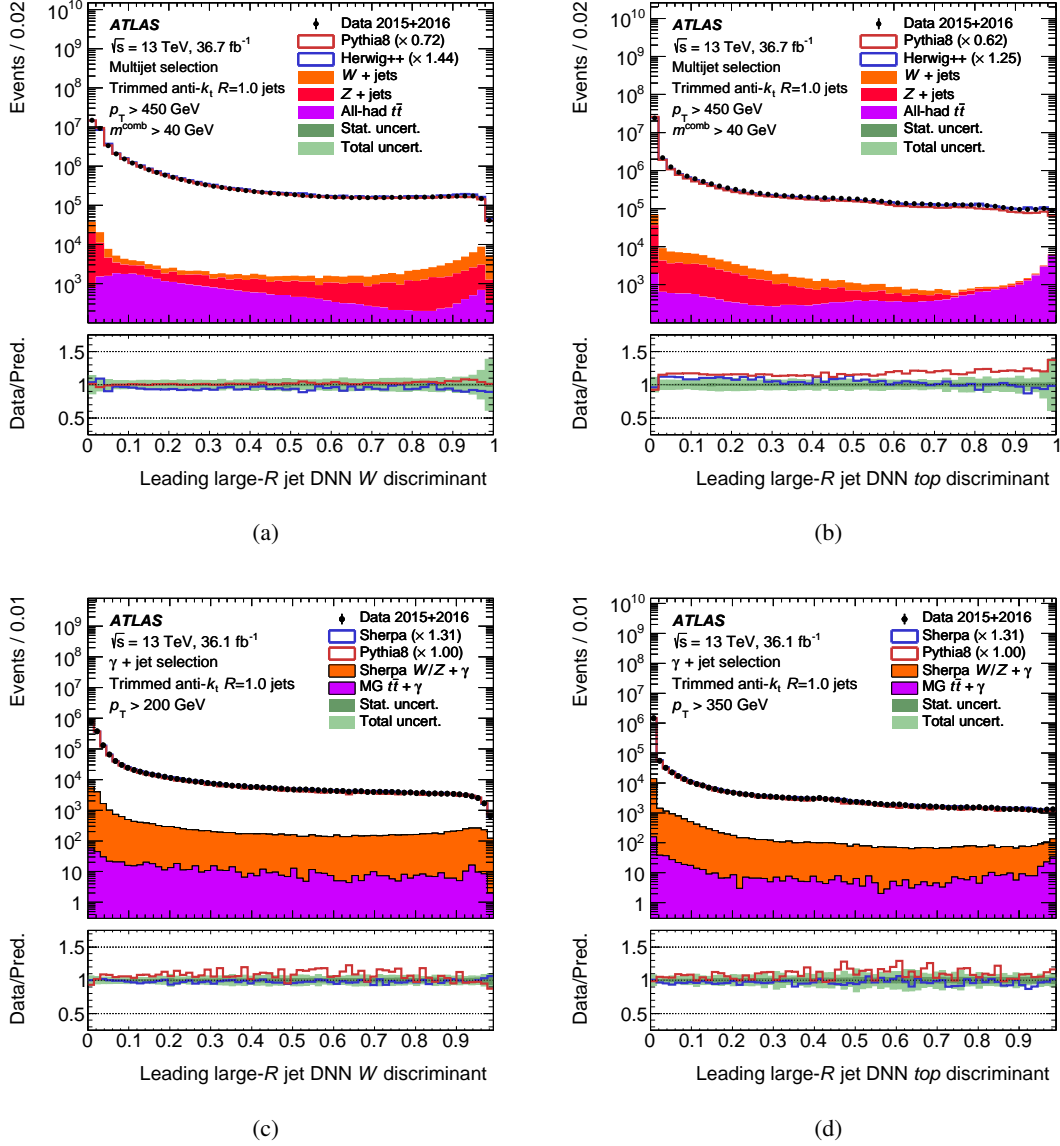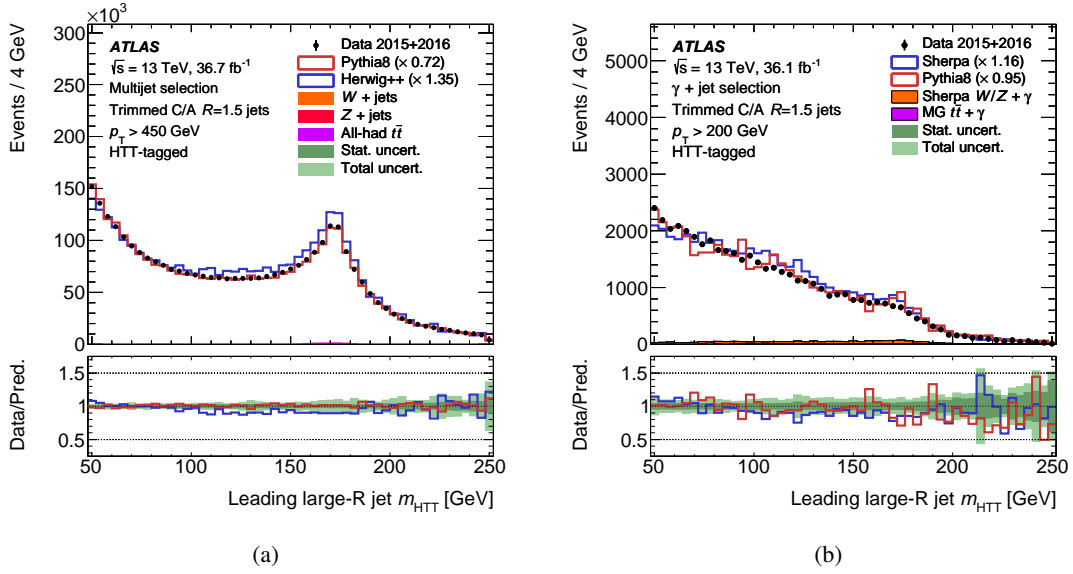
Figure 30: A comparison of the observed data and predicted MC distributions in the multijet (a) and γ + jet (b) event samples for the HEPTopTagger mass. The data-driven normalisation correction, described in Section 6.2.1, is shown in the legend beside the specific sample to which it applies. Systematic uncertainties are indicated as a band in the lower panel and include all experimental uncertainties related to the selection of events, as well as the reconstruction and calibration of the large-R jet. The difference in the shape of the HEPTopTagger mass distribution between the multijet and the γ + jet selections, in particular the absence of a pronounced top-mass peak in the γ + jet selection, is caused by the difference in the jet p_T thresholds.
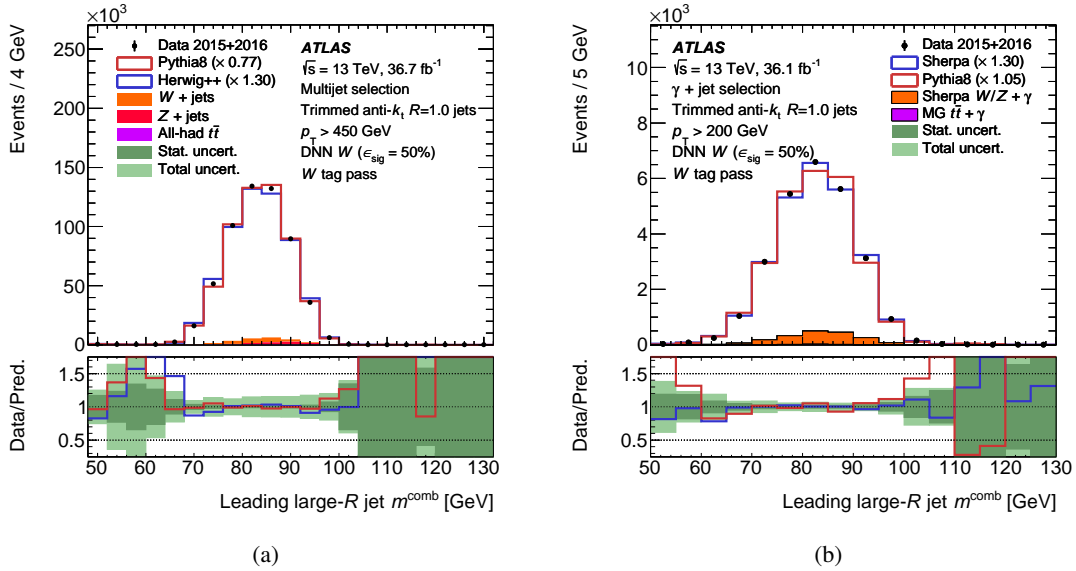
Figure 31: A comparison of the observed data and predicted MC distributions of the anti-k_t R =1.0 trimmed jet m^{comb} observable for events from the multijet (a) or γ + jet (b) selections that pass the selection on the jet-shape-based W-boson DNN tagger. The data-driven normalisation correction, described in Section 6.2.1, is shown in the legend beside the specific sample to which it applies. Systematic uncertainties are indicated as a band in the lower panel and include all experimental uncertainties related to the selection of events, as well as the reconstruction and calibration of the large-R jet.
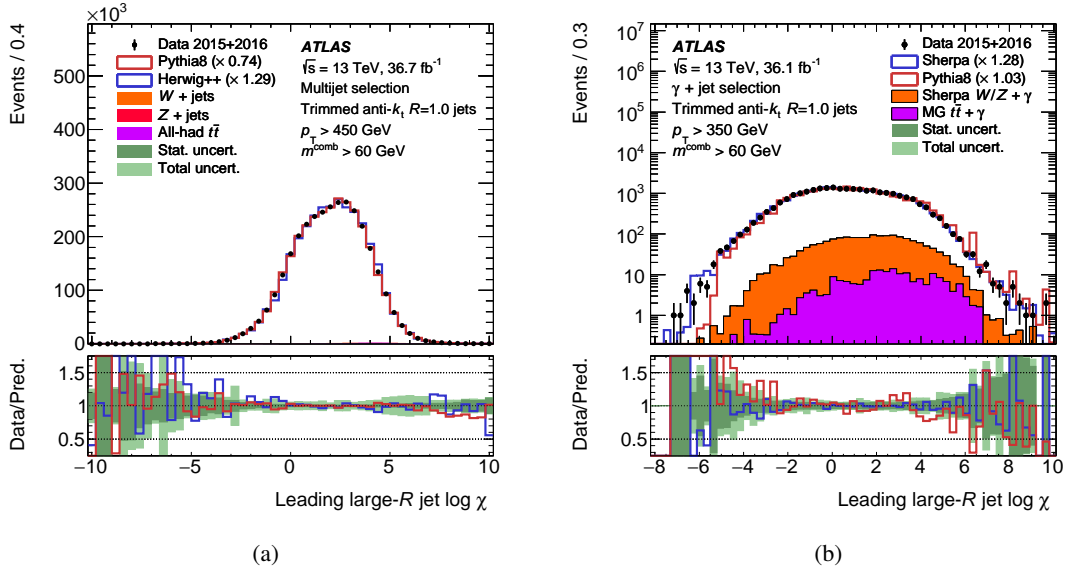
(a)

(b)
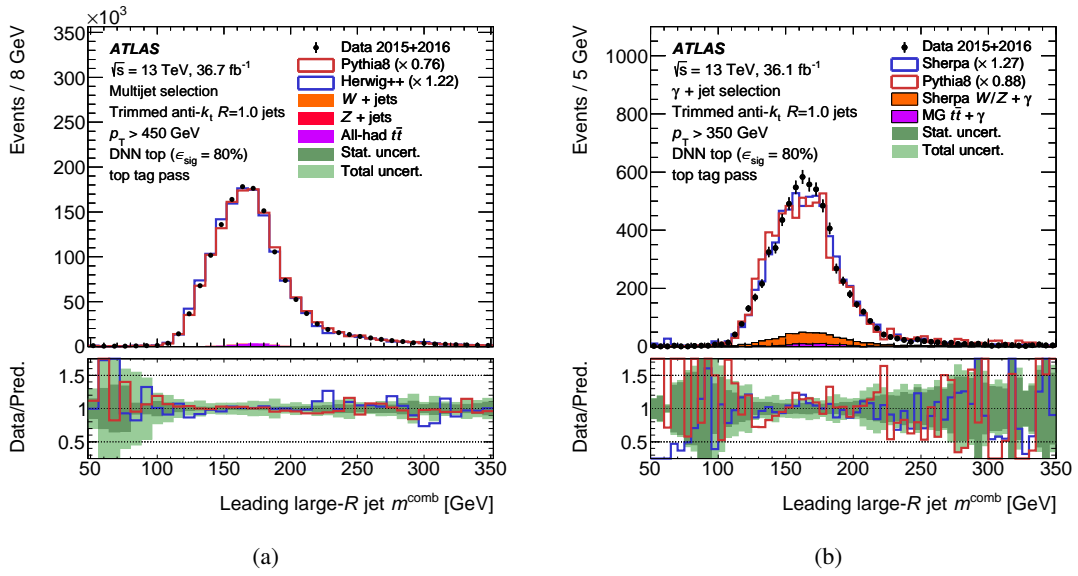
Figure 32: A comparison of the observed data and predicted MC distributions of the anti-k_t R =1.0 trimmed jet m^{comb} observable for events from the multijet (a) or γ + jet (b) selections that pass the selection on the jet-shape-based top quark DNN tagger. The data-driven normalisation correction, described in Section 6.2.1, is shown in the legend beside the specific sample to which it applies. Systematic uncertainties are indicated as a band in the lower panel and include all experimental uncertainties related to the selection of events, as well as the reconstruction and calibration of the large-R jet.

6.2.2 Background rejection measurements

In a similar manner to the measurement of the signal efficiency in Section 6.1.2, the background rejection $1/\epsilon_{\mathrm{bkg}}$ is measured for the W-boson and top-quark tagging working points described in Section 6.1.2. This measurement is performed in both the multijet and $\gamma + $ jet topologies as a function of the transverse momentum of the highest-p_{T} jet in the event, taken to be the leading jet studied in Section 6.2.1, as well as μ.

The approach in this measurement is simpler than the chi-square fit approach used in Section 6.1.2 due to the purity of these samples. In particular, after subtracting the signal contamination from data and performing the normalisation of the multijet and $\gamma + $ jet samples in the inclusive selection described in Section 6.2.1, the background efficiency is calculated directly as the fraction of events that satisfy the full set of tagging criteria in data and in Monte Carlo simulation. The results are shown in Figures 33–39, for the full set of tagging techniques. In the case of W-boson tagging (Figures 33 and 34), the dependence of the background rejection on jet p_{T} arises from the requirement of a fixed signal efficiency. At low jet p_{T}, there is a non-negligible fraction of signal W-boson jets which are not sufficiently collimated, thereby requiring a broad jet-mass selection to obtain the required 50% signal efficiency. As the jet p_{T} increases, the sample of signal jets becomes better contained within a radius of 1.0, thereby allowing a stricter mass requirement, and the background rejection increases. However, the W-boson signal jets become fully contained at $p_{\mathrm{T}} \sim 800$ GeV, and with increasing jet p_{T} the experimental resolution worsens and the Sudakov peak of the light-jet mass migrates into the signal region, thereby leading to a degradation of the background rejection.

Good agreement is generally observed between the predicted and measured rejections. For the multijet topology, the PYTHIA8 prediction of the background rejection describes the observed one, while the HERWIG++ prediction is lower than the rejection in data. Although the rejections for the two topologies are similar, there are relatively large uncertainties at higher jet p_{T}, with clear differences observed between the generators examined for the dominant samples in each topology. In particular, in the case of W-boson tagging, it is observed that these generator differences are larger for the more complex jet-shape DNN tagger, shown in Figure 34, than for the cut-based tagger, shown in Figure 33. In the case of top-quark tagging, the same trend can be seen: a more algorithmically involved classifier, namely the TopoDNN tagger, shown in Figure 37, shows larger differences between generators than the jet-shape DNN tagger, shown in Figure 36. In the case of top-quark tagging, in addition to the trend between the jet-shape DNN and cut-based taggers, a similar trend can be seen in which a more algorithmically involved classifier, namely the TopoDNN tagger, shown in Figure 37, shows larger differences between generators than the jet-shape DNN tagger, shown in Figure 36.

When examining the background rejection with respect to μ, in the case of W-boson tagging, a trend of increasing background rejection for higher μ exists. This is observed in both the multijet and $\gamma + $ jet topologies and found to be the same size for both the $m^{\mathrm{comb}} + D_2$ W-boson tagger and the jet shape-based DNN W-boson tagger. In the case of top-quark tagging, the $m^{\mathrm{comb}} + \tau_{32}$ top-quark tagger, the jet shape-based DNN top-quark tagger, and the TopoDNN tagger show no clear trend as a function of pile-up, likely due to the high-p_{T} regime selected by the top-quark taggers. However, the Shower Deconstruction top-quark tagger shows minor trends with the background rejection decreasing as the level of pile-up increases. The background rejection of the HEPTopTagger shows little dependence on μ. In all cases, this trend is well-described by the Monte Carlo simulation.

Figure 33: The estimated light-jet rejection $1/\epsilon_{\mathrm{bkg}}$ as a function of the leading jet p_{T} and the average number of interactions per bunch crossing μ for the two-variable W-boson tagger in the multijet (a) (c) and γ + jet (b) (d) selection.

Figure 34: The estimated light-jet rejection $1/\epsilon_{\mathrm{bkg}}$ as a function of the leading jet p_{T} and the average number of interactions per bunch crossing μ for the DNN W-boson tagger in the multijet (a) (c) and γ + jet (b) (d) selection.

Figure 35: The estimated light-jet rejection $1/\epsilon_{\mathrm{bkg}}$ as a function of the leading jet p_{T} and the average number of interactions per bunch crossing μ for the two-variable top-quark tagger in the multijet (a) (c) and γ + jet (b) (d) selection.

Figure 36: The estimated light-jet rejection $1/\epsilon_{bkg}$ as a function of the leading jet p_T and the average number of interactions per bunch crossing μ for the DNN top-quark tagger in the multijet (a) (c) and γ + jet (b) (d) selection.

Figure 37: The estimated light-jet rejection $1/\epsilon_{\text{bkg}}$ as a function of the leading jet p_{T} and the average number of interactions per bunch crossing μ for the TopoDNN top-quark tagger in the multijet (a) (c) and γ + jet (b) (d) selection.

Figure 38: The estimated light-jet rejection $1/\epsilon_{bkg}$ as a function of the leading jet p_T and the average number of interactions per bunch crossing μ for the shower deconstruction top-quark tagger in the multijet (a) (c) and $\gamma + \text{jet}$ (b) (d) selection.
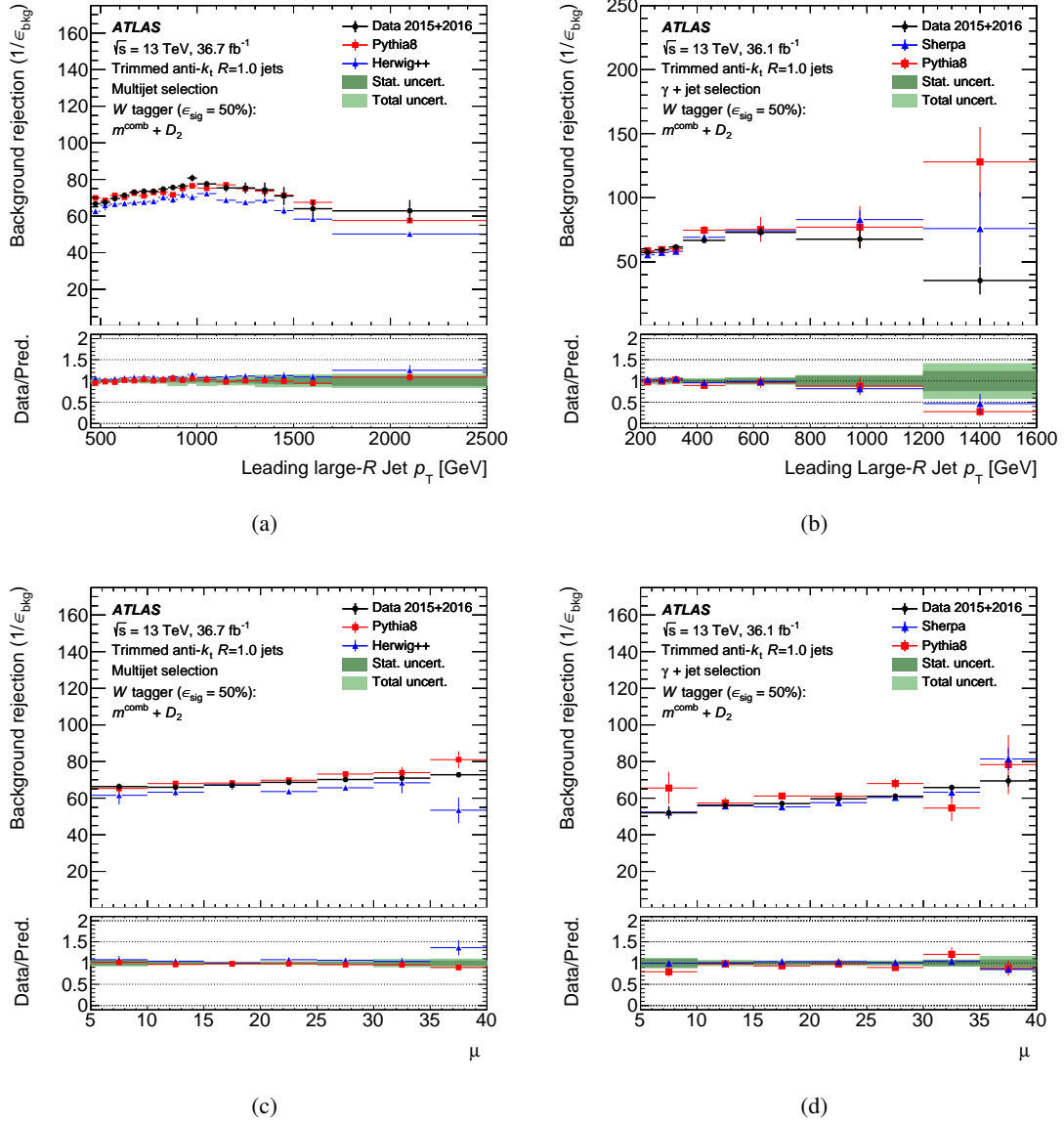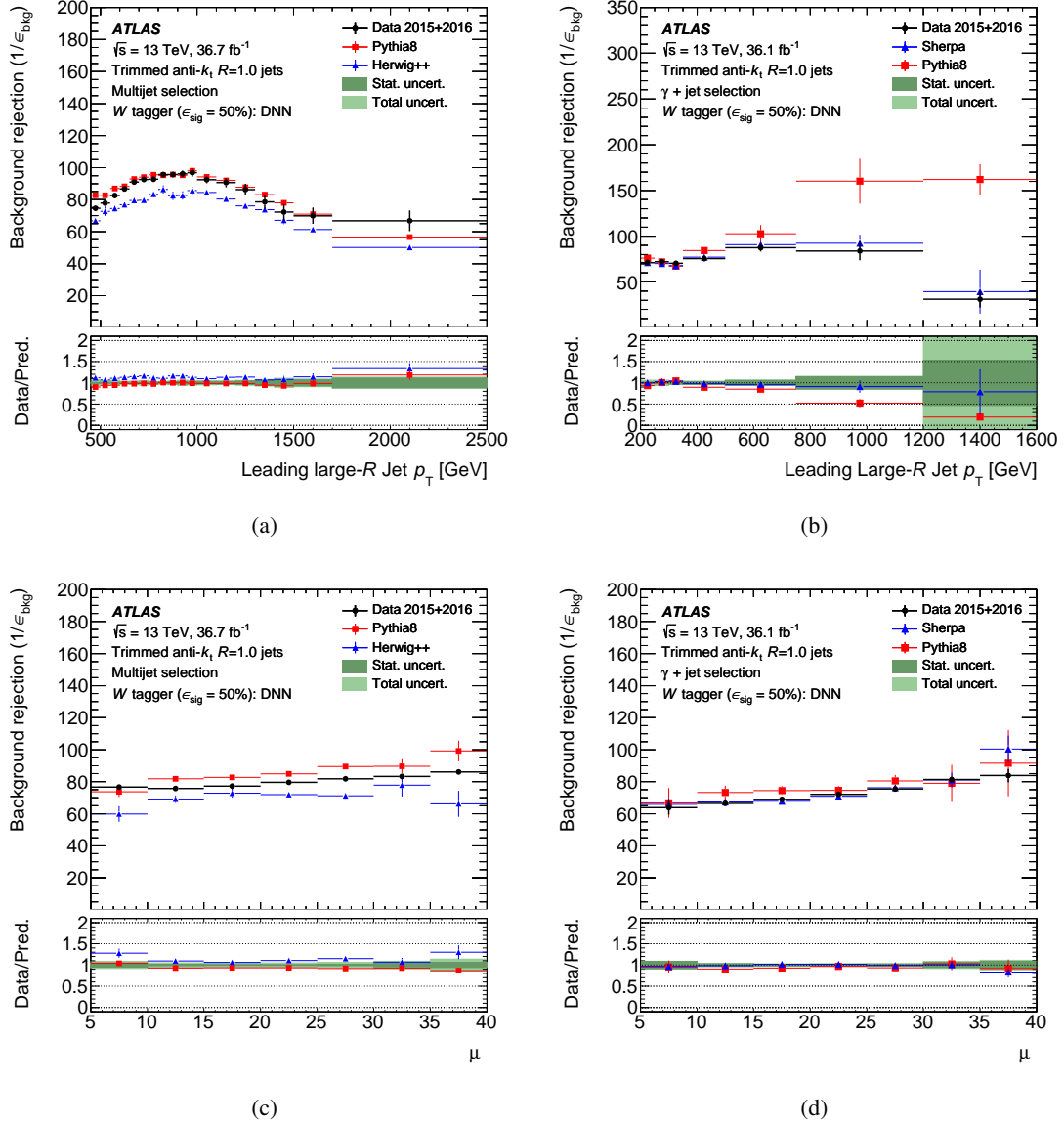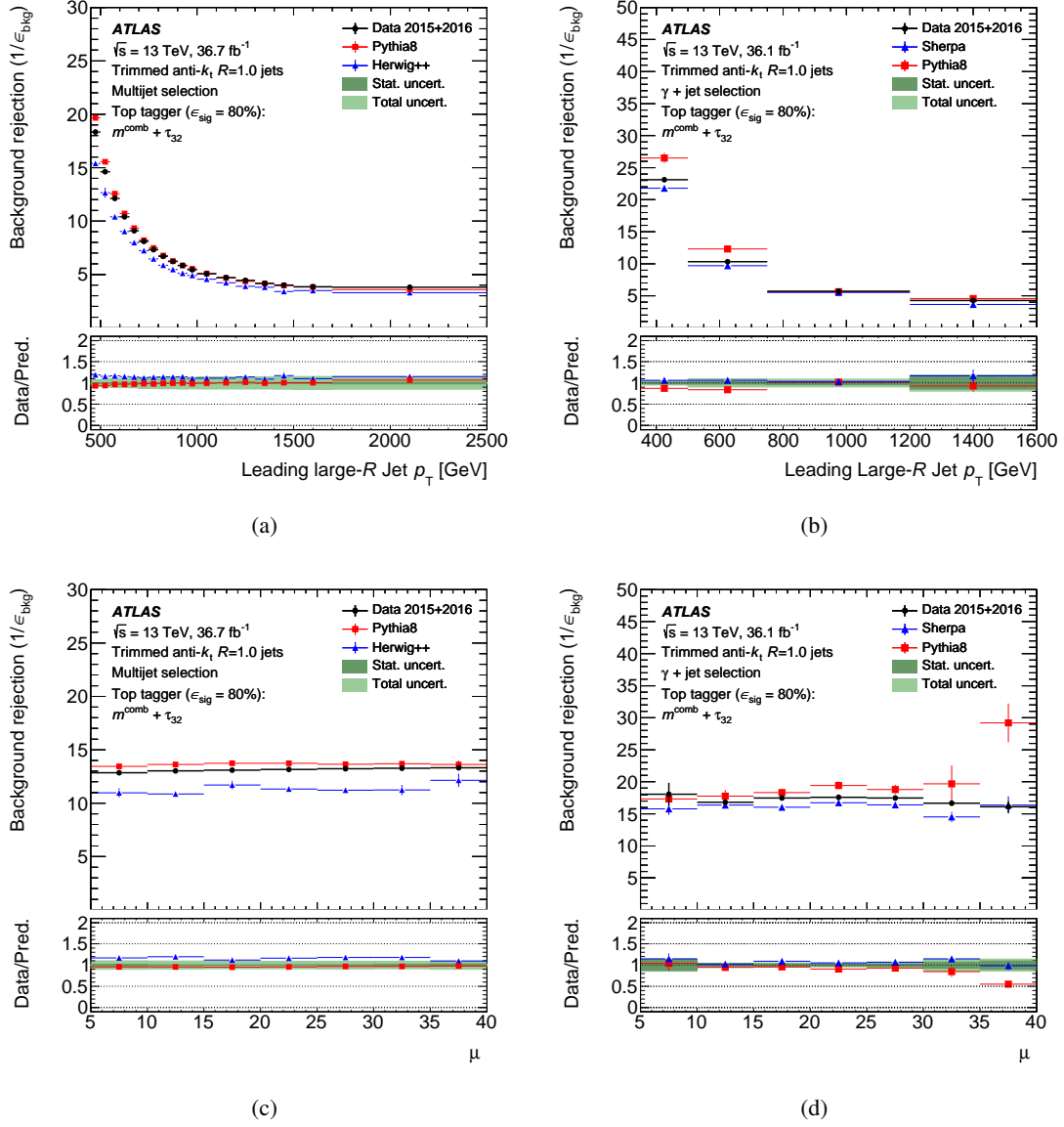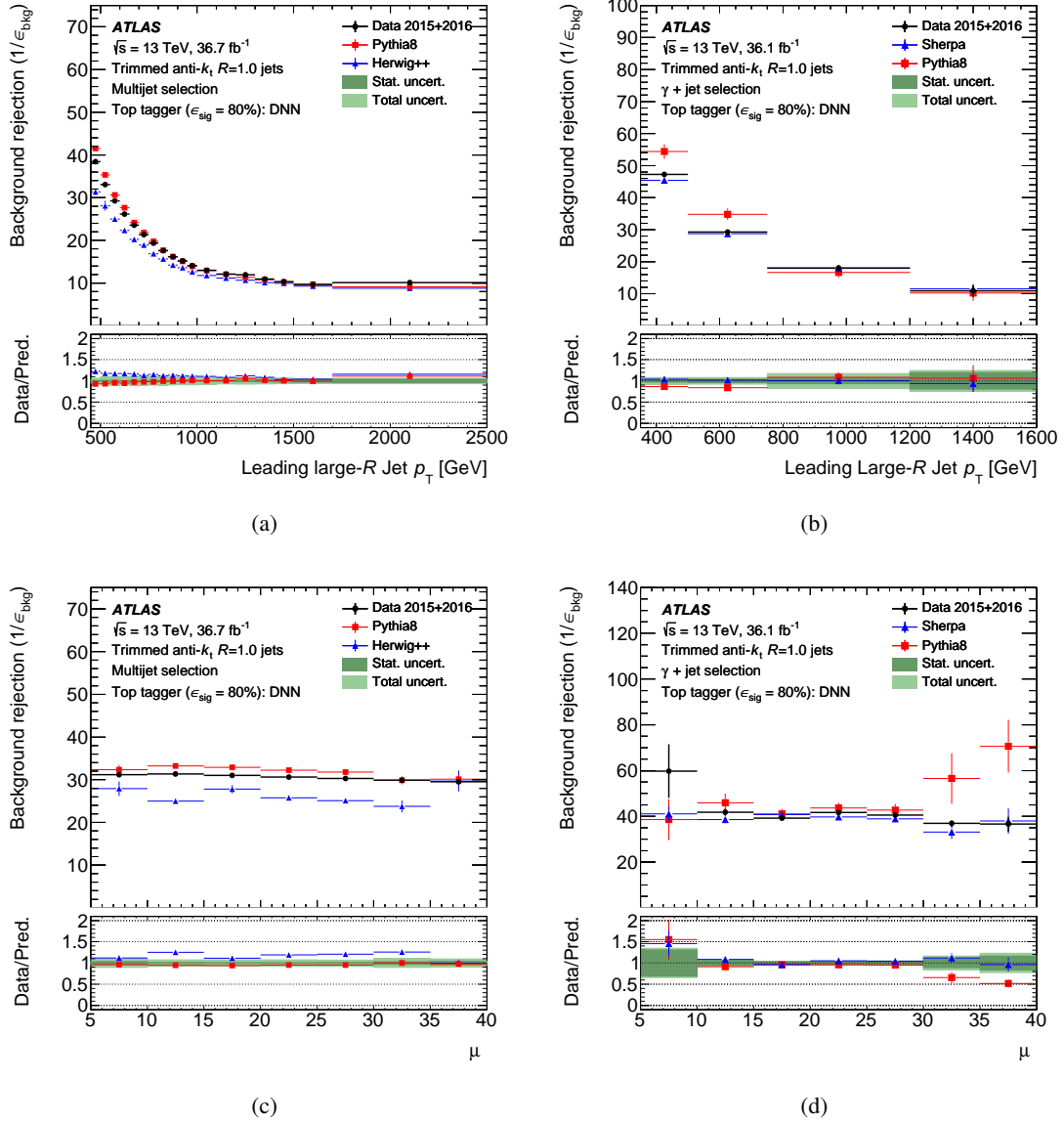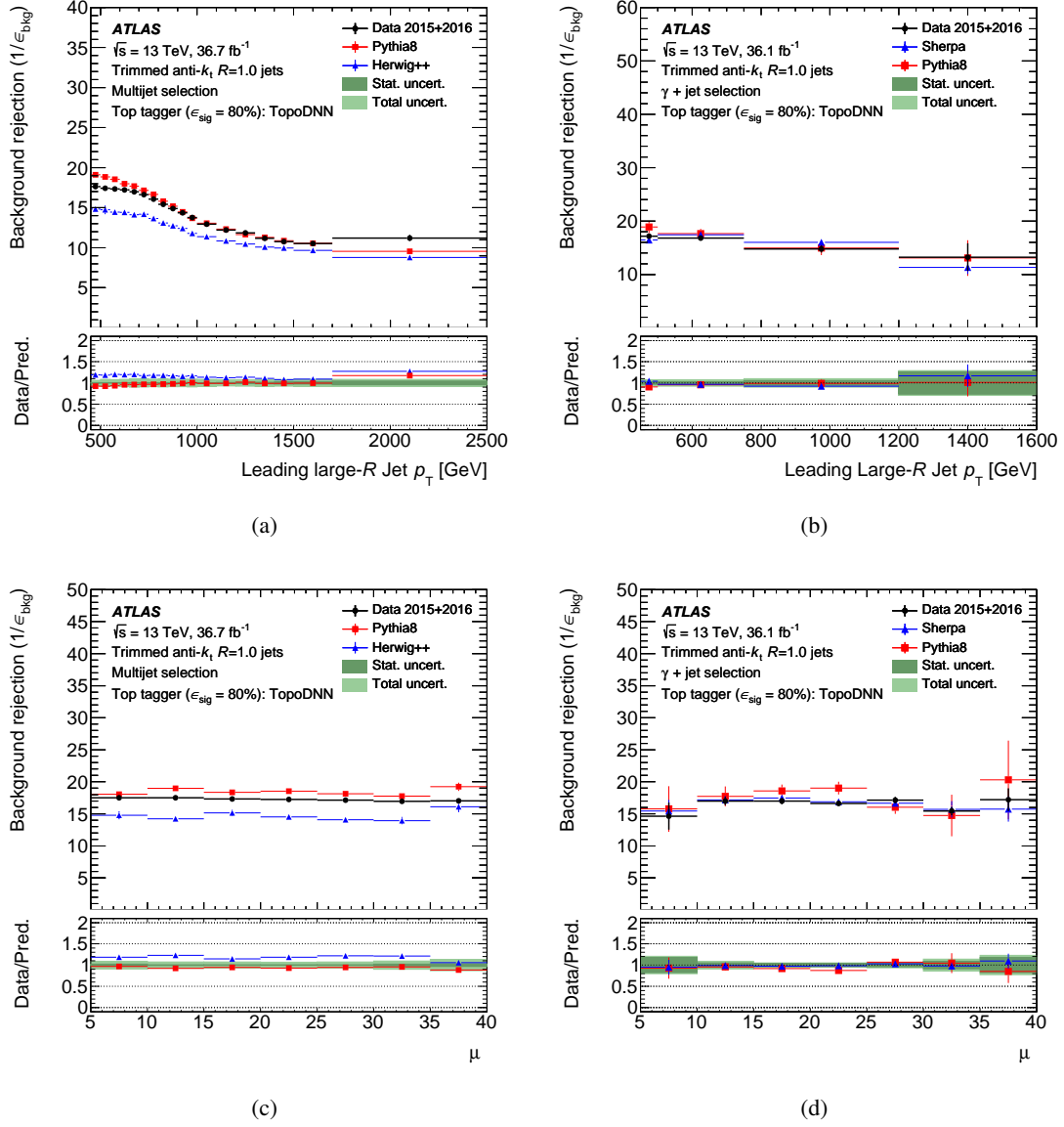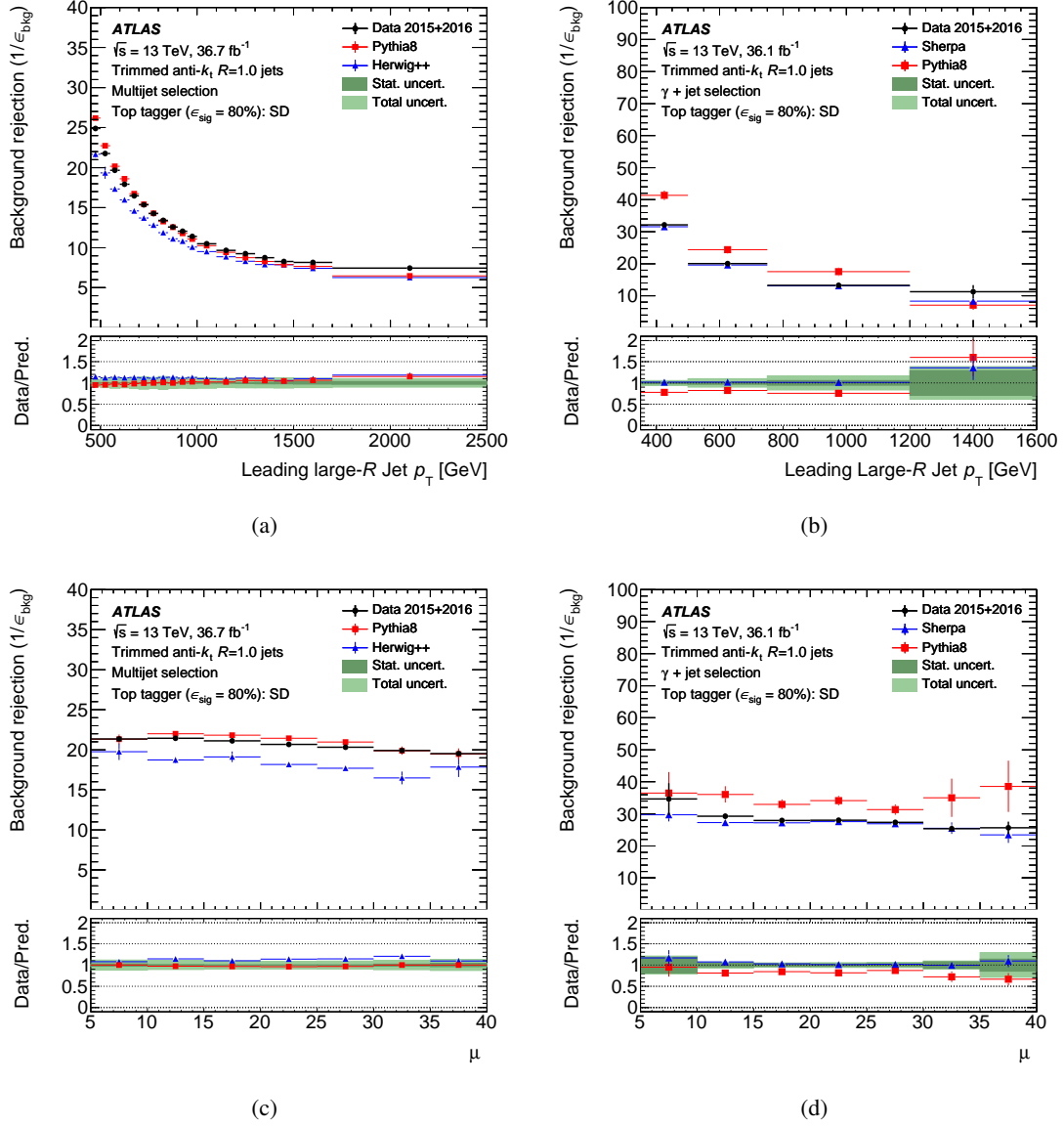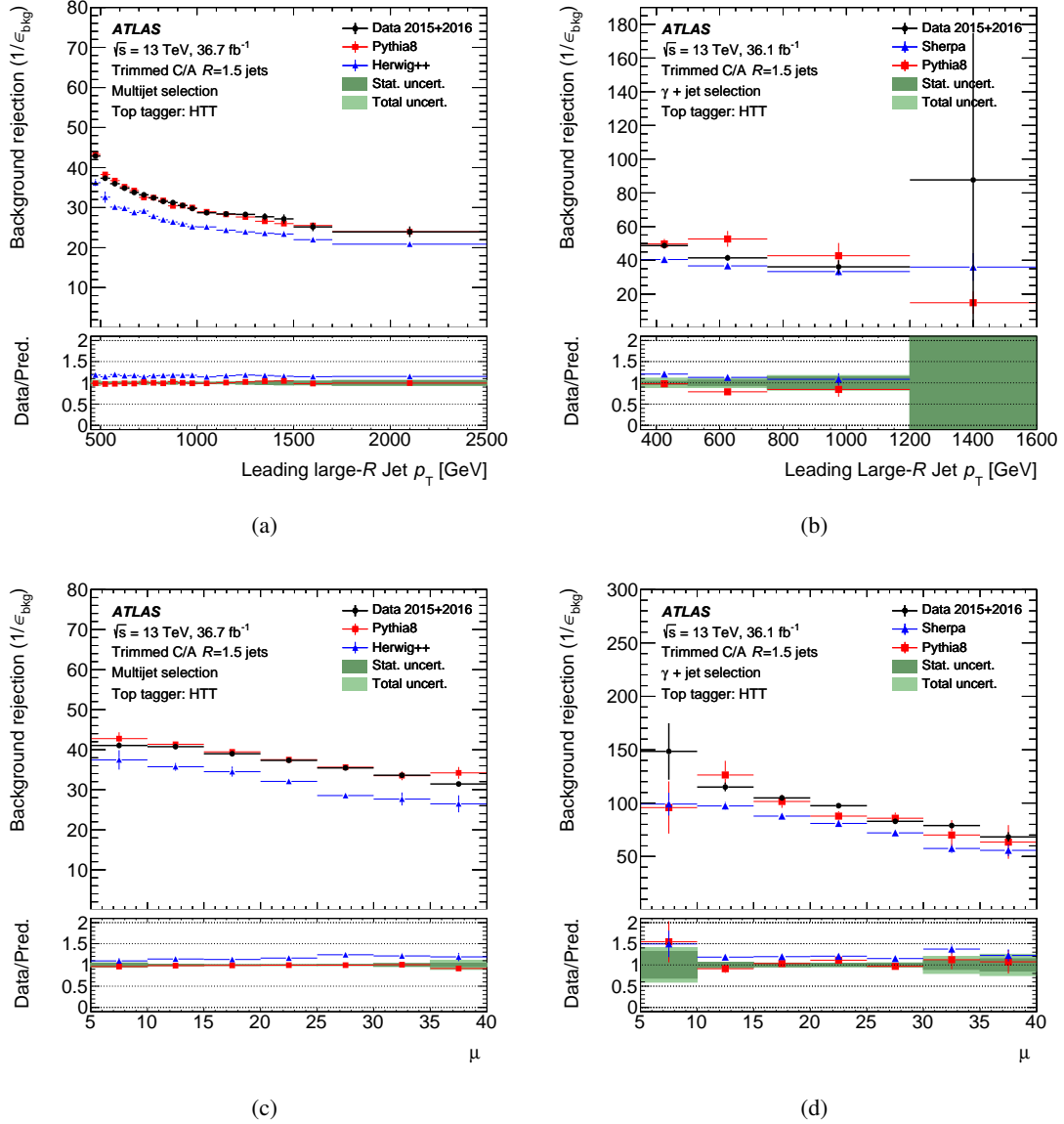
Figure 39: The estimated light-jet rejection $1/\epsilon_{bkg}$ as a function of the leading jet p_T and the average number of interactions per bunch crossing μ for the HEPTopTagger in the multijet (a) (c) and γ + jet (b) (d) selection.

6.3 Systematic uncertainties

A number of sources of systematic uncertainty enter into the evaluation of the modelling of data by the Monte Carlo simulation. These uncertainties derive both from theoretical assumptions within the Monte Carlo predictions and from the reconstruction and calibration of the detector response to the physics objects and therefore affect the three topologies to varying degrees. These sources of uncertainty, their effect in this analysis, and the manner in which they are estimated are summarised in Tables 3 and 4. Systematic uncertainties are propagated to the signal efficiency measurement by repeating the fit for varied templates that correspond to each systematic uncertainty source and comparing the extracted efficiency for the varied and nominal templates.

From this set of uncertainties, those originating from the measurement of leptons, photons, anti-k_t $R = 0.4$ calorimeter jets, and the $E_{\mathrm{T}}^{\mathrm{miss}}$ soft term are found to be negligible in all cases. Additionally, the uncertainty related to the estimation and subsequent subtraction of the multijet background in the $t\bar{t}$ analysis in Section 6.1 and the background with a real hadronic W/Z-boson or top-quark decay in the multijet and γ + jet analysis in Section 6.2 are found to be negligible. The uncertainties due to the application of flavour tagging in the $t\bar{t}$ analysis of signal jets are subdominant and affect the yield results with an impact of the order of 20% in the region of m^{comb} below 100 GeV, with negligible impact on the measurement of the signal efficiency. The uncertainties in both the scale and resolution of the observable of interest (e.g. m^{calo}, D_2 and τ_{32}) are evaluated by comparing the large-R jets formed from calorimeter cell topoclusters to those formed from ID tracks [88]. These sources of uncertainty generally cause small (10%) changes in the yield of events near the most highly populated regions of the distributions of observables but are generally the dominant uncertainties when examining both the tails of these distributions and the regions near m_W and m_{top} in Section 6.1. Likewise, in the case of the HEPTopTagger, the subjet energy scale uncertainty, which itself is based on Run 1 studies, is a dominant source of systematic uncertainty in the shape of the HEPTopTagger mass near m_{top} but this uncertainty does not propagate strongly into the final evaluation of the signal efficiency due to the broad mass window selection described in Section 4.3.4.

The dominant systematic uncertainties of these techniques are those related to the theoretical modelling of the Monte Carlo predictions. In particular, in Section 6.1, the contribution of the uncertainty in the modelling of parton shower and hadronisation is dominant in all cases, leading to variations in the yield of the Monte Carlo when examining the distributions of m^{comb}, D_2, and τ_{32} of up to 30%. In the tails of these distributions, the uncertainty in the modelling of additional radiation in $t\bar{t}$ events yields variations that are comparable in size. The same behaviour can be observed in the study of the modelling of light jets, particularly in Section 6.2.1, where predictions from both Pythia8 and Herwig++ show shape differences ranging up to approximately 25% for certain jet moments as well as for the DNN top tagger. As seen in Sections 6.1.2 and 6.2.2, these uncertainties manifest themselves as large variations in the measured signal efficiency and background rejection. In the case of the tagging efficiency measurement of top quarks in particular, the measured signal efficiency is found to be susceptible to both the truth-level labelling of the top quark and the particular working point chosen for the tagger.

Table 3: Summary of theoretical systematic uncertainties considered in the performance measurements in data.

Source	Affected topologies	Description
Event generator choice	$t\bar{t}$	Hard-scattering modelling uncertainty estimated as the difference between Powheg+Herwig and MC@NLO+Herwig [27].
Showering choice	$t\bar{t}$	Parton shower and hadronisation modelling uncertainty estimated from the difference between Powheg+Pythia6 and Powheg+Herwig [27].
Modelling of extra QCD radiation	$t\bar{t}$	Uncertainty in amount of initial/final-state radiation estimated as the difference between the nominal Powheg+Pythia6 generator and *radLo* and *radHi* tunes of Powheg+Pythia6. The radiation variations include variation of renormalisation and factorisation scales and the h_{damp} parameters [27].
$t\bar{t}$ total cross-section uncertainty	$t\bar{t}$	Uncertainty in normalisation of $t\bar{t}$ MC contribution of magnitude ±5.5% [24]
Single-top total cross-section uncertainty	$t\bar{t}$	Uncertainty in normalisation of single-top MC contribution of magnitude ±5.3% (a conservative estimate enveloping the uncertainties on t-channel, s-channel and Wt-channel)
W +jets total cross-section uncertainty	$t\bar{t}$	Uncertainty in normalisation of W +jets MC contribution of magnitude ±5.0% [92]
W +jets theory scale uncertainties	$t\bar{t}$	Uncertainty arising from the choice of renormalisation and factorisation scale, CKKW matching scale and QSF scale [93]. For the renormalisation and factorisation scale, ×0.5 and ×2 variations are considered and the renormalisation and factorisation scales are varied independently as well as in correlated and anti-correlated ways. The envelope of the variations is considered as the final renormalisation+factorisation scale uncertainty.
Signal normalisation	multijet, γ + jet	The uncertainty in the subtraction of processes containing a hadronically decaying top quark or vector boson, conservatively taken to be 25%.

Table 4: Summary of experimental systematic uncertainties considered in the performance measurements in data.

Source	Affected topologies	Description
anti-k_t R =1.0 trimmed jet moment scale	$t\bar{t}$, multijet, γ + jet	The uncertainty in the scale of the detector response for all jet moments derived by comparing the calorimeter quantity with the reference track jet [6].
anti-k_t R =1.0 trimmed jet moment resolution	$t\bar{t}$, multijet, γ + jet	The uncertainty in the resolution of the detector response conservatively estimated as a 2% absolute uncertainty in p_{T}, a 20% relative uncertainty in jet mass, and a 15% relative uncertainty in all other jet moments [88].
C/A R = 1.5 subjet energy scale	$t\bar{t}$, multijet, γ + jet	The uncertainty in the scale of the detector energy response for subjets used in the HEPTopTagger algorithm conservatively estimated to be 3% based on Run 1 studies [7]
anti-k_t R = 0.4 jet energy scale and resolution	$t\bar{t}$	The uncertainty in the scale and resolution of the detector response for the jet p_{T} derived from simulation and *in situ* calibration measurements [38].
$E_{\mathrm{T}}^{\mathrm{miss}}$ track soft term	$t\bar{t}$	The uncertainty on the component of the $E_{\mathrm{T}}^{\mathrm{miss}}$ calculation due to energy flow that is unassigned to a calibrated physics object, estimated in-situ in Z+jet events [87].
Flavour tagging	$t\bar{t}$	The uncertainty in the scale factor correcting the efficiency response of the detector to identify heavy-flavour b- and c-jets as well as light-flavour jets derived *in situ* using $t\bar{t}$ events [85, 89].
Lepton reconstruction and calibration	$t\bar{t}$	The uncertainty in the scale factor correcting the efficiency to trigger on, reconstruct, and identify leptons as well as uncertainties in their energy and p_{T} scale and resolution [81, 82, 94].
Photon reconstruction and calibration	γ + jet	The uncertainty in the scale factor correcting the efficiency to trigger on, reconstruct, and identify photons [95] as well as uncertainties in their energy scale and resolution [96].
Multijet background normalisation	$t\bar{t}$	The uncertainty in the data-driven prediction of the yield of multijet events, conservatively taken to be 50% based on the estimate in Ref. [2].
Multijet lepton misreconstructin efficiencies	$t\bar{t}$	The statistical uncertainty of the real and fake/non-prompt lepton reconstruction efficiencies estimated in Ref. [2] is propagated through the matrix method.
Luminosity uncetainty	$t\bar{t}$, multijet, γ + jet	A 2.1 % relative uncertainty in the MC yield, based on the luminosity uncertainty of the combined 2015+2016 dataset based on [97].
Pile-up uncertainty	$t\bar{t}$, multijet, γ + jet	Uncertainty in the reweighting of MC pile-up profile to the measured pile-up profile in data based on disagreement between instantaneous luminosity in data and in simulation [97].

7 Conclusion

Various methods to tag boosted, hadronically decaying W bosons and top quarks are studied in data and simulation. A number of techniques, including the use of physically motivated jet moments, shower deconstruction and the HEPTopTagger which were studied in Run 1 are re-optimised for use in LHC Run 2 conditions. Additionally, the multivariate combination of high-level jet moments using boosted decision trees and neural networks as well as the combination of low-level energy flow information in the form of topoclusters using a deep neural network is studied both in data and Monte Carlo simulation. The performance of these techniques is evaluated using Monte Carlo simulation for jets in the p_T range from 500 to 2000 GeV and compared in terms of the central value of the background rejection at fixed signal efficiency. This study indicates that a multivariate combination of information can enhance performance to exceed that of techniques based on more physically motivated individual features across the full jet p_T range for both W-boson and top-quark tagging.

The performance of the various tagging techniques is studied using a sample of 36.1fb^{-1} of 13 TeV proton–proton collision data collected by the ATLAS detector at the LHC in 2015 and 2016. A sample of lepton-plus-jets $t\bar{t}$ events is used to study the signal W-boson and top-quark jet tagging efficiency and compare the predicted efficiency in Monte Carlo simulation to that in data for a set of working points for the tagging strategies from which *in situ* calibrations and systematic uncertainties can be derived. Likewise, background light-jet-enriched event topologies are studied using multijet and γ + jet samples. In general, it is found that the inputs to and the performance of the studied W-boson and top-quark taggers currently in use in physics analyses are well-modelled by Monte Carlo simulations. However, in all studies, it is found that the primary limiting factor in the description of the tagging efficiency by the Monte Carlo prediction derives from the theoretical modelling of the Monte Carlo processes studied, particularly the parton shower and hadronisation model of the $t\bar{t}$ process. Finally, the small pile-up dependence of each tagger working point is characterised to understand the relative susceptibility of each strategy to pile-up contamination within the jet. In general, the signal efficiency is found to be quite robust against increased levels of event pile-up whereas the background rejection shows residual pile-up dependence, particularly in the case of the W taggers. In all cases, however, the dependence is well-described by the Monte Carlo simulation.

Appendix

A BDT & DNN Hyper-parameters

In this section, a description of the tuned hyper-parameters of the BDT and DNN are presented in Tables 5 and 6.

Table 5: Brief description of the BDT parameters and the chosen parameters.

Setting Name	Description	Choice
Software package	Package used for training	TMVA 4.2.1 [98]
BoostType	Type of boosting technique	GradientBoost
NTrees	Number of trees in the forest	500
MaxDepth	Max depth of the decision tree allowed	20
MinimumNodeSize	Minimum fraction of training events required in a leaf node	1.0%
Shrinkage	Learning rate for GradientBoost algorithm	0.5
UseBaggedBoost	Use only a random (bagged) subsample of all events for growing the trees in each iteration	True
BaggedSampleFraction	Relative size of bagged event sample to original size of the data sample	0.5
SeparationType	Separation criterion for node splitting	GiniIndex
nCuts	Number of grid points in variable range used in finding optimal cut in node splitting	500

Table 6: Chosen DNN parameters and architecture for shape-based W-boson and top-quark tagging.

	W-Boson Tagging	Top-Quark Tagging	Reference
Software package	Keras 1.0.8 with Theano backend, lwtnn 2.0		[99–101]
Layer type	Dense	Dense	[99]
Number of hidden layers	4	5	[99]
Architecture	16, 14, 9, 6	18, 16, 14, 10, 5	-
Activation function	rectified linear unit (relu)	rectified linear unit (relu)	[102]
Optimizer	Adam	Adam	[103]
Learning rate	0.0001	0.00005	[103]
L1 Regulariser	0.001	0.001	[102]
NN weight initialisation	Glorot uniform	Glorot uniform	[104]
Batch size	200	200	[102]
Batch normalisation	Yes	Yes	[105]
Number of epochs	100 with early stopping	100 with early stopping	[99]
Training input group	Group 8	Group 9	-

Acknowledgements

References

[1] L. Evans and P. Bryant, *LHC Machine*, JINST **3** (2008) S08001, ed. by L. Evans.

[2] M. Aaboud et al., *Search for heavy particles decaying into top-quark pairs using lepton-plus-jets events in proton–proton collisions at $\sqrt{s} = 13$ TeV with the ATLAS detector*, Eur. Phys. J. C **78** (2018) 565, arXiv: `1804.10823 [hep-ex]`.

[3] ATLAS Collaboration, *Search for heavy resonances decaying to a W or Z boson and a Higgs boson in the $q\bar{q}^{(\prime)}b\bar{b}$ final state in pp collisions at $\sqrt{s} = 13$ TeV with the ATLAS detector*, Phys. Lett. B **774** (2017) 494, arXiv: `1707.06958 [hep-ex]`.

[4] ATLAS Collaboration, *Search for diboson resonances with boson-tagged jets in pp collisions at $\sqrt{s} = 13$ TeV with the ATLAS detector*, Phys. Lett. B **777** (2018) 91, arXiv: `1708.04445 [hep-ex]`.

[5] ATLAS Collaboration, *Measurements of $t\bar{t}$ differential cross-sections of highly boosted top quarks decaying to all-hadronic final states in pp collisions at $\sqrt{s} = 13$ TeV using the ATLAS detector*, (2018), arXiv: `1801.02052 [hep-ex]`.

[6] ATLAS Collaboration, *Identification of Boosted, Hadronically Decaying W Bosons and Comparisons with ATLAS Data Taken at $\sqrt{s} = 8$ TeV*, Eur. Phys. J. C **76** (2016) 154, arXiv: `1510.05821 [hep-ex]`.

[7] ATLAS Collaboration, *Identification of high transverse momentum top quarks in pp collisions at $\sqrt{s} = 8$ TeV with the ATLAS detector*, JHEP **06** (2016) 093, arXiv: `1603.03127 [hep-ex]`.

[8] CMS Collaboration, *Identification techniques for highly boosted W bosons that decay into hadrons*, JHEP **12** (2014) 017, arXiv: `1410.4227 [hep-ex]`.

[9] CMS Collaboration, *Boosted Top Jet Tagging at CMS*, 2014, URL: `https://cds.cern.ch/record/1647419`.

[10] ATLAS Collaboration, *The ATLAS Experiment at the CERN Large Hadron Collider*, JINST **3** (2008) S08003.

[11] B. Abbott et al., *Production and integration of the ATLAS Insertable B-Layer*, JINST **13** (2018) T05008, arXiv: `1803.00844 [physics.ins-det]`.

[12] ATLAS Collaboration, *Performance of the ATLAS trigger system in 2015*, Eur. Phys. J. C **77** (2017) 317, arXiv: `1611.09661 [hep-ex]`.

[13] T. Sjostrand, S. Mrenna and P. Z. Skands, *A brief introduction to PYTHIA 8.1*, Comput. Phys. Commun. **178** (2008) 852, arXiv: `0710.3820 [hep-ph]`.

[14] R. D. Ball et al., *Parton distributions with QED corrections*, Nucl. Phys. B **877** (2013) 290, arXiv: `1308.0598 [hep-ph]`.

[15] ATLAS Collaboration, *ATLAS Pythia 8 tunes to 7 TeV data*, ATL-PHYS-PUB-2014-021, 2014, URL: `https://cds.cern.ch/record/1966419`.

[16] G. Altarelli, B. Mele and M. Ruiz-Altaba, *Searching for new heavy vector bosons in $p\bar{p}$ colliders*, Z. Phys. C **45** (1989) 109, [Erratum: Z. Phys. C 47,676(1990)].

[17] S. Alioli, P. Nason, C. Oleari and E. Re, *A general framework for implementing NLO calculations in shower Monte Carlo programs: the POWHEG BOX*, JHEP **06** (2010) 043, arXiv: 1002.2581 [hep-ph].

[18] S. Frixione, P. Nason and C. Oleari,
Matching NLO QCD computations with parton shower simulations: the POWHEG method,
JHEP **11** (2007) 070, arXiv: 0709.2092 [hep-ph].

[19] P. Nason, *A new method for combining NLO QCD with shower Monte Carlo algorithms*,
JHEP **11** (2004) 040, arXiv: hep-ph/0409146 [hep-ph].

[20] H.-L. Lai et al., *New parton distributions for collider physics*, Phys. Rev. D **82** (2010) 074024,
arXiv: 1007.2241 [hep-ph].

[21] T. Sjostrand, S. Mrenna and P. Z. Skands, *PYTHIA 6.4 physics and manual*, JHEP **05** (2006) 026,
arXiv: hep-ph/0603175 [hep-ph].

[22] J. Pumplin et al.,
New Generation of Parton Distributions with Uncertainties from Global QCD Analysis,
JHEP **07** (2002) 012, arXiv: hep-ph/0201195 [hep-ph].

[23] P. Skands, *Tuning Monte Carlo generators: The Perugia tunes*, Phys. Rev. D **82** (2010) 074018,
arXiv: 1005.3457 [hep-ph].

[24] M. Czakon, P. Fiedler and A. Mitov,
Total Top-Quark Pair-Production Cross Section at Hadron Colliders Through $O(\alpha_s^4)$,
Phys. Rev. Lett. **110** (2013) 252004, arXiv: 1303.6254 [hep-ph].

[25] M. Bahr et al., *Herwig++ physics and manual*, Eur. Phys. J. C **58** (2008) 639,
arXiv: 0803.0883 [hep-ph].

[26] J. Alwall et al., *The automated computation of tree-level and next-to-leading order differential cross sections, and their matching to parton shower simulations*, JHEP **07** (2014) 079,
arXiv: 1405.0301 [hep-ph].

[27] ATLAS Collaboration,
Simulation of top-quark production for the ATLAS experiment at $\sqrt{s}$ = 13 TeV,
ATL-PHYS-PUB-2016-004, 2016, URL: https://cds.cern.ch/record/2120417.

[28] T. Gleisberg et al., *Event generation with SHERPA 1.1*, JHEP **02** (2009) 007,
arXiv: 0811.4622 [hep-ph].

[29] S. Catani, L. Cieri, G. Ferrera, D. de Florian and M. Grazzini, *Vector Boson Production at Hadron Colliders: A Fully Exclusive QCD Calculation at Next-to-Next-to-Leading Order*,
Phys. Rev. Lett. **103** (2009) 082001, arXiv: 0903.2120 [hep-ph].

[30] S. Schumann and F. Krauss,
A Parton shower algorithm based on Catani-Seymour dipole factorisation, JHEP **03** (2008) 038,
arXiv: 0709.1027 [hep-ph].

[31] S. Höche, F. Krauss, S. Schumann and F. Siegert, *QCD matrix elements and truncated showers*,
JHEP **05** (2009) 053, arXiv: 0903.1219 [hep-ph].

[32] ATLAS Collaboration, *The ATLAS Simulation Infrastructure*, Eur. Phys. J. C **70** (2010) 823,
arXiv: 1005.4568 [physics.ins-det].

[33] S. Agostinelli et al., *GEANT4: a simulation toolkit*, Nucl. Instrum. Meth. A **506** (2003) 250.

[34] A. D. Martin, W. J. Stirling, R. S. Thorne and G. Watt, *Parton distributions for the LHC*, Eur. Phys. J. C **63** (2009) 189, arXiv: `0901.0002 [hep-ph]`.

[35] ATLAS Collaboration, *Reconstruction of primary vertices at the ATLAS experiment in Run 1 proton–proton collisions at the LHC*, Eur. Phys. J. C **77** (2017) 332, arXiv: `1611.10235 [hep-ex]`.

[36] ATLAS Collaboration, *A new method to distinguish hadronically decaying boosted Z bosons from W bosons using the ATLAS detector*, Eur. Phys. J. C **76** (2016) 238, arXiv: `1509.04939 [hep-ex]`.

[37] ATLAS Collaboration, *Topological cell clustering in the ATLAS calorimeters and its performance in LHC Run 1*, Eur. Phys. J. C **77** (2017) 490, arXiv: `1603.02934 [hep-ex]`.

[38] ATLAS Collaboration, *Jet energy scale measurements and their systematic uncertainties in proton–proton collisions at $\sqrt{s}$ = 13 TeV with the ATLAS detector*, Phys. Rev. D **96** (2017) 072002, arXiv: `1703.09665 [hep-ex]`.

[39] M. Cacciari, G. P. Salam and G. Soyez, *The anti-k_t jet clustering algorithm*, JHEP **04** (2008) 063, arXiv: `0802.1189 [hep-ph]`.

[40] S. D. Ellis, C. K. Vermilion and J. R. Walsh, *Recombination algorithms and jet substructure: Pruning as a tool for heavy particle searches*, Phys. Rev. D **81** (2010) 094023, arXiv: `0912.0033 [hep-ph]`.

[41] J. M. Butterworth, A. R. Davison, M. Rubin and G. P. Salam, *Jet Substructure as a New Higgs-Search Channel at the Large Hadron Collider*, Phys. Rev. Lett. **100** (2008) 242001, arXiv: `0802.2470 [hep-ph]`.

[42] D. Krohn, J. Thaler and L.-T. Wang, *Jet trimming*, JHEP **02** (2010) 084, arXiv: `0912.1342 [hep-ph]`.

[43] S. D. Ellis and D. E. Soper, *Successive combination jet algorithm for hadron collisions*, Phys. Rev. D **48** (1993) 3160, arXiv: `hep-ph/9305266 [hep-ph]`.

[44] ATLAS Collaboration, *Jet mass reconstruction with the ATLAS Detector in early Run 2 data*, ATLAS-CONF-2016-035, 2016, URL: `https://cds.cern.ch/record/2200211`.

[45] T. Plehn, G. P. Salam and M. Spannowsky, *Fat Jets for a Light Higgs*, Phys. Rev. Lett. **104** (2010) 111801, arXiv: `0910.5472 [hep-ph]`.

[46] T. Plehn, M. Spannowsky, M. Takeuchi and D. Zerwas, *Stop reconstruction with tagged tops*, JHEP **10** (2010) 078, arXiv: `1006.2833 [hep-ph]`.

[47] Y. L. Dokshitzer, G. D. Leder, S. Moretti and B. R. Webber, *Better jet clustering algorithms*, JHEP **08** (1997) 001, arXiv: `hep-ph/9707323 [hep-ph]`.

[48] M. Wobisch and T. Wengler, 'Hadronization corrections to jet cross-sections in deep inelastic scattering', *Monte Carlo generators for HERA physics. Proceedings, Workshop, Hamburg, Germany, 1998-1999*, 1998 270, arXiv: `hep-ph/9907280 [hep-ph]`.

[49] M. Cacciari, G. P. Salam and G. Soyez, *The catchment area of jets*, JHEP **04** (2008) 005, arXiv: `0802.1188 [hep-ph]`.

[50] A. J. Larkoski, G. P. Salam and J. Thaler, *Energy correlation functions for jet substructure*, JHEP **06** (2013) 108, arXiv: `1305.0007 [hep-ph]`.

[51] J. Gallicchio et al., *Multivariate discrimination and the Higgs + W/Z search*, JHEP **04** (2011) 069, arXiv: 1010.3698 [hep-ph].

[52] D. Adams et al., *Towards an understanding of the correlations in jet substructure*, Eur. Phys. J. C **75** (2015) 409, arXiv: 1504.00679 [hep-ph].

[53] A. J. Larkoski, D. Neill and J. Thaler, *Jet shapes with the broadening axis*, JHEP **04** (2014) 017, arXiv: 1401.2158 [hep-ph].

[54] A. J. Larkoski, I. Moult and D. Neill, *Power counting to better jet observables*, JHEP **12** (2014) 009, arXiv: 1409.6298 [hep-ph].

[55] J. Thaler and K. Van Tilburg, *Identifying boosted objects with N-subjettiness*, JHEP **03** (2011) 015, arXiv: 1011.2268 [hep-ph].

[56] J. Thaler and K. Van Tilburg, *Maximizing boosted top identification by minimizing N-subjettiness*, JHEP **02** (2012) 093, arXiv: 1108.2701 [hep-ph].

[57] G. C. Fox and S. Wolfram, *Observables for the Analysis of Event Shapes in e+ e- Annihilation and Other Processes*, Phys. Rev. Lett. **41** (1978) 1581.

[58] C. Chen, *New approach to identifying boosted hadronically-decaying particle using jet substructure in its center-of-mass frame*, Phys. Rev. D **85** (2012) 034007, arXiv: 1112.2567 [hep-ph].

[59] J. Thaler and L.-T. Wang, *Strategies to identify boosted tops*, JHEP **07** (2008) 092, arXiv: 0806.0023 [hep-ph].

[60] ATLAS Collaboration, *Measurement of k_T splitting scales in $W \rightarrow \ell\nu$ events at $\sqrt{s}$ = 7 TeV with the ATLAS detector*, Eur. Phys. J. C **73** (2013) 2432, arXiv: 1302.1415 [hep-ex].

[61] L. G. Almeida, S. J. Lee, G. Perez, I. Sung and J. Virzi, *Top quark jets at the LHC*, Phys. Rev. **D79** (2009) 074012, arXiv: 0810.0934 [hep-ph].

[62] ATLAS Collaboration, *ATLAS measurements of the properties of jets for boosted particle searches*, Phys. Rev. D **86** (2012) 072006, arXiv: 1206.5369 [hep-ex].

[63] S. Catani, Y. L. Dokshitzer, M. H. Seymour and B. R. Webber, *Longitudinally invariant K_t clustering algorithms for hadron hadron collisions*, Nucl. Phys. **B406** (1993) 187.

[64] L. de Oliveira, M. Kagan, L. Mackey, B. Nachman and A. Schwartzman, *Jet-images — deep learning edition*, JHEP **07** (2016) 069, arXiv: 1511.05190 [hep-ph].

[65] P. Baldi, K. Bauer, C. Eng, P. Sadowski and D. Whiteson, *Jet substructure classification in high-energy physics with deep neural networks*, Phys. Rev. D **93** (2016) 094034, arXiv: 1603.09349 [hep-ex].

[66] J. Pearkes, W. Fedorko, A. Lister and C. Gay, *Jet Constituents for Deep Neural Network Based Top Quark Tagging*, (2017), arXiv: 1704.02124 [hep-ex].

[67] G. Kasieczka, T. Plehn, M. Russell and T. Schell, *Deep-learning top taggers or the end of QCD?*, JHEP **05** (2017) 006, arXiv: 1701.08784 [hep-ph].

[68] D. E. Soper and M. Spannowsky, *Finding physics signals with shower deconstruction*,
Phys. Rev. D **84** (2011) 074002, arXiv: 1102.3480 [hep-ph].

[69] J. S. Gainer, J. Lykken, K. T. Matchev, S. Mrenna and M. Park,
'The Matrix Element Method: Past, Present, and Future',
Proceedings, 2013 Community Summer Study on the Future of U.S. Particle Physics: Snowmass on the Mississippi (CSS2013): Minneapolis, MN, USA, July 29-August 6, 2013, 2013,
arXiv: 1307.3546 [hep-ph],
URL: https://inspirehep.net/record/1242444/files/arXiv:1307.3546.pdf.

[70] G. Kasieczka, T. Plehn, T. Schell, T. Strebler and G. P. Salam,
Resonance searches with an updated top tagger, JHEP **06** (2015) 203,
arXiv: 1503.05921 [hep-ph].

[71] ATLAS Collaboration, *Identification of Boosted, Hadronically-Decaying W and Z Bosons in $\sqrt{s}$ = 13 TeV Monte Carlo Simulations for ATLAS*, ATL-PHYS-PUB-2015-033, 2015,
URL: https://cds.cern.ch/record/2041461.

[72] ATLAS Collaboration, *Boosted hadronic top identification at ATLAS for early* 13 *TeV data*,
ATL-PHYS-PUB-2015-053, 2015, URL: https://cds.cern.ch/record/2116351.

[73] ATLAS Collaboration,
Search for pair production of heavy vector-like quarks decaying into high-p_T W bosons and top quarks in the lepton-plus-jets final state in pp collisions at $\sqrt{s}$ = 13 TeV with the ATLAS detector,
(2018), arXiv: 1806.01762 [hep-ex].

[74] ATLAS Collaboration,
Searches for heavy diboson resonances in pp collisions at $\sqrt{s}$ = 13 TeV with the ATLAS detector,
JHEP **09** (2016) 173, arXiv: 1606.04833 [hep-ex].

[75] ATLAS Collaboration, *Search for heavy resonances decaying to a photon and a hadronically decaying Z/W/H boson in pp collisions at $\sqrt{s}$ = 13* TeV *with the ATLAS detector*, (2018),
arXiv: 1805.01908 [hep-ex].

[76] CMS Collaboration, *Top Tagging with New Approaches*, CMS-PAS-JME-15-002, 2016,
URL: https://cds.cern.ch/record/2126325.

[77] ATLAS Collaboration,
Identification of Hadronically-Decaying W Bosons and Top Quarks Using High-Level Features as Input to Boosted Decision Trees and Deep Neural Networks in ATLAS at $\sqrt{s}$ = 13 TeV,
ATL-PHYS-PUB-2017-004, 2017, URL: https://cds.cern.ch/record/2259646.

[78] ATLAS Collaboration, *Search for $W' \rightarrow tb$ decays in the hadronic final state using pp collisions at $\sqrt{s}$ = 13 TeV with the ATLAS detector*, Phys. Lett. B **781** (2018) 327,
arXiv: 1801.07893 [hep-ex].

[79] ATLAS Collaboration, *Electron efficiency measurements with the ATLAS detector using 2012 LHC proton–proton collision data*, Eur. Phys. J. C **77** (2017) 195,
arXiv: 1612.01456 [hep-ex].

[80] ATLAS Collaboration, *Electron identification measurements in ATLAS using $\sqrt{s}$ = 13 TeV data with* 50 *ns bunch spacing*, ATL-PHYS-PUB-2015-041, 2015,
URL: https://cds.cern.ch/record/2048202.

[81] ATLAS Collaboration, *Muon reconstruction performance of the ATLAS detector in proton–proton collision data at $\sqrt{s}$ = 13 TeV*, Eur. Phys. J. C **76** (2016) 292, arXiv: 1603.05598 [hep-ex].

[82] ATLAS Collaboration, *Electron efficiency measurements with the ATLAS detector using the 2015 LHC proton–proton collision data*, ATLAS-CONF-2016-024, 2016, URL: https://cds.cern.ch/record/2157687.

[83] ATLAS Collaboration, *Selection of jets produced in* 13 *TeV proton–proton collisions with the ATLAS detector*, ATLAS-CONF-2015-029, 2015, URL: https://cds.cern.ch/record/2037702.

[84] ATLAS Collaboration, *Performance of pile-up mitigation techniques for jets in pp collisions at $\sqrt{s}$ = 8 TeV using the ATLAS detector*, Eur. Phys. J. C **76** (2016) 581, arXiv: 1510.03823 [hep-ex].

[85] ATLAS Collaboration, *Optimisation of the ATLAS b-tagging performance for the 2016 LHC Run*, ATL-PHYS-PUB-2016-012, 2016, URL: https://cds.cern.ch/record/2160731.

[86] ATLAS Collaboration, *Measurements of b-jet tagging efficiency with the ATLAS detector using $t\bar{t}$ events at $\sqrt{s}$ = 13 TeV*, (2018), arXiv: 1805.01845 [hep-ex].

[87] ATLAS Collaboration, *Performance of missing transverse momentum reconstruction with the ATLAS detector using proton-proton collisions at $\sqrt{s}$ = 13 TeV*, (2018), arXiv: 1802.08168 [hep-ex].

[88] ATLAS Collaboration, *In-situ measurements of the ATLAS large-radius jet response in* 13 *TeV pp collisions*, ATLAS-CONF-2017-063, 2017, URL: https://cds.cern.ch/record/2275655.

[89] ATLAS Collaboration, *Performance of b-jet identification in the ATLAS experiment*, JINST **11** (2016) P04008, arXiv: 1512.01094 [hep-ex].

[90] P. Gras et al., *Systematics of quark/gluon tagging*, JHEP **07** (2017) 091, arXiv: 1704.03878 [hep-ph].

[91] ATLAS Collaboration, *Photon identification in 2015 ATLAS data*, ATL-PHYS-PUB-2016-014, 2016, URL: https://cds.cern.ch/record/2203125.

[92] ATLAS Collaboration, *Measurement of W$^\pm$ and Z Boson Production Cross Sections in pp Collisions at $\sqrt{s}$ = 13 TeV with the ATLAS Detector*, ATLAS-CONF-2015-039, 2015, URL: https://cds.cern.ch/record/2045487.

[93] ATLAS Collaboration, *ATLAS simulation of boson plus jets processes in Run 2*, ATL-PHYS-PUB-2017-006, 2017, URL: https://cds.cern.ch/record/2261937.

[94] ATLAS Collaboration, *Electron and photon energy calibration with the ATLAS detector using data collected in 2015 at $\sqrt{s}$ = 13 TeV*, ATL-PHYS-PUB-2016-015, 2016, URL: https://cds.cern.ch/record/2203514.

[95] ATLAS Collaboration, *Measurement of the photon identification efficiencies with the ATLAS detector using LHC Run-1 data*, Eur. Phys. J. C **76** (2016) 666, arXiv: 1606.01813 [hep-ex].

[96] ATLAS Collaboration, *Electron and photon energy calibration with the ATLAS detector using LHC Run 1 data*, Eur. Phys. J. C **74** (2014) 3071, arXiv: 1407.5063 [hep-ex].

[97] ATLAS Collaboration,
Luminosity determination in pp collisions at $\sqrt{s} = 8$ TeV using the ATLAS detector at the LHC,
Eur. Phys. J. C **76** (2016) 653, arXiv: 1608.03953 [hep-ex].

[98] P. Speckmayer, A. Hocker, J. Stelzer and H. Voss,
The toolkit for multivariate data analysis, TMVA 4, J. Phys. Conf. Ser. **219** (2010) 032057.

[99] F. Chollet, *Keras*, https://github.com/fchollet/keras, 2015.

[100] Theano Development Team,
Theano: A Python framework for fast computation of mathematical expressions,
arXiv e-prints **abs/1605.02688** (2016), URL: http://arxiv.org/abs/1605.02688.

[101] D. H. Guest, M. Paganini, M. Kagan, J. W. Smith and M. Lanfermann,
lwtnn/lwtnn: Release for Athena v21, 2017,
URL: https://doi.org/10.5281/zenodo.290682.

[102] I. Goodfellow, Y. Bengio and A. Courville, *Deep Learning*,
http://www.deeplearningbook.org, MIT Press, 2016.

[103] D. P. Kingma and J. Ba, *Adam: A Method for Stochastic Optimization*,
CoRR **abs/1412.6980** (2014), arXiv: 1412.6980.

[104] X. Glorot and Y. Bengio,
'Understanding the difficulty of training deep feedforward neural networks',
*Proceedings of the Thirteenth International Conference on Artificial Intelligence and Statistics,
AISTATS 2010, Chia Laguna Resort, Sardinia, Italy, May 13-15*, 2010, 249,
URL: http://www.jmlr.org/proceedings/papers/v9/glorot10a.html.

[105] S. Ioffe and C. Szegedy,
Batch Normalization: Accelerating Deep Network Training by Reducing Internal Covariate Shift,
CoRR **abs/1502.03167** (2015), arXiv: 1502.03167.

[106] ATLAS Collaboration, *ATLAS Computing Acknowledgements*, ATL-GEN-PUB-2016-002,
URL: https://cds.cern.ch/record/2202407.

The ATLAS Collaboration

M. Aaboud[34d], G. Aad[99], B. Abbott[124], O. Abdinov[13,*], B. Abeloos[128], D.K. Abhayasinghe[91],
S.H. Abidi[164], O.S. AbouZeid[39], N.L. Abraham[153], H. Abramowicz[158], H. Abreu[157], Y. Abulaiti[6],
B.S. Acharya[64a,64b,o], S. Adachi[160], L. Adam[97], L. Adamczyk[81a], J. Adelman[119], M. Adersberger[112],
A. Adiguzel[12c,ah], T. Adye[141], A.A. Affolder[143], Y. Afik[157], C. Agheorghiesei[27c],
J.A. Aguilar-Saavedra[136f,136a], F. Ahmadov[77,af], G. Aielli[71a,71b], S. Akatsuka[83], T.P.A. Åkesson[94],
E. Akilli[52], A.V. Akimov[108], G.L. Alberghi[23b,23a], J. Albert[173], P. Albicocco[49], M.J. Alconada Verzini[86],
S. Alderweireldt[117], M. Aleksa[35], I.N. Aleksandrov[77], C. Alexa[27b], T. Alexopoulos[10], M. Alhroob[124],
B. Ali[138], G. Alimonti[66a], J. Alison[36], S.P. Alkire[145], C. Allaire[128], B.M.M. Allbrooke[153], B.W. Allen[127],
P.P. Allport[21], A. Aloisio[67a,67b], A. Alonso[39], F. Alonso[86], C. Alpigiani[145], A.A. Alshehri[55],
M.I. Alstaty[99], B. Alvarez Gonzalez[35], D. Álvarez Piqueras[171], M.G. Alviggi[67a,67b], B.T. Amadio[18],
Y. Amaral Coutinho[78b], A. Ambler[101], L. Ambroz[131], C. Amelung[26], D. Amidei[103],
S.P. Amor Dos Santos[136a,136c], S. Amoroso[44], C.S. Amrouche[52], C. Anastopoulos[146], L.S. Ancu[52],
N. Andari[142], T. Andeen[11], C.F. Anders[59b], J.K. Anders[20], K.J. Anderson[36], A. Andreazza[66a,66b],
V. Andrei[59a], C.R. Anelli[173], S. Angelidakis[37], I. Angelozzi[118], A. Angerami[38], A.V. Anisenkov[120b,120a],
A. Annovi[69a], C. Antel[59a], M.T. Anthony[146], M. Antonelli[49], D.J.A. Antrim[168], F. Anulli[70a], M. Aoki[79],
J.A. Aparisi Pozo[171], L. Aperio Bella[35], G. Arabidze[104], J.P. Araque[136a], V. Araujo Ferraz[78b],
R. Araujo Pereira[78b], A.T.H. Arce[47], R.E. Ardell[91], F.A. Arduh[86], J-F. Arguin[107], S. Argyropoulos[75],
A.J. Armbruster[35], L.J. Armitage[90], A Armstrong[168], O. Arnaez[164], H. Arnold[118], M. Arratia[31],
O. Arslan[24], A. Artamonov[109,*], G. Artoni[131], S. Artz[97], S. Asai[160], N. Asbah[57],
E.M. Asimakopoulou[169], L. Asquith[153], K. Assamagan[29], R. Astalos[28a], R.J. Atkin[32a], M. Atkinson[170],
N.B. Atlay[148], K. Augsten[138], G. Avolio[35], R. Avramidou[58a], M.K. Ayoub[15a], A.M. Azoulay[165b],
G. Azuelos[107,at], A.E. Baas[59a], M.J. Baca[21], H. Bachacou[142], K. Bachas[65a,65b], M. Backes[131],
P. Bagnaia[70a,70b], M. Bahmani[82], H. Bahrasemani[149], A.J. Bailey[171], J.T. Baines[141], M. Bajic[39],
C. Bakalis[10], O.K. Baker[180], P.J. Bakker[118], D. Bakshi Gupta[8], S. Balaji[154], E.M. Baldin[120b,120a],
P. Balek[177], F. Balli[142], W.K. Balunas[133], J. Balz[97], E. Banas[82], A. Bandyopadhyay[24], S. Banerjee[178,k],
A.A.E. Bannoura[179], L. Barak[158], W.M. Barbe[37], E.L. Barberio[102], D. Barberis[53b,53a], M. Barbero[99],
T. Barillari[113], M-S. Barisits[35], J. Barkeloo[127], T. Barklow[150], R. Barnea[157], S.L. Barnes[58c],
B.M. Barnett[141], R.M. Barnett[18], Z. Barnovska-Blenessy[58a], A. Baroncelli[72a], G. Barone[26], A.J. Barr[131],
L. Barranco Navarro[171], F. Barreiro[96], J. Barreiro Guimarães da Costa[15a], R. Bartoldus[150],
A.E. Barton[87], P. Bartos[28a], A. Basalaev[134], A. Bassalat[128], R.L. Bates[55], S.J. Batista[164],
S. Batlamous[34e], J.R. Batley[31], M. Battaglia[143], M. Bauce[70a,70b], F. Bauer[142], K.T. Bauer[168],
H.S. Bawa[150,m], J.B. Beacham[122], T. Beau[132], P.H. Beauchemin[167], P. Bechtle[24], H.C. Beck[51],
H.P. Beck[20,r], K. Becker[50], M. Becker[97], C. Becot[44], A. Beddall[12d], A.J. Beddall[12a], V.A. Bednyakov[77],
M. Bedognetti[118], C.P. Bee[152], T.A. Beermann[74], M. Begalli[78b], M. Begel[29], A. Behera[152], J.K. Behr[44],
A.S. Bell[92], G. Bella[158], L. Bellagamba[23b], A. Bellerive[33], M. Bellomo[157], P. Bellos[9], K. Belotskiy[110],
N.L. Belyaev[110], O. Benary[158,*], D. Benchekroun[34a], M. Bender[112], N. Benekos[10], Y. Benhammou[158],
E. Benhar Noccioli[180], J. Benitez[75], D.P. Benjamin[47], M. Benoit[52], J.R. Bensinger[26], S. Bentvelsen[118],
L. Beresford[131], M. Beretta[49], D. Berge[44], E. Bergeaas Kuutmann[169], N. Berger[5], L.J. Bergsten[26],
J. Beringer[18], S. Berlendis[7], N.R. Bernard[100], G. Bernardi[132], C. Bernius[150], F.U. Bernlochner[24],
T. Berry[91], P. Berta[97], C. Bertella[15a], G. Bertoli[43a,43b], I.A. Bertram[87], G.J. Besjes[39],
O. Bessidskaia Bylund[179], M. Bessner[44], N. Besson[142], A. Bethani[98], S. Bethke[113], A. Betti[24],
A.J. Bevan[90], J. Beyer[113], R. Bi[135], R.M. Bianchi[135], O. Biebel[112], D. Biedermann[19], R. Bielski[35],
K. Bierwagen[97], N.V. Biesuz[69a,69b], M. Biglietti[72a], T.R.V. Billoud[107], M. Bindi[51], A. Bingul[12d],
C. Bini[70a,70b], S. Biondi[23b,23a], M. Birman[177], T. Bisanz[51], J.P. Biswal[158], C. Bittrich[46],

D.M. Bjergaard[47], J.E. Black[150], K.M. Black[25], T. Blazek[28a], I. Bloch[44], C. Blocker[26], A. Blue[55],
U. Blumenschein[90], Dr. Blunier[144a], G.J. Bobbink[118], V.S. Bobrovnikov[120b,120a], S.S. Bocchetta[94],
A. Bocci[47], D. Boerner[179], D. Bogavac[112], A.G. Bogdanchikov[120b,120a], C. Bohm[43a], V. Boisvert[91],
P. Bokan[169], T. Bold[81a], A.S. Boldyrev[111], A.E. Bolz[59b], M. Bomben[132], M. Bona[90], J.S. Bonilla[127],
M. Boonekamp[142], A. Borisov[140], G. Borissov[87], J. Bortfeldt[35], D. Bortoletto[131], V. Bortolotto[71a,71b],
D. Boscherini[23b], M. Bosman[14], J.D. Bossio Sola[30], K. Bouaouda[34a], J. Boudreau[135],
E.V. Bouhova-Thacker[87], D. Boumediene[37], C. Bourdarios[128], S.K. Boutle[55], A. Boveia[122], J. Boyd[35],
D. Boye[32b], I.R. Boyko[77], A.J. Bozson[91], J. Bracinik[21], N. Brahimi[99], A. Brandt[8], G. Brandt[179],
O. Brandt[59a], F. Braren[44], U. Bratzler[161], B. Brau[100], J.E. Brau[127], W.D. Breaden Madden[55],
K. Brendlinger[44], L. Brenner[44], R. Brenner[169], S. Bressler[177], B. Brickwedde[97], D.L. Briglin[21],
D. Britton[55], D. Britzger[113], I. Brock[24], R. Brock[104], G. Brooijmans[38], T. Brooks[91], W.K. Brooks[144b],
E. Brost[119], J.H Broughton[21], P.A. Bruckman de Renstrom[82], D. Bruncko[28b], A. Bruni[23b], G. Bruni[23b],
L.S. Bruni[118], S. Bruno[71a,71b], B.H. Brunt[31], M. Bruschi[23b], N. Bruscino[135], P. Bryant[36],
L. Bryngemark[44], T. Buanes[17], Q. Buat[35], P. Buchholz[148], A.G. Buckley[55], I.A. Budagov[77],
F. Buehrer[50], M.K. Bugge[130], O. Bulekov[110], D. Bullock[8], T.J. Burch[119], S. Burdin[88], C.D. Burgard[118],
A.M. Burger[5], B. Burghgrave[119], K. Burka[82], S. Burke[141], I. Burmeister[45], J.T.P. Burr[131], V. Büscher[97],
E. Buschmann[51], P. Bussey[55], J.M. Butler[25], C.M. Buttar[55], J.M. Butterworth[92], P. Butti[35],
W. Buttinger[35], A. Buzatu[155], A.R. Buzykaev[120b,120a], G. Cabras[23b,23a], S. Cabrera Urbán[171],
D. Caforio[138], H. Cai[170], V.M.M. Cairo[2], O. Cakir[4a], N. Calace[52], P. Calafiura[18], A. Calandri[99],
G. Calderini[132], P. Calfayan[63], G. Callea[40b,40a], L.P. Caloba[78b], S. Calvente Lopez[96], D. Calvet[37],
S. Calvet[37], T.P. Calvet[152], M. Calvetti[69a,69b], R. Camacho Toro[132], S. Camarda[35],
D. Camarero Munoz[96], P. Camarri[71a,71b], D. Cameron[130], R. Caminal Armadans[100], C. Camincher[35],
S. Campana[35], M. Campanelli[92], A. Camplani[39], A. Campoverde[148], V. Canale[67a,67b], M. Cano Bret[58c],
J. Cantero[125], T. Cao[158], Y. Cao[170], M.D.M. Capeans Garrido[35], I. Caprini[27b], M. Caprini[27b],
M. Capua[40b,40a], R.M. Carbone[38], R. Cardarelli[71a], F.C. Cardillo[146], I. Carli[139], T. Carli[35], G. Carlino[67a],
B.T. Carlson[135], L. Carminati[66a,66b], R.M.D. Carney[43a,43b], S. Caron[117], E. Carquin[144b], S. Carrá[66a,66b],
G.D. Carrillo-Montoya[35], D. Casadei[32b], M.P. Casado[14,g], A.F. Casha[164], D.W. Casper[168],
R. Castelijn[118], F.L. Castillo[171], V. Castillo Gimenez[171], N.F. Castro[136a,136e], A. Catinaccio[35],
J.R. Catmore[130], A. Cattai[35], J. Caudron[24], V. Cavaliere[29], E. Cavallaro[14], D. Cavalli[66a],
M. Cavalli-Sforza[14], V. Cavasinni[69a,69b], E. Celebi[12b], F. Ceradini[72a,72b], L. Cerda Alberich[171],
A.S. Cerqueira[78a], A. Cerri[153], L. Cerrito[71a,71b], F. Cerutti[18], A. Cervelli[23b,23a], S.A. Cetin[12b],
A. Chafaq[34a], D Chakraborty[119], S.K. Chan[57], W.S. Chan[118], Y.L. Chan[61a], J.D. Chapman[31],
B. Chargeishvili[156b], D.G. Charlton[21], C.C. Chau[33], C.A. Chavez Barajas[153], S. Che[122],
A. Chegwidden[104], S. Chekanov[6], S.V. Chekulaev[165a], G.A. Chelkov[77,as], M.A. Chelstowska[35],
C. Chen[58a], C.H. Chen[76], H. Chen[29], J. Chen[58a], J. Chen[38], S. Chen[133], S.J. Chen[15c], X. Chen[15b,ar],
Y. Chen[80], Y-H. Chen[44], H.C. Cheng[103], H.J. Cheng[15d], A. Cheplakov[77], E. Cheremushkina[140],
R. Cherkaoui El Moursli[34e], E. Cheu[7], K. Cheung[62], L. Chevalier[142], V. Chiarella[49], G. Chiarelli[69a],
G. Chiodini[65a], A.S. Chisholm[35,21], A. Chitan[27b], I. Chiu[160], Y.H. Chiu[173], M.V. Chizhov[77], K. Choi[63],
A.R. Chomont[128], S. Chouridou[159], Y.S. Chow[118], V. Christodoulou[92], M.C. Chu[61a], J. Chudoba[137],
A.J. Chuinard[101], J.J. Chwastowski[82], L. Chytka[126], D. Cinca[45], V. Cindro[89], I.A. Cioară[24], A. Ciocio[18],
F. Cirotto[67a,67b], Z.H. Citron[177], M. Citterio[66a], A. Clark[52], M.R. Clark[38], P.J. Clark[48], C. Clement[43a,43b],
Y. Coadou[99], M. Cobal[64a,64c], A. Coccaro[53b,53a], J. Cochran[76], H. Cohen[158], A.E.C. Coimbra[177],
L. Colasurdo[117], B. Cole[38], A.P. Colijn[118], J. Collot[56], P. Conde Muiño[136a,136b], E. Coniavitis[50],
S.H. Connell[32b], I.A. Connelly[98], S. Constantinescu[27b], F. Conventi[67a,au], A.M. Cooper-Sarkar[131],
F. Cormier[172], K.J.R. Cormier[164], L.D. Corpe[92], M. Corradi[70a,70b], E.E. Corrigan[94], F. Corriveau[101,ad],
A. Cortes-Gonzalez[35], M.J. Costa[171], F. Costanza[5], D. Costanzo[146], G. Cottin[31], G. Cowan[91],
B.E. Cox[98], J. Crane[98], K. Cranmer[121], S.J. Crawley[55], R.A. Creager[133], G. Cree[33], S. Crépé-Renaudin[56],

F. Crescioli[132], M. Cristinziani[24], V. Croft[121], G. Crosetti[40b,40a], A. Cueto[96],
T. Cuhadar Donszelmann[146], A.R. Cukierman[150], S. Czekierda[82], P. Czodrowski[35],
M.J. Da Cunha Sargedas De Sousa[58b,136b], C. Da Via[98], W. Dabrowski[81a], T. Dado[28a,y], S. Dahbi[34e],
T. Dai[103], F. Dallaire[107], C. Dallapiccola[100], M. Dam[39], G. D'amen[23b,23a], J. Damp[97], J.R. Dandoy[133],
M.F. Daneri[30], N.P. Dang[178,k], N.D Dann[98], M. Danninger[172], V. Dao[35], G. Darbo[53b], S. Darmora[8],
O. Dartsi[5], A. Dattagupta[127], T. Daubney[44], S. D'Auria[55], W. Davey[24], C. David[44], T. Davidek[139],
D.R. Davis[47], E. Dawe[102], I. Dawson[146], K. De[8], R. De Asmundis[67a], A. De Benedetti[124],
M. De Beurs[118], S. De Castro[23b,23a], S. De Cecco[70a,70b], N. De Groot[117], P. de Jong[118], H. De la Torre[104],
F. De Lorenzi[76], A. De Maria[51,t], D. De Pedis[70a], A. De Salvo[70a], U. De Sanctis[71a,71b],
M. De Santis[71a,71b], A. De Santo[153], K. De Vasconcelos Corga[99], J.B. De Vivie De Regie[128],
C. Debenedetti[143], D.V. Dedovich[77], N. Dehghanian[3], M. Del Gaudio[40b,40a], J. Del Peso[96],
Y. Delabat Diaz[44], D. Delgove[128], F. Deliot[142], C.M. Delitzsch[7], M. Della Pietra[67a,67b], D. Della Volpe[52],
A. Dell'Acqua[35], L. Dell'Asta[25], M. Delmastro[5], C. Delporte[128], P.A. Delsart[56], D.A. DeMarco[164],
S. Demers[180], M. Demichev[77], S.P. Denisov[140], D. Denysiuk[118], L. D'Eramo[132], D. Derendarz[82],
J.E. Derkaoui[34d], F. Derue[132], P. Dervan[88], K. Desch[24], C. Deterre[44], K. Dette[164], M.R. Devesa[30],
P.O. Deviveiros[35], A. Dewhurst[141], S. Dhaliwal[26], F.A. Di Bello[52], A. Di Ciaccio[71a,71b], L. Di Ciaccio[5],
W.K. Di Clemente[133], C. Di Donato[67a,67b], A. Di Girolamo[35], G. Di Gregorio[69a,69b], B. Di Micco[72a,72b],
R. Di Nardo[100], K.F. Di Petrillo[57], R. Di Sipio[164], D. Di Valentino[33], C. Diaconu[99], M. Diamond[164],
F.A. Dias[39], T. Dias Do Vale[136a], M.A. Diaz[144a], J. Dickinson[18], E.B. Diehl[103], J. Dietrich[19],
S. Díez Cornell[44], A. Dimitrievska[18], J. Dingfelder[24], F. Dittus[35], F. Djama[99], T. Djobava[156b],
J.I. Djuvsland[59a], M.A.B. Do Vale[78c], M. Dobre[27b], D. Dodsworth[26], C. Doglioni[94], J. Dolejsi[139],
Z. Dolezal[139], M. Donadelli[78d], J. Donini[37], A. D'onofrio[90], M. D'Onofrio[88], J. Dopke[141], A. Doria[67a],
M.T. Dova[86], A.T. Doyle[55], E. Drechsler[51], E. Dreyer[149], T. Dreyer[51], Y. Du[58b], F. Dubinin[108],
M. Dubovsky[28a], A. Dubreuil[52], E. Duchovni[177], G. Duckeck[112], A. Ducourthial[132], O.A. Ducu[107,x],
D. Duda[113], A. Dudarev[35], A.C. Dudder[97], E.M. Duffield[18], L. Duflot[128], M. Dührssen[35], C. Dülsen[179],
M. Dumancic[177], A.E. Dumitriu[27b,e], A.K. Duncan[55], M. Dunford[59a], A. Duperrin[99], H. Duran Yildiz[4a],
M. Düren[54], A. Durglishvili[156b], D. Duschinger[46], B. Dutta[44], D. Duvnjak[1], M. Dyndal[44], S. Dysch[98],
B.S. Dziedzic[82], C. Eckardt[44], K.M. Ecker[113], R.C. Edgar[103], T. Eifert[35], G. Eigen[17], K. Einsweiler[18],
T. Ekelof[169], M. El Kacimi[34c], R. El Kosseifi[99], V. Ellajosyula[99], M. Ellert[169], F. Ellinghaus[179],
A.A. Elliot[90], N. Ellis[35], J. Elmsheuser[29], M. Elsing[35], D. Emeliyanov[141], A. Emerman[38], Y. Enari[160],
J.S. Ennis[175], M.B. Epland[47], J. Erdmann[45], A. Ereditato[20], S. Errede[170], M. Escalier[128], C. Escobar[171],
O. Estrada Pastor[171], A.I. Etienvre[142], E. Etzion[158], H. Evans[63], A. Ezhilov[134], M. Ezzi[34e], F. Fabbri[55],
L. Fabbri[23b,23a], V. Fabiani[117], G. Facini[92], R.M. Faisca Rodrigues Pereira[136a], R.M. Fakhrutdinov[140],
S. Falciano[70a], P.J. Falke[5], S. Falke[5], J. Faltova[139], Y. Fang[15a], M. Fanti[66a,66b], A. Farbin[8], A. Farilla[72a],
E.M. Farina[68a,68b], T. Farooque[104], S. Farrell[18], S.M. Farrington[175], P. Farthouat[35], F. Fassi[34e],
P. Fassnacht[35], D. Fassouliotis[9], M. Faucci Giannelli[48], A. Favareto[53b,53a], W.J. Fawcett[31], L. Fayard[128],
O.L. Fedin[134,p], W. Fedorko[172], M. Feickert[41], S. Feigl[130], L. Feligioni[99], C. Feng[58b], E.J. Feng[35],
M. Feng[47], M.J. Fenton[55], A.B. Fenyuk[140], L. Feremenga[8], J. Ferrando[44], A. Ferrari[169], P. Ferrari[118],
R. Ferrari[68a], D.E. Ferreira de Lima[59b], A. Ferrer[171], D. Ferrere[52], C. Ferretti[103], F. Fiedler[97],
A. Filipčič[89], F. Filthaut[117], K.D. Finelli[25], M.C.N. Fiolhais[136a,136c,a], L. Fiorini[171], C. Fischer[14],
W.C. Fisher[104], N. Flaschel[44], I. Fleck[148], P. Fleischmann[103], R.R.M. Fletcher[133], T. Flick[179],
B.M. Flierl[112], L.M. Flores[133], L.R. Flores Castillo[61a], F.M. Follega[73a,73b], N. Fomin[17],
G.T. Forcolin[73a,73b], A. Formica[142], F.A. Förster[14], A.C. Forti[98], A.G. Foster[21], D. Fournier[128], H. Fox[87],
S. Fracchia[146], P. Francavilla[69a,69b], M. Franchini[23b,23a], S. Franchino[59a], D. Francis[35], L. Franconi[143],
M. Franklin[57], M. Frate[168], M. Fraternali[68a,68b], A.N. Fray[90], D. Freeborn[92],
S.M. Fressard-Batraneanu[35], B. Freund[107], W.S. Freund[78b], E.M. Freundlich[45], D.C. Frizzell[124],
D. Froidevaux[35], J.A. Frost[131], C. Fukunaga[161], E. Fullana Torregrosa[171], T. Fusayasu[114], J. Fuster[171],

O. Gabizon[157], A. Gabrielli[23b,23a], A. Gabrielli[18], G.P. Gach[81a], S. Gadatsch[52], P. Gadow[113],
G. Gagliardi[53b,53a], L.G. Gagnon[107], C. Galea[27b], B. Galhardo[136a,136c], E.J. Gallas[131], B.J. Gallop[141],
P. Gallus[138], G. Galster[39], R. Gamboa Goni[90], K.K. Gan[122], S. Ganguly[177], J. Gao[58a], Y. Gao[88],
Y.S. Gao[150,m], C. García[171], J.E. García Navarro[171], J.A. García Pascual[15a], M. Garcia-Sciveres[18],
R.W. Gardner[36], N. Garelli[150], V. Garonne[130], K. Gasnikova[44], A. Gaudiello[53b,53a], G. Gaudio[68a],
I.L. Gavrilenko[108], A. Gavrilyuk[109], C. Gay[172], G. Gaycken[24], E.N. Gazis[10], C.N.P. Gee[141], J. Geisen[51],
M. Geisen[97], M.P. Geisler[59a], K. Gellerstedt[43a,43b], C. Gemme[53b], M.H. Genest[56], C. Geng[103],
S. Gentile[70a,70b], S. George[91], D. Gerbaudo[14], G. Gessner[45], S. Ghasemi[148], M. Ghasemi Bostanabad[173],
M. Ghneimat[24], B. Giacobbe[23b], S. Giagu[70a,70b], N. Giangiacomi[23b,23a], P. Giannetti[69a],
A. Giannini[67a,67b], S.M. Gibson[91], M. Gignac[143], D. Gillberg[33], G. Gilles[179], D.M. Gingrich[3,at],
M.P. Giordani[64a,64c], F.M. Giorgi[23b], P.F. Giraud[142], P. Giromini[57], G. Giugliarelli[64a,64c], D. Giugni[66a],
F. Giuli[131], M. Giulini[59b], S. Gkaitatzis[159], I. Gkialas[9,j], E.L. Gkougkousis[14], P. Gkountoumis[10],
L.K. Gladilin[111], C. Glasman[96], J. Glatzer[14], P.C.F. Glaysher[44], A. Glazov[44], M. Goblirsch-Kolb[26],
J. Godlewski[82], S. Goldfarb[102], T. Golling[52], D. Golubkov[140], A. Gomes[136a,136b,136d],
R. Goncalves Gama[78a], R. Gonçalo[136a], G. Gonella[50], L. Gonella[21], A. Gongadze[77], F. Gonnella[21],
J.L. Gonski[57], S. González de la Hoz[171], S. Gonzalez-Sevilla[52], L. Goossens[35], P.A. Gorbounov[109],
H.A. Gordon[29], B. Gorini[35], E. Gorini[65a,65b], A. Gorišek[89], A.T. Goshaw[47], C. Gössling[45],
M.I. Gostkin[77], C.A. Gottardo[24], C.R. Goudet[128], D. Goujdami[34c], A.G. Goussiou[145], N. Govender[32b,c],
C. Goy[5], E. Gozani[157], I. Grabowska-Bold[81a], P.O.J. Gradin[169], E.C. Graham[88], J. Gramling[168],
E. Gramstad[130], S. Grancagnolo[19], V. Gratchev[134], P.M. Gravila[27f], F.G. Gravili[65a,65b], C. Gray[55],
H.M. Gray[18], Z.D. Greenwood[93,aj], C. Grefe[24], K. Gregersen[94], I.M. Gregor[44], P. Grenier[150],
K. Grevtsov[44], N.A. Grieser[124], J. Griffiths[8], A.A. Grillo[143], K. Grimm[150,b], S. Grinstein[14,z], Ph. Gris[37],
J.-F. Grivaz[128], S. Groh[97], E. Gross[177], J. Grosse-Knetter[51], G.C. Grossi[93], Z.J. Grout[92], C. Grud[103],
A. Grummer[116], L. Guan[103], W. Guan[178], J. Guenther[35], A. Guerguichon[128], F. Guescini[165a],
D. Guest[168], R. Gugel[50], B. Gui[122], T. Guillemin[5], S. Guindon[35], U. Gul[55], C. Gumpert[35], J. Guo[58c],
W. Guo[103], Y. Guo[58a,s], Z. Guo[99], R. Gupta[44], S. Gurbuz[12c], G. Gustavino[124], B.J. Gutelman[157],
P. Gutierrez[124], C. Gutschow[92], C. Guyot[142], M.P. Guzik[81a], C. Gwenlan[131], C.B. Gwilliam[88],
A. Haas[121], C. Haber[18], H.K. Hadavand[8], N. Haddad[34e], A. Hadef[58a], S. Hageböck[24], M. Hagihara[166],
H. Hakobyan[181,*], M. Haleem[174], J. Haley[125], G. Halladjian[104], G.D. Hallewell[99], K. Hamacher[179],
P. Hamal[126], K. Hamano[173], A. Hamilton[32a], G.N. Hamity[146], K. Han[58a,ai], L. Han[58a], S. Han[15d],
K. Hanagaki[79,v], M. Hance[143], D.M. Handl[112], B. Haney[133], R. Hankache[132], P. Hanke[59a], E. Hansen[94],
J.B. Hansen[39], J.D. Hansen[39], M.C. Hansen[24], P.H. Hansen[39], K. Hara[166], A.S. Hard[178], T. Harenberg[179],
S. Harkusha[105], P.F. Harrison[175], N.M. Hartmann[112], Y. Hasegawa[147], A. Hasib[48], S. Hassani[142],
S. Haug[20], R. Hauser[104], L. Hauswald[46], L.B. Havener[38], M. Havranek[138], C.M. Hawkes[21],
R.J. Hawkings[35], D. Hayden[104], C. Hayes[152], C.P. Hays[131], J.M. Hays[90], H.S. Hayward[88],
S.J. Haywood[141], M.P. Heath[48], V. Hedberg[94], L. Heelan[8], S. Heer[24], K.K. Heidegger[50], J. Heilman[33],
S. Heim[44], T. Heim[18], B. Heinemann[44,ao], J.J. Heinrich[112], L. Heinrich[121], C. Heinz[54], J. Hejbal[137],
L. Helary[35], A. Held[172], S. Hellesund[130], S. Hellman[43a,43b], C. Helsens[35], R.C.W. Henderson[87],
Y. Heng[178], S. Henkelmann[172], A.M. Henriques Correia[35], G.H. Herbert[19], H. Herde[26], V. Herget[174],
Y. Hernández Jiménez[32c], H. Herr[97], M.G. Herrmann[112], T. Herrmann[46], G. Herten[50],
R. Hertenberger[112], L. Hervas[35], T.C. Herwig[133], G.G. Hesketh[92], N.P. Hessey[165a], S. Higashino[79],
E. Higón-Rodriguez[171], K. Hildebrand[36], E. Hill[173], J.C. Hill[31], K.K. Hill[29], K.H. Hiller[44], S.J. Hillier[21],
M. Hils[46], I. Hinchliffe[18], M. Hirose[129], D. Hirschbuehl[179], B. Hiti[89], O. Hladik[137], D.R. Hlaluku[32c],
X. Hoad[48], J. Hobbs[152], N. Hod[165a], M.C. Hodgkinson[146], A. Hoecker[35], M.R. Hoeferkamp[116],
F. Hoenig[112], D. Hohn[24], D. Hohov[128], T.R. Holmes[36], M. Holzbock[112], M. Homann[45], S. Honda[166],
T. Honda[79], T.M. Hong[135], A. Hönle[113], B.H. Hooberman[170], W.H. Hopkins[127], Y. Horii[115], P. Horn[46],
A.J. Horton[149], L.A. Horyn[36], J-Y. Hostachy[56], A. Hostiuc[145], S. Hou[155], A. Hoummada[34a],

J. Howarth[98], J. Hoya[86], M. Hrabovsky[126], I. Hristova[19], J. Hrivnac[128], A. Hrynevich[106], T. Hryn'ova[5], P.J. Hsu[62], S.-C. Hsu[145], Q. Hu[29], S. Hu[58c], Y. Huang[15a], Z. Hubacek[138], F. Hubaut[99], M. Huebner[24], F. Huegging[24], T.B. Huffman[131], E.W. Hughes[38], M. Huhtinen[35], R.F.H. Hunter[33], P. Huo[152], A.M. Hupe[33], N. Huseynov[77,af], J. Huston[104], J. Huth[57], R. Hyneman[103], G. Iacobucci[52], G. Iakovidis[29], I. Ibragimov[148], L. Iconomidou-Fayard[128], Z. Idrissi[34e], P. Iengo[35], R. Ignazzi[39], O. Igonkina[118,ab], R. Iguchi[160], T. Iizawa[52], Y. Ikegami[79], M. Ikeno[79], D. Iliadis[159], N. Ilic[150], F. Iltzsche[46], G. Introzzi[68a,68b], M. Iodice[72a], K. Iordanidou[38], V. Ippolito[70a,70b], M.F. Isacson[169], N. Ishijima[129], M. Ishino[160], M. Ishitsuka[162], W. Islam[125], C. Issever[131], S. Istin[157], F. Ito[166], J.M. Iturbe Ponce[61a], R. Iuppa[73a,73b], A. Ivina[177], H. Iwasaki[79], J.M. Izen[42], V. Izzo[67a], P. Jacka[137], P. Jackson[1], R.M. Jacobs[24], V. Jain[2], G. Jäkel[179], K.B. Jakobi[97], K. Jakobs[50], S. Jakobsen[74], T. Jakoubek[137], D.O. Jamin[125], R. Jansky[52], J. Janssen[24], M. Janus[51], P.A. Janus[81a], G. Jarlskog[94], N. Javadov[77,af], T. Javůrek[35], M. Javurkova[50], F. Jeanneau[142], L. Jeanty[18], J. Jejelava[156a,ag], A. Jelinskas[175], P. Jenni[50,d], J. Jeong[44], N. Jeong[44], S. Jézéquel[5], H. Ji[178], J. Jia[152], H. Jiang[76], Y. Jiang[58a], Z. Jiang[150,q], S. Jiggins[50], F.A. Jimenez Morales[37], J. Jimenez Pena[171], S. Jin[15c], A. Jinaru[27b], O. Jinnouchi[162], H. Jivan[32c], P. Johansson[146], K.A. Johns[7], C.A. Johnson[63], W.J. Johnson[145], K. Jon-And[43a,43b], R.W.L. Jones[87], S.D. Jones[153], S. Jones[7], T.J. Jones[88], J. Jongmanns[59a], P.M. Jorge[136a,136b], J. Jovicevic[165a], X. Ju[18], J.J. Junggeburth[113], A. Juste Rozas[14,z], A. Kaczmarska[82], M. Kado[128], H. Kagan[122], M. Kagan[150], T. Kaji[176], E. Kajomovitz[157], C.W. Kalderon[94], A. Kaluza[97], S. Kama[41], A. Kamenshchikov[140], L. Kanjir[89], Y. Kano[160], V.A. Kantserov[110], J. Kanzaki[79], B. Kaplan[121], L.S. Kaplan[178], D. Kar[32c], M.J. Kareem[165b], E. Karentzos[10], S.N. Karpov[77], Z.M. Karpova[77], V. Kartvelishvili[87], A.N. Karyukhin[140], L. Kashif[178], R.D. Kass[122], A. Kastanas[43a,43b], Y. Kataoka[160], C. Kato[58d,58c], J. Katzy[44], K. Kawade[80], K. Kawagoe[85], T. Kawamoto[160], G. Kawamura[51], E.F. Kay[88], V.F. Kazanin[120b,120a], R. Keeler[173], R. Kehoe[41], J.S. Keller[33], E. Kellermann[94], J.J. Kempster[21], J. Kendrick[21], O. Kepka[137], S. Kersten[179], B.P. Kerševan[89], S. Ketabchi Haghighat[164], R.A. Keyes[101], M. Khader[170], F. Khalil-Zada[13], A. Khanov[125], A.G. Kharlamov[120b,120a], T. Kharlamova[120b,120a], E.E. Khoda[172], A. Khodinov[163], T.J. Khoo[52], E. Khramov[77], J. Khubua[156b], S. Kido[80], M. Kiehn[52], C.R. Kilby[91], Y.K. Kim[36], N. Kimura[64a,64c], O.M. Kind[19], B.T. King[88], D. Kirchmeier[46], J. Kirk[141], A.E. Kiryunin[113], T. Kishimoto[160], D. Kisielewska[81a], V. Kitali[44], O. Kivernyk[5], E. Kladiva[28b,*], T. Klapdor-Kleingrothaus[50], M.H. Klein[103], M. Klein[88], U. Klein[88], K. Kleinknecht[97], P. Klimek[119], A. Klimentov[29], T. Klingl[24], T. Klioutchnikova[35], F.F. Klitzner[112], P. Kluit[118], S. Kluth[113], E. Kneringer[74], E.B.F.G. Knoops[99], A. Knue[50], A. Kobayashi[160], D. Kobayashi[85], T. Kobayashi[160], M. Kobel[46], M. Kocian[150], P. Kodys[139], P.T. Koenig[24], T. Koffas[33], E. Koffeman[118], N.M. Köhler[113], T. Koi[150], M. Kolb[59b], I. Koletsou[5], T. Kondo[79], N. Kondrashova[58c], K. Köneke[50], A.C. König[117], T. Kono[79], R. Konoplich[121,al], V. Konstantinides[92], N. Konstantinidis[92], B. Konya[94], R. Kopeliansky[63], S. Koperny[81a], K. Korcyl[82], K. Kordas[159], G. Koren[158], A. Korn[92], I. Korolkov[14], E.V. Korolkova[146], N. Korotkova[111], O. Kortner[113], S. Kortner[113], T. Kosek[139], V.V. Kostyukhin[24], A. Kotwal[47], A. Koulouris[10], A. Kourkoumeli-Charalampidi[68a,68b], C. Kourkoumelis[9], E. Kourlitis[146], V. Kouskoura[29], A.B. Kowalewska[82], R. Kowalewski[173], T.Z. Kowalski[81a], C. Kozakai[160], W. Kozanecki[142], A.S. Kozhin[140], V.A. Kramarenko[111], G. Kramberger[89], D. Krasnopevtsev[58a], M.W. Krasny[132], A. Krasznahorkay[35], D. Krauss[113], J.A. Kremer[81a], J. Kretzschmar[88], P. Krieger[164], K. Krizka[18], K. Kroeninger[45], H. Kroha[113], J. Kroll[137], J. Kroll[133], J. Krstic[16], U. Kruchonak[77], H. Krüger[24], N. Krumnack[76], M.C. Kruse[47], T. Kubota[102], S. Kuday[4b], J.T. Kuechler[179], S. Kuehn[35], A. Kugel[59a], F. Kuger[174], T. Kuhl[44], V. Kukhtin[77], R. Kukla[99], Y. Kulchitsky[105], S. Kuleshov[144b], Y.P. Kulinich[170], M. Kuna[56], T. Kunigo[83], A. Kupco[137], T. Kupfer[45], O. Kuprash[158], H. Kurashige[80], L.L. Kurchaninov[165a], Y.A. Kurochkin[105], A. Kurova[110], M.G. Kurth[15d], E.S. Kuwertz[35], M. Kuze[162], J. Kvita[126], T. Kwan[101], A. La Rosa[113], J.L. La Rosa Navarro[78d], L. La Rotonda[40b,40a], F. La Ruffa[40b,40a], C. Lacasta[171], F. Lacava[70a,70b], J. Lacey[44], D.P.J. Lack[98], H. Lacker[19], D. Lacour[132], E. Ladygin[77],

R. Lafaye[5], B. Laforge[132], T. Lagouri[32c], S. Lai[51], S. Lammers[63], W. Lampl[7], E. Lançon[29],
U. Landgraf[50], M.P.J. Landon[90], M.C. Lanfermann[52], V.S. Lang[44], J.C. Lange[51], R.J. Langenberg[35],
A.J. Lankford[168], F. Lanni[29], K. Lantzsch[24], A. Lanza[68a], A. Lapertosa[53b,53a], S. Laplace[132],
J.F. Laporte[142], T. Lari[66a], F. Lasagni Manghi[23b,23a], M. Lassnig[35], T.S. Lau[61a], A. Laudrain[128],
M. Lavorgna[67a,67b], A.T. Law[143], M. Lazzaroni[66a,66b], B. Le[102], O. Le Dortz[132], E. Le Guirriec[99],
E.P. Le Quilleuc[142], M. LeBlanc[7], T. LeCompte[6], F. Ledroit-Guillon[56], C.A. Lee[29], G.R. Lee[144a],
L. Lee[57], S.C. Lee[155], B. Lefebvre[101], M. Lefebvre[173], F. Legger[112], C. Leggett[18], K. Lehmann[149],
N. Lehmann[179], G. Lehmann Miotto[35], W.A. Leight[44], A. Leisos[159,w], M.A.L. Leite[78d], R. Leitner[139],
D. Lellouch[177], K.J.C. Leney[92], T. Lenz[24], B. Lenzi[35], R. Leone[7], S. Leone[69a], C. Leonidopoulos[48],
G. Lerner[153], C. Leroy[107], R. Les[164], A.A.J. Lesage[142], C.G. Lester[31], M. Levchenko[134], J. Levêque[5],
D. Levin[103], L.J. Levinson[177], D. Lewis[90], B. Li[103], C-Q. Li[58a,ak], H. Li[58b], L. Li[58c], M. Li[15a], Q. Li[15d],
Q.Y. Li[58a], S. Li[58d,58c], X. Li[58c], Y. Li[148], Z. Liang[15a], B. Liberti[71a], A. Liblong[164], K. Lie[61c], S. Liem[118],
A. Limosani[154], C.Y. Lin[31], K. Lin[104], T.H. Lin[97], R.A. Linck[63], J.H. Lindon[21], B.E. Lindquist[152],
A.L. Lionti[52], E. Lipeles[133], A. Lipniacka[17], M. Lisovyi[59b], T.M. Liss[170,aq], A. Lister[172], A.M. Litke[143],
J.D. Little[8], B. Liu[76], B.L Liu[6], H.B. Liu[29], H. Liu[103], J.B. Liu[58a], J.K.K. Liu[131], K. Liu[132], M. Liu[58a],
P. Liu[18], Y. Liu[15a], Y.L. Liu[58a], Y.W. Liu[58a], M. Livan[68a,68b], A. Lleres[56], J. Llorente Merino[15a],
S.L. Lloyd[90], C.Y. Lo[61b], F. Lo Sterzo[41], E.M. Lobodzinska[44], P. Loch[7], T. Lohse[19], K. Lohwasser[146],
M. Lokajicek[137], J.D. Long[170], R.E. Long[87], L. Longo[65a,65b], K.A. Looper[122], J.A. Lopez[144b],
I. Lopez Paz[98], A. Lopez Solis[146], J. Lorenz[112], N. Lorenzo Martinez[5], M. Losada[22], P.J. Lösel[112],
A. Lösle[50], X. Lou[44], X. Lou[15a], A. Lounis[128], J. Love[6], P.A. Love[87], J.J. Lozano Bahilo[171], H. Lu[61a],
M. Lu[58a], N. Lu[103], Y.J. Lu[62], H.J. Lubatti[145], C. Luci[70a,70b], A. Lucotte[56], C. Luedtke[50], F. Luehring[63],
I. Luise[132], L. Luminari[70a], B. Lund-Jensen[151], M.S. Lutz[100], P.M. Luzi[132], D. Lynn[29], R. Lysak[137],
E. Lytken[94], F. Lyu[15a], V. Lyubushkin[77], T. Lyubushkina[77], H. Ma[29], L.L. Ma[58b], Y. Ma[58b],
G. Maccarrone[49], A. Macchiolo[113], C.M. Macdonald[146], J. Machado Miguens[133,136b], D. Madaffari[171],
R. Madar[37], W.F. Mader[46], A. Madsen[44], N. Madysa[46], J. Maeda[80], K. Maekawa[160], S. Maeland[17],
T. Maeno[29], A.S. Maevskiy[111], V. Magerl[50], C. Maidantchik[78b], T. Maier[112], A. Maio[136a,136b,136d],
O. Majersky[28a], S. Majewski[127], Y. Makida[79], N. Makovec[128], B. Malaescu[132], Pa. Malecki[82],
V.P. Maleev[134], F. Malek[56], U. Mallik[75], D. Malon[6], C. Malone[31], S. Maltezos[10], S. Malyukov[35],
J. Mamuzic[171], G. Mancini[49], I. Mandić[89], J. Maneira[136a], L. Manhaes de Andrade Filho[78a],
J. Manjarres Ramos[46], K.H. Mankinen[94], A. Mann[112], A. Manousos[74], B. Mansoulie[142],
J.D. Mansour[15a], M. Mantoani[51], S. Manzoni[66a,66b], A. Marantis[159], G. Marceca[30], L. March[52],
L. Marchese[131], G. Marchiori[132], M. Marcisovsky[137], C.A. Marin Tobon[35], M. Marjanovic[37],
D.E. Marley[103], F. Marroquim[78b], Z. Marshall[18], M.U.F Martensson[169], S. Marti-Garcia[171],
C.B. Martin[122], T.A. Martin[175], V.J. Martin[48], B. Martin dit Latour[17], M. Martinez[14,z],
V.I. Martinez Outschoorn[100], S. Martin-Haugh[141], V.S. Martoiu[27b], A.C. Martyniuk[92], A. Marzin[35],
L. Masetti[97], T. Mashimo[160], R. Mashinistov[108], J. Masik[98], A.L. Maslennikov[120b,120a], L.H. Mason[102],
L. Massa[71a,71b], P. Massarotti[67a,67b], P. Mastrandrea[5], A. Mastroberardino[40b,40a], T. Masubuchi[160],
P. Mättig[179], J. Maurer[27b], B. Maček[89], S.J. Maxfield[88], D.A. Maximov[120b,120a], R. Mazini[155],
I. Maznas[159], S.M. Mazza[143], N.C. Mc Fadden[116], G. Mc Goldrick[164], S.P. Mc Kee[103], A. McCarn[103],
T.G. McCarthy[113], L.I. McClymont[92], E.F. McDonald[102], J.A. Mcfayden[35], G. Mchedlidze[51],
M.A. McKay[41], K.D. McLean[173], S.J. McMahon[141], P.C. McNamara[102], C.J. McNicol[175],
R.A. McPherson[173,ad], J.E. Mdhluli[32c], Z.A. Meadows[100], S. Meehan[145], T.M. Megy[50], S. Mehlhase[112],
A. Mehta[88], T. Meideck[56], B. Meirose[42], D. Melini[171,h], B.R. Mellado Garcia[32c], J.D. Mellenthin[51],
M. Melo[28a], F. Meloni[44], A. Melzer[24], S.B. Menary[98], E.D. Mendes Gouveia[136a], L. Meng[88],
X.T. Meng[103], A. Mengarelli[23b,23a], S. Menke[113], E. Meoni[40b,40a], S. Mergelmeyer[19], S.A.M. Merkt[135],
C. Merlassino[20], P. Mermod[52], L. Merola[67a,67b], C. Meroni[66a], F.S. Merritt[36], A. Messina[70a,70b],
J. Metcalfe[6], A.S. Mete[168], C. Meyer[133], J. Meyer[157], J-P. Meyer[142], H. Meyer Zu Theenhausen[59a],

F. Miano[153], R.P. Middleton[141], L. Mijović[48], G. Mikenberg[177], M. Mikestikova[137], M. Mikuž[89], M. Milesi[102], A. Milic[164], D.A. Millar[90], D.W. Miller[36], A. Milov[177], D.A. Milstead[43a,43b], A.A. Minaenko[140], M. Miñano Moya[171], I.A. Minashvili[156b], A.I. Mincer[121], B. Mindur[81a], M. Mineev[77], Y. Minegishi[160], Y. Ming[178], L.M. Mir[14], A. Mirto[65a,65b], K.P. Mistry[133], T. Mitani[176], J. Mitrevski[112], V.A. Mitsou[171], A. Miucci[20], P.S. Miyagawa[146], A. Mizukami[79], J.U. Mjörnmark[94], T. Mkrtchyan[181], M. Mlynarikova[139], T. Moa[43a,43b], K. Mochizuki[107], P. Mogg[50], S. Mohapatra[38], S. Molander[43a,43b], R. Moles-Valls[24], M.C. Mondragon[104], K. Mönig[44], J. Monk[39], E. Monnier[99], A. Montalbano[149], J. Montejo Berlingen[35], F. Monticelli[86], S. Monzani[66a], N. Morange[128], D. Moreno[22], M. Moreno Llácer[35], P. Morettini[53b], M. Morgenstern[118], S. Morgenstern[46], D. Mori[149], M. Morii[57], M. Morinaga[176], V. Morisbak[130], A.K. Morley[35], G. Mornacchi[35], A.P. Morris[92], J.D. Morris[90], L. Morvaj[152], P. Moschovakos[10], M. Mosidze[156b], H.J. Moss[146], J. Moss[150,n], K. Motohashi[162], R. Mount[150], E. Mountricha[35], E.J.W. Moyse[100], S. Muanza[99], F. Mueller[113], J. Mueller[135], R.S.P. Mueller[112], D. Muenstermann[87], G.A. Mullier[94], F.J. Munoz Sanchez[98], P. Murin[28b], W.J. Murray[175,141], A. Murrone[66a,66b], M. Muškinja[89], C. Mwewa[32a], A.G. Myagkov[140,am], J. Myers[127], M. Myska[138], B.P. Nachman[18], O. Nackenhorst[45], K. Nagai[131], K. Nagano[79], Y. Nagasaka[60], M. Nagel[50], E. Nagy[99], A.M. Nairz[35], Y. Nakahama[115], K. Nakamura[79], T. Nakamura[160], I. Nakano[123], H. Nanjo[129], F. Napolitano[59a], R.F. Naranjo Garcia[44], R. Narayan[11], D.I. Narrias Villar[59a], I. Naryshkin[134], T. Naumann[44], G. Navarro[22], R. Nayyar[7], H.A. Neal[103,*], P.Y. Nechaeva[108], T.J. Neep[142], A. Negri[68a,68b], M. Negrini[23b], S. Nektarijevic[117], C. Nellist[51], M.E. Nelson[131], S. Nemecek[137], P. Nemethy[121], M. Nessi[35,f], M.S. Neubauer[170], M. Neumann[179], R. Newhouse[172], P.R. Newman[21], T.Y. Ng[61c], Y.S. Ng[19], H.D.N. Nguyen[99], T. Nguyen Manh[107], E. Nibigira[37], R.B. Nickerson[131], R. Nicolaidou[142], D.S. Nielsen[39], J. Nielsen[143], N. Nikiforou[11], V. Nikolaenko[140,am], I. Nikolic-Audit[132], K. Nikolopoulos[21], P. Nilsson[29], Y. Ninomiya[79], A. Nisati[70a], N. Nishu[58c], R. Nisius[113], I. Nitsche[45], T. Nitta[176], T. Nobe[160], Y. Noguchi[83], M. Nomachi[129], I. Nomidis[132], M.A. Nomura[29], T. Nooney[90], M. Nordberg[35], N. Norjoharuddeen[131], T. Novak[89], O. Novgorodova[46], R. Novotny[138], L. Nozka[126], K. Ntekas[168], E. Nurse[92], F. Nuti[102], F.G. Oakham[33,at], H. Oberlack[113], J. Ocariz[132], A. Ochi[80], I. Ochoa[38], J.P. Ochoa-Ricoux[144a], K. O'Connor[26], S. Oda[85], S. Odaka[79], S. Oerdek[51], A. Oh[98], S.H. Oh[47], C.C. Ohm[151], H. Oide[53b,53a], M.L. Ojeda[164], H. Okawa[166], Y. Okazaki[83], Y. Okumura[160], T. Okuyama[79], A. Olariu[27b], L.F. Oleiro Seabra[136a], S.A. Olivares Pino[144a], D. Oliveira Damazio[29], J.L. Oliver[1], M.J.R. Olsson[36], A. Olszewski[82], J. Olszowska[82], D.C. O'Neil[149], A. Onofre[136a,136e], K. Onogi[115], P.U.E. Onyisi[11], H. Oppen[130], M.J. Oreglia[36], G.E. Orellana[86], Y. Oren[158], D. Orestano[72a,72b], E.C. Orgill[98], N. Orlando[61b], A.A. O'Rourke[44], R.S. Orr[164], B. Osculati[53b,53a,*], V. O'Shea[55], R. Ospanov[58a], G. Otero y Garzon[30], H. Otono[85], M. Ouchrif[34d], F. Ould-Saada[130], A. Ouraou[142], Q. Ouyang[15a], M. Owen[55], R.E. Owen[21], V.E. Ozcan[12c], N. Ozturk[8], J. Pacalt[126], H.A. Pacey[31], K. Pachal[149], A. Pacheco Pages[14], L. Pacheco Rodriguez[142], C. Padilla Aranda[14], S. Pagan Griso[18], M. Paganini[180], G. Palacino[63], S. Palazzo[40b,40a], S. Palestini[35], M. Palka[81b], D. Pallin[37], I. Panagoulias[10], C.E. Pandini[35], J.G. Panduro Vazquez[91], P. Pani[35], G. Panizzo[64a,64c], L. Paolozzi[52], T.D. Papadopoulou[10], K. Papageorgiou[9,j], A. Paramonov[6], D. Paredes Hernandez[61b], S.R. Paredes Saenz[131], B. Parida[163], A.J. Parker[87], K.A. Parker[44], M.A. Parker[31], F. Parodi[53b,53a], J.A. Parsons[38], U. Parzefall[50], V.R. Pascuzzi[164], J.M.P. Pasner[143], E. Pasqualucci[70a], S. Passaggio[53b], F. Pastore[91], P. Pasuwan[43a,43b], S. Pataraia[97], J.R. Pater[98], A. Pathak[178,k], T. Pauly[35], J. Pearkes[150], B. Pearson[113], M. Pedersen[130], L. Pedraza Diaz[117], R. Pedro[136a,136b], S.V. Peleganchuk[120b,120a], O. Penc[137], C. Peng[15d], H. Peng[58a], B.S. Peralva[78a], M.M. Perego[128], A.P. Pereira Peixoto[136a], D.V. Perepelitsa[29], F. Peri[19], L. Perini[66a,66b], H. Pernegger[35], S. Perrella[67a,67b], V.D. Peshekhonov[77,*], K. Peters[44], R.F.Y. Peters[98], B.A. Petersen[35], T.C. Petersen[39], E. Petit[56], A. Petridis[1], C. Petridou[159], P. Petroff[128], M. Petrov[131], F. Petrucci[72a,72b], M. Pettee[180], N.E. Pettersson[100], A. Peyaud[142], R. Pezoa[144b], T. Pham[102], F.H. Phillips[104], P.W. Phillips[141], M.W. Phipps[170], G. Piacquadio[152], E. Pianori[18],

A. Picazio[100], M.A. Pickering[131], R.H. Pickles[98], R. Piegaia[30], J.E. Pilcher[36], A.D. Pilkington[98],
M. Pinamonti[71a,71b], J.L. Pinfold[3], M. Pitt[177], L. Pizzimento[71a,71b], M.-A. Pleier[29], V. Pleskot[139],
E. Plotnikova[77], D. Pluth[76], P. Podberezko[120b,120a], R. Poettgen[94], R. Poggi[52], L. Poggioli[128],
I. Pogrebnyak[104], D. Pohl[24], I. Pokharel[51], G. Polesello[68a], A. Poley[18], A. Policicchio[70a,70b], R. Polifka[35],
A. Polini[23b], C.S. Pollard[44], V. Polychronakos[29], D. Ponomarenko[110], L. Pontecorvo[70a],
G.A. Popeneciu[27d], D.M. Portillo Quintero[132], S. Pospisil[138], K. Potamianos[44], I.N. Potrap[77],
C.J. Potter[31], H. Potti[11], T. Poulsen[94], J. Poveda[35], T.D. Powell[146], M.E. Pozo Astigarraga[35],
P. Pralavorio[99], S. Prell[76], D. Price[98], M. Primavera[65a], S. Prince[101], N. Proklova[110], K. Prokofiev[61c],
F. Prokoshin[144b], S. Protopopescu[29], J. Proudfoot[6], M. Przybycien[81a], A. Puri[170], P. Puzo[128], J. Qian[103],
Y. Qin[98], A. Quadt[51], M. Queitsch-Maitland[44], A. Qureshi[1], P. Rados[102], F. Ragusa[66a,66b], G. Rahal[95],
J.A. Raine[52], S. Rajagopalan[29], A. Ramirez Morales[90], T. Rashid[128], S. Raspopov[5], M.G. Ratti[66a,66b],
D.M. Rauch[44], F. Rauscher[112], S. Rave[97], B. Ravina[146], I. Ravinovich[177], J.H. Rawling[98],
M. Raymond[35], A.L. Read[130], N.P. Readioff[56], M. Reale[65a,65b], D.M. Rebuzzi[68a,68b], A. Redelbach[174],
G. Redlinger[29], R. Reece[143], R.G. Reed[32c], K. Reeves[42], L. Rehnisch[19], J. Reichert[133], D. Reikher[158],
A. Reiss[97], C. Rembser[35], H. Ren[15d], M. Rescigno[70a], S. Resconi[66a], E.D. Resseguie[133], S. Rettie[172],
E. Reynolds[21], O.L. Rezanova[120b,120a], P. Reznicek[139], E. Ricci[73a,73b], R. Richter[113], S. Richter[44],
E. Richter-Was[81b], O. Ricken[24], M. Ridel[132], P. Rieck[113], C.J. Riegel[179], O. Rifki[44], M. Rijssenbeek[152],
A. Rimoldi[68a,68b], M. Rimoldi[20], L. Rinaldi[23b], G. Ripellino[151], B. Ristić[87], E. Ritsch[35], I. Riu[14],
J.C. Rivera Vergara[144a], F. Rizatdinova[125], E. Rizvi[90], C. Rizzi[14], R.T. Roberts[98], S.H. Robertson[101,ad],
D. Robinson[31], J.E.M. Robinson[44], A. Robson[55], E. Rocco[97], C. Roda[69a,69b], Y. Rodina[99],
S. Rodriguez Bosca[171], A. Rodriguez Perez[14], D. Rodriguez Rodriguez[171], A.M. Rodríguez Vera[165b],
S. Roe[35], C.S. Rogan[57], O. Røhne[130], R. Röhrig[113], C.P.A. Roland[63], J. Roloff[57], A. Romaniouk[110],
M. Romano[23b,23a], N. Rompotis[88], M. Ronzani[121], L. Roos[132], S. Rosati[70a], K. Rosbach[50], P. Rose[143],
N-A. Rosien[51], B.J. Rosser[133], E. Rossi[44], E. Rossi[72a,72b], E. Rossi[67a,67b], L.P. Rossi[53b], L. Rossini[66a,66b],
J.H.N. Rosten[31], R. Rosten[14], M. Rotaru[27b], J. Rothberg[145], D. Rousseau[128], D. Roy[32c], A. Rozanov[99],
Y. Rozen[157], X. Ruan[32c], F. Rubbo[150], F. Rühr[50], A. Ruiz-Martinez[171], Z. Rurikova[50],
N.A. Rusakovich[77], H.L. Russell[101], J.P. Rutherfoord[7], E.M. Rüttinger[44,l], Y.F. Ryabov[134], M. Rybar[170],
G. Rybkin[128], S. Ryu[6], A. Ryzhov[140], G.F. Rzehorz[51], P. Sabatini[51], G. Sabato[118], S. Sacerdoti[128],
H.F-W. Sadrozinski[143], R. Sadykov[77], F. Safai Tehrani[70a], P. Saha[119], M. Sahinsoy[59a], A. Sahu[179],
M. Saimpert[44], M. Saito[160], T. Saito[160], H. Sakamoto[160], A. Sakharov[121,al], D. Salamani[52],
G. Salamanna[72a,72b], J.E. Salazar Loyola[144b], P.H. Sales De Bruin[169], D. Salihagic[113], A. Salnikov[150],
J. Salt[171], D. Salvatore[40b,40a], F. Salvatore[153], A. Salvucci[61a,61b,61c], A. Salzburger[35], J. Samarati[35],
D. Sammel[50], D. Sampsonidis[159], D. Sampsonidou[159], J. Sánchez[171], A. Sanchez Pineda[64a,64c],
H. Sandaker[130], C.O. Sander[44], M. Sandhoff[179], C. Sandoval[22], D.P.C. Sankey[141], M. Sannino[53b,53a],
Y. Sano[115], A. Sansoni[49], C. Santoni[37], H. Santos[136a], I. Santoyo Castillo[153], A. Santra[171],
A. Sapronov[77], J.G. Saraiva[136a,136d], O. Sasaki[79], K. Sato[166], E. Sauvan[5], P. Savard[164,at], N. Savic[113],
R. Sawada[160], C. Sawyer[141], L. Sawyer[93,aj], C. Sbarra[23b], A. Sbrizzi[23b,23a], T. Scanlon[92],
J. Schaarschmidt[145], P. Schacht[113], B.M. Schachtner[112], D. Schaefer[36], L. Schaefer[133], J. Schaeffer[97],
S. Schaepe[35], U. Schäfer[97], A.C. Schaffer[128], D. Schaile[112], R.D. Schamberger[152], N. Scharmberg[98],
V.A. Schegelsky[134], D. Scheirich[139], F. Schenck[19], M. Schernau[168], C. Schiavi[53b,53a], S. Schier[143],
L.K. Schildgen[24], Z.M. Schillaci[26], E.J. Schioppa[35], M. Schioppa[40b,40a], K.E. Schleicher[50],
S. Schlenker[35], K.R. Schmidt-Sommerfeld[113], K. Schmieden[35], C. Schmitt[97], S. Schmitt[44], S. Schmitz[97],
J.C. Schmoeckel[44], U. Schnoor[50], L. Schoeffel[142], A. Schoening[59b], E. Schopf[131], M. Schott[97],
J.F.P. Schouwenberg[117], J. Schovancova[35], S. Schramm[52], A. Schulte[97], H-C. Schultz-Coulon[59a],
M. Schumacher[50], B.A. Schumm[143], Ph. Schune[142], A. Schwartzman[150], T.A. Schwarz[103],
Ph. Schwemling[142], R. Schwienhorst[104], A. Sciandra[24], G. Sciolla[26], M. Scornajenghi[40b,40a], F. Scuri[69a],
F. Scutti[102], L.M. Scyboz[113], J. Searcy[103], C.D. Sebastiani[70a,70b], P. Seema[19], S.C. Seidel[116],

A. Seiden[143], T. Seiss[36], J.M. Seixas[78b], G. Sekhniaidze[67a], K. Sekhon[103], S.J. Sekula[41],
N. Semprini-Cesari[23b,23a], S. Sen[47], S. Senkin[37], C. Serfon[130], L. Serin[128], L. Serkin[64a,64b], M. Sessa[58a],
H. Severini[124], F. Sforza[167], A. Sfyrla[52], E. Shabalina[51], J.D. Shahinian[143], N.W. Shaikh[43a,43b],
L.Y. Shan[15a], R. Shang[170], J.T. Shank[25], M. Shapiro[18], A.S. Sharma[1], A. Sharma[131], P.B. Shatalov[109],
K. Shaw[153], S.M. Shaw[98], A. Shcherbakova[134], Y. Shen[124], N. Sherafati[33], A.D. Sherman[25],
P. Sherwood[92], L. Shi[155,ap], S. Shimizu[79], C.O. Shimmin[180], M. Shimojima[114], I.P.J. Shipsey[131],
S. Shirabe[85], M. Shiyakova[77], J. Shlomi[177], A. Shmeleva[108], D. Shoaleh Saadi[107], M.J. Shochet[36],
S. Shojaii[102], D.R. Shope[124], S. Shrestha[122], E. Shulga[110], P. Sicho[137], A.M. Sickles[170], P.E. Sidebo[151],
E. Sideras Haddad[32c], O. Sidiropoulou[35], A. Sidoti[23b,23a], F. Siegert[46], Dj. Sijacki[16], J. Silva[136a],
M. Silva Jr.[178], M.V. Silva Oliveira[78a], S.B. Silverstein[43a], S. Simion[128], E. Simioni[97], M. Simon[97],
R. Simoniello[97], P. Sinervo[164], N.B. Sinev[127], M. Sioli[23b,23a], G. Siragusa[174], I. Siral[103],
S.Yu. Sivoklokov[111], J. Sjölin[43a,43b], P. Skubic[124], M. Slater[21], T. Slavicek[138], M. Slawinska[82],
K. Sliwa[167], R. Slovak[139], V. Smakhtin[177], B.H. Smart[5], J. Smiesko[28a], N. Smirnov[110],
S.Yu. Smirnov[110], Y. Smirnov[110], L.N. Smirnova[111], O. Smirnova[94], J.W. Smith[51], M.N.K. Smith[38],
M. Smizanska[87], K. Smolek[138], A. Smykiewicz[82], A.A. Snesarev[108], I.M. Snyder[127], S. Snyder[29],
R. Sobie[173,ad], A.M. Soffa[168], A. Soffer[158], A. Søgaard[48], D.A. Soh[155], G. Sokhrannyi[89],
C.A. Solans Sanchez[35], M. Solar[138], E.Yu. Soldatov[110], U. Soldevila[171], A.A. Solodkov[140],
A. Soloshenko[77], O.V. Solovyanov[140], V. Solovyev[134], P. Sommer[146], H. Son[167], W. Song[141],
W.Y. Song[165b], A. Sopczak[138], F. Sopkova[28b], C.L. Sotiropoulou[69a,69b], S. Sottocornola[68a,68b],
R. Soualah[64a,64c,i], A.M. Soukharev[120b,120a], D. South[44], B.C. Sowden[91], S. Spagnolo[65a,65b],
M. Spalla[113], M. Spangenberg[175], F. Spanò[91], D. Sperlich[19], T.M. Spieker[59a], R. Spighi[23b], G. Spigo[35],
L.A. Spiller[102], D.P. Spiteri[55], M. Spousta[139], A. Stabile[66a,66b], R. Stamen[59a], S. Stamm[19], E. Stanecka[82],
R.W. Stanek[6], C. Stanescu[72a], B. Stanislaus[131], M.M. Stanitzki[44], B. Stapf[118], S. Stapnes[130],
E.A. Starchenko[140], G.H. Stark[36], J. Stark[56], S.H Stark[39], P. Staroba[137], P. Starovoitov[59a], S. Stärz[35],
R. Staszewski[82], M. Stegler[44], P. Steinberg[29], B. Stelzer[149], H.J. Stelzer[35], O. Stelzer-Chilton[165a],
H. Stenzel[54], T.J. Stevenson[90], G.A. Stewart[55], M.C. Stockton[35], G. Stoicea[27b], P. Stolte[51], S. Stonjek[113],
A. Straessner[46], J. Strandberg[151], S. Strandberg[43a,43b], M. Strauss[124], P. Strizenec[28b], R. Ströhmer[174],
D.M. Strom[127], R. Stroynowski[41], A. Strubig[48], S.A. Stucci[29], B. Stugu[17], J. Stupak[124], N.A. Styles[44],
D. Su[150], J. Su[135], S. Suchek[59a], Y. Sugaya[129], M. Suk[138], V.V. Sulin[108], M.J. Sullivan[88],
D.M.S. Sultan[52], S. Sultansoy[4c], T. Sumida[83], S. Sun[103], X. Sun[3], K. Suruliz[153], C.J.E. Suster[154],
M.R. Sutton[153], S. Suzuki[79], M. Svatos[137], M. Swiatlowski[36], S.P. Swift[2], A. Sydorenko[97], I. Sykora[28a],
T. Sykora[139], D. Ta[97], K. Tackmann[44,aa], J. Taenzer[158], A. Taffard[168], R. Tafirout[165a], E. Tahirovic[90],
N. Taiblum[158], H. Takai[29], R. Takashima[84], E.H. Takasugi[113], K. Takeda[80], T. Takeshita[147], Y. Takubo[79],
M. Talby[99], A.A. Talyshev[120b,120a], J. Tanaka[160], M. Tanaka[162], R. Tanaka[128], B.B. Tannenwald[122],
S. Tapia Araya[144b], S. Tapprogge[97], A. Tarek Abouelfadl Mohamed[132], S. Tarem[157], G. Tarna[27b,e],
G.F. Tartarelli[66a], P. Tas[139], M. Tasevsky[137], T. Tashiro[83], E. Tassi[40b,40a], A. Tavares Delgado[136a,136b],
Y. Tayalati[34e], A.C. Taylor[116], A.J. Taylor[48], G.N. Taylor[102], P.T.E. Taylor[102], W. Taylor[165b], A.S. Tee[87],
P. Teixeira-Dias[91], H. Ten Kate[35], J.J. Teoh[118], S. Terada[79], K. Terashi[160], J. Terron[96], S. Terzo[14],
M. Testa[49], R.J. Teuscher[164,ad], S.J. Thais[180], T. Theveneaux-Pelzer[44], F. Thiele[39], D.W. Thomas[91],
J.P. Thomas[21], A.S. Thompson[55], P.D. Thompson[21], L.A. Thomsen[180], E. Thomson[133], Y. Tian[38],
R.E. Ticse Torres[51], V.O. Tikhomirov[108,an], Yu.A. Tikhonov[120b,120a], S. Timoshenko[110], P. Tipton[180],
S. Tisserant[99], K. Todome[162], S. Todorova-Nova[5], S. Todt[46], J. Tojo[85], S. Tokár[28a], K. Tokushuku[79],
E. Tolley[122], K.G. Tomiwa[32c], M. Tomoto[115], L. Tompkins[150,q], K. Toms[116], B. Tong[57], P. Tornambe[50],
E. Torrence[127], H. Torres[46], E. Torró Pastor[145], C. Tosciri[131], J. Toth[99,ac], F. Touchard[99], D.R. Tovey[146],
C.J. Treado[121], T. Trefzger[174], F. Tresoldi[153], A. Tricoli[29], I.M. Trigger[165a], S. Trincaz-Duvoid[132],
M.F. Tripiana[14], W. Trischuk[164], B. Trocmé[56], A. Trofymov[128], C. Troncon[66a], M. Trovatelli[173],
F. Trovato[153], L. Truong[32b], M. Trzebinski[82], A. Trzupek[82], F. Tsai[44], J.C-L. Tseng[131], P.V. Tsiareshka[105],

71

A. Tsirigotis[159], N. Tsirintanis[9], V. Tsiskaridze[152], E.G. Tskhadadze[156a], I.I. Tsukerman[109], V. Tsulaia[18], S. Tsuno[79], D. Tsybychev[152,163], Y. Tu[61b], A. Tudorache[27b], V. Tudorache[27b], T.T. Tulbure[27a], A.N. Tuna[57], S. Turchikhin[77], D. Turgeman[177], I. Turk Cakir[4b,u], R. Turra[66a], P.M. Tuts[38], E. Tzovara[97], G. Ucchielli[23b,23a], I. Ueda[79], M. Ughetto[43a,43b], F. Ukegawa[166], G. Unal[35], A. Undrus[29], G. Unel[168], F.C. Ungaro[102], Y. Unno[79], K. Uno[160], J. Urban[28b], P. Urquijo[102], P. Urrejola[97], G. Usai[8], J. Usui[79], L. Vacavant[99], V. Vacek[138], B. Vachon[101], K.O.H. Vadla[130], A. Vaidya[92], C. Valderanis[112], E. Valdes Santurio[43a,43b], M. Valente[52], S. Valentinetti[23b,23a], A. Valero[171], L. Valéry[44], R.A. Vallance[21], A. Vallier[5], J.A. Valls Ferrer[171], T.R. Van Daalen[14], H. Van der Graaf[118], P. Van Gemmeren[6], J. Van Nieuwkoop[149], I. Van Vulpen[118], M. Vanadia[71a,71b], W. Vandelli[35], A. Vaniachine[163], P. Vankov[118], R. Vari[70a], E.W. Varnes[7], C. Varni[53b,53a], T. Varol[41], D. Varouchas[128], K.E. Varvell[154], G.A. Vasquez[144b], J.G. Vasquez[180], F. Vazeille[37], D. Vazquez Furelos[14], T. Vazquez Schroeder[35], J. Veatch[51], V. Vecchio[72a,72b], L.M. Veloce[164], F. Veloso[136a,136c], S. Veneziano[70a], A. Ventura[65a,65b], M. Venturi[173], N. Venturi[35], V. Vercesi[68a], M. Verducci[72a,72b], C.M. Vergel Infante[76], C. Vergis[24], W. Verkerke[118], A.T. Vermeulen[118], J.C. Vermeulen[118], M.C. Vetterli[149,at], N. Viaux Maira[144b], M. Vicente Barreto Pinto[52], I. Vichou[170,*], T. Vickey[146], O.E. Vickey Boeriu[146], G.H.A. Viehhauser[131], S. Viel[18], L. Vigani[131], M. Villa[23b,23a], M. Villaplana Perez[66a,66b], E. Vilucchi[49], M.G. Vincter[33], V.B. Vinogradov[77], A. Vishwakarma[44], C. Vittori[23b,23a], I. Vivarelli[153], S. Vlachos[10], M. Vogel[179], P. Vokac[138], G. Volpi[14], S.E. von Buddenbrock[32c], E. Von Toerne[24], V. Vorobel[139], K. Vorobev[110], M. Vos[171], J.H. Vossebeld[88], N. Vranjes[16], M. Vranjes Milosavljevic[16], V. Vrba[138], M. Vreeswijk[118], T. Šfiligoj[89], R. Vuillermet[35], I. Vukotic[36], T. Ženiš[28a], L. Živković[16], P. Wagner[24], W. Wagner[179], J. Wagner-Kuhr[112], H. Wahlberg[86], S. Wahrmund[46], K. Wakamiya[80], V.M. Walbrecht[113], J. Walder[87], R. Walker[112], S.D. Walker[91], W. Walkowiak[148], V. Wallangen[43a,43b], A.M. Wang[57], C. Wang[58b,e], F. Wang[178], H. Wang[18], H. Wang[3], J. Wang[154], J. Wang[59b], P. Wang[41], Q. Wang[124], R.-J. Wang[132], R. Wang[58a], R. Wang[6], S.M. Wang[155], W.T. Wang[58a], W. Wang[15c,ae], W.X. Wang[58a,ae], Y. Wang[58a,ak], Z. Wang[58c], C. Wanotayaroj[44], A. Warburton[101], C.P. Ward[31], D.R. Wardrope[92], A. Washbrook[48], P.M. Watkins[21], A.T. Watson[21], M.F. Watson[21], G. Watts[145], S. Watts[98], B.M. Waugh[92], A.F. Webb[11], S. Webb[97], C. Weber[180], M.S. Weber[20], S.A. Weber[33], S.M. Weber[59a], A.R. Weidberg[131], B. Weinert[63], J. Weingarten[45], M. Weirich[97], C. Weiser[50], P.S. Wells[35], T. Wenaus[29], T. Wengler[35], S. Wenig[35], N. Wermes[24], M.D. Werner[76], P. Werner[35], M. Wessels[59a], T.D. Weston[20], K. Whalen[127], N.L. Whallon[145], A.M. Wharton[87], A.S. White[103], A. White[8], M.J. White[1], R. White[144b], D. Whiteson[168], B.W. Whitmore[87], F.J. Wickens[141], W. Wiedenmann[178], M. Wielers[141], C. Wiglesworth[39], L.A.M. Wiik-Fuchs[50], F. Wilk[98], H.G. Wilkens[35], L.J. Wilkins[91], H.H. Williams[133], S. Williams[31], C. Willis[104], S. Willocq[100], J.A. Wilson[21], I. Wingerter-Seez[5], E. Winkels[153], F. Winklmeier[127], O.J. Winston[153], B.T. Winter[50], M. Wittgen[150], M. Wobisch[93], A. Wolf[97], T.M.H. Wolf[118], R. Wolff[99], M.W. Wolter[82], H. Wolters[136a,136c], V.W.S. Wong[172], N.L. Woods[143], S.D. Worm[21], B.K. Wosiek[82], K.W. Woźniak[82], K. Wraight[55], M. Wu[36], S.L. Wu[178], X. Wu[52], Y. Wu[58a], T.R. Wyatt[98], B.M. Wynne[48], S. Xella[39], Z. Xi[103], L. Xia[175], D. Xu[15a], H. Xu[58a,e], L. Xu[29], T. Xu[142], W. Xu[103], B. Yabsley[154], S. Yacoob[32a], K. Yajima[129], D.P. Yallup[92], D. Yamaguchi[162], Y. Yamaguchi[162], A. Yamamoto[79], T. Yamanaka[160], F. Yamane[80], M. Yamatani[160], T. Yamazaki[160], Y. Yamazaki[80], Z. Yan[25], H.J. Yang[58c,58d], H.T. Yang[18], S. Yang[75], Y. Yang[160], Z. Yang[17], W-M. Yao[18], Y.C. Yap[44], Y. Yasu[79], E. Yatsenko[58c,58d], J. Ye[41], S. Ye[29], I. Yeletskikh[77], E. Yigitbasi[25], E. Yildirim[97], K. Yorita[176], K. Yoshihara[133], C.J.S. Young[35], C. Young[150], J. Yu[8], J. Yu[76], X. Yue[59a], S.P.Y. Yuen[24], B. Zabinski[82], G. Zacharis[10], E. Zaffaroni[52], R. Zaidan[14], A.M. Zaitsev[140,am], T. Zakareishvili[156b], N. Zakharchuk[33], J. Zalieckas[17], S. Zambito[57], D. Zanzi[35], D.R. Zaripovas[55], S.V. Zeißner[45], C. Zeitnitz[179], G. Zemaityte[131], J.C. Zeng[170], Q. Zeng[150], O. Zenin[140], D. Zerwas[128], M. Zgubič[131], D.F. Zhang[58b], D. Zhang[103], F. Zhang[178], G. Zhang[58a], H. Zhang[15c], J. Zhang[6], L. Zhang[15c], L. Zhang[58a], M. Zhang[170], P. Zhang[15c], R. Zhang[58a], R. Zhang[24], X. Zhang[58b], Y. Zhang[15d], Z. Zhang[128], P. Zhao[47],

Y. Zhao[58b,128,ai], Z. Zhao[58a], A. Zhemchugov[77], Z. Zheng[103], D. Zhong[170], B. Zhou[103], C. Zhou[178], L. Zhou[41], M.S. Zhou[15d], M. Zhou[152], N. Zhou[58c], Y. Zhou[7], C.G. Zhu[58b], H.L. Zhu[58a], H. Zhu[15a], J. Zhu[103], Y. Zhu[58a], X. Zhuang[15a], K. Zhukov[108], V. Zhulanov[120b,120a], A. Zibell[174], D. Zieminska[63], N.I. Zimine[77], S. Zimmermann[50], Z. Zinonos[113], M. Zinser[97], M. Ziolkowski[148], G. Zobernig[178], A. Zoccoli[23b,23a], K. Zoch[51], T.G. Zorbas[146], R. Zou[36], M. Zur Nedden[19], L. Zwalinski[35].

[1]Department of Physics, University of Adelaide, Adelaide; Australia.

[2]Physics Department, SUNY Albany, Albany NY; United States of America.

[3]Department of Physics, University of Alberta, Edmonton AB; Canada.

[4][(a)]Department of Physics, Ankara University, Ankara;[(b)]Istanbul Aydin University, Istanbul;[(c)]Division of Physics, TOBB University of Economics and Technology, Ankara; Turkey.

[5]LAPP, Université Grenoble Alpes, Université Savoie Mont Blanc, CNRS/IN2P3, Annecy; France.

[6]High Energy Physics Division, Argonne National Laboratory, Argonne IL; United States of America.

[7]Department of Physics, University of Arizona, Tucson AZ; United States of America.

[8]Department of Physics, University of Texas at Arlington, Arlington TX; United States of America.

[9]Physics Department, National and Kapodistrian University of Athens, Athens; Greece.

[10]Physics Department, National Technical University of Athens, Zografou; Greece.

[11]Department of Physics, University of Texas at Austin, Austin TX; United States of America.

[12][(a)]Bahcesehir University, Faculty of Engineering and Natural Sciences, Istanbul;[(b)]Istanbul Bilgi University, Faculty of Engineering and Natural Sciences, Istanbul;[(c)]Department of Physics, Bogazici University, Istanbul;[(d)]Department of Physics Engineering, Gaziantep University, Gaziantep; Turkey.

[13]Institute of Physics, Azerbaijan Academy of Sciences, Baku; Azerbaijan.

[14]Institut de Física d'Altes Energies (IFAE), Barcelona Institute of Science and Technology, Barcelona; Spain.

[15][(a)]Institute of High Energy Physics, Chinese Academy of Sciences, Beijing;[(b)]Physics Department, Tsinghua University, Beijing;[(c)]Department of Physics, Nanjing University, Nanjing;[(d)]University of Chinese Academy of Science (UCAS), Beijing; China.

[16]Institute of Physics, University of Belgrade, Belgrade; Serbia.

[17]Department for Physics and Technology, University of Bergen, Bergen; Norway.

[18]Physics Division, Lawrence Berkeley National Laboratory and University of California, Berkeley CA; United States of America.

[19]Institut für Physik, Humboldt Universität zu Berlin, Berlin; Germany.

[20]Albert Einstein Center for Fundamental Physics and Laboratory for High Energy Physics, University of Bern, Bern; Switzerland.

[21]School of Physics and Astronomy, University of Birmingham, Birmingham; United Kingdom.

[22]Centro de Investigaciónes, Universidad Antonio Nariño, Bogota; Colombia.

[23][(a)]Dipartimento di Fisica e Astronomia, Università di Bologna, Bologna;[(b)]INFN Sezione di Bologna; Italy.

[24]Physikalisches Institut, Universität Bonn, Bonn; Germany.

[25]Department of Physics, Boston University, Boston MA; United States of America.

[26]Department of Physics, Brandeis University, Waltham MA; United States of America.

[27][(a)]Transilvania University of Brasov, Brasov;[(b)]Horia Hulubei National Institute of Physics and Nuclear Engineering, Bucharest;[(c)]Department of Physics, Alexandru Ioan Cuza University of Iasi, Iasi;[(d)]National Institute for Research and Development of Isotopic and Molecular Technologies, Physics Department, Cluj-Napoca;[(e)]University Politehnica Bucharest, Bucharest;[(f)]West University in Timisoara, Timisoara; Romania.

[28][(a)]Faculty of Mathematics, Physics and Informatics, Comenius University, Bratislava;[(b)]Department of

Subnuclear Physics, Institute of Experimental Physics of the Slovak Academy of Sciences, Kosice; Slovak Republic.

[29]Physics Department, Brookhaven National Laboratory, Upton NY; United States of America.

[30]Departamento de Física, Universidad de Buenos Aires, Buenos Aires; Argentina.

[31]Cavendish Laboratory, University of Cambridge, Cambridge; United Kingdom.

[32](a)Department of Physics, University of Cape Town, Cape Town;(b)Department of Mechanical Engineering Science, University of Johannesburg, Johannesburg;(c)School of Physics, University of the Witwatersrand, Johannesburg; South Africa.

[33]Department of Physics, Carleton University, Ottawa ON; Canada.

[34](a)Faculté des Sciences Ain Chock, Réseau Universitaire de Physique des Hautes Energies - Université Hassan II, Casablanca;(b)Centre National de l'Energie des Sciences Techniques Nucleaires (CNESTEN), Rabat;(c)Faculté des Sciences Semlalia, Université Cadi Ayyad, LPHEA-Marrakech;(d)Faculté des Sciences, Université Mohamed Premier and LPTPM, Oujda;(e)Faculté des sciences, Université Mohammed V, Rabat; Morocco.

[35]CERN, Geneva; Switzerland.

[36]Enrico Fermi Institute, University of Chicago, Chicago IL; United States of America.

[37]LPC, Université Clermont Auvergne, CNRS/IN2P3, Clermont-Ferrand; France.

[38]Nevis Laboratory, Columbia University, Irvington NY; United States of America.

[39]Niels Bohr Institute, University of Copenhagen, Copenhagen; Denmark.

[40](a)Dipartimento di Fisica, Università della Calabria, Rende;(b)INFN Gruppo Collegato di Cosenza, Laboratori Nazionali di Frascati; Italy.

[41]Physics Department, Southern Methodist University, Dallas TX; United States of America.

[42]Physics Department, University of Texas at Dallas, Richardson TX; United States of America.

[43](a)Department of Physics, Stockholm University;(b)Oskar Klein Centre, Stockholm; Sweden.

[44]Deutsches Elektronen-Synchrotron DESY, Hamburg and Zeuthen; Germany.

[45]Lehrstuhl für Experimentelle Physik IV, Technische Universität Dortmund, Dortmund; Germany.

[46]Institut für Kern- und Teilchenphysik, Technische Universität Dresden, Dresden; Germany.

[47]Department of Physics, Duke University, Durham NC; United States of America.

[48]SUPA - School of Physics and Astronomy, University of Edinburgh, Edinburgh; United Kingdom.

[49]INFN e Laboratori Nazionali di Frascati, Frascati; Italy.

[50]Physikalisches Institut, Albert-Ludwigs-Universität Freiburg, Freiburg; Germany.

[51]II. Physikalisches Institut, Georg-August-Universität Göttingen, Göttingen; Germany.

[52]Département de Physique Nucléaire et Corpusculaire, Université de Genève, Genève; Switzerland.

[53](a)Dipartimento di Fisica, Università di Genova, Genova;(b)INFN Sezione di Genova; Italy.

[54]II. Physikalisches Institut, Justus-Liebig-Universität Giessen, Giessen; Germany.

[55]SUPA - School of Physics and Astronomy, University of Glasgow, Glasgow; United Kingdom.

[56]LPSC, Université Grenoble Alpes, CNRS/IN2P3, Grenoble INP, Grenoble; France.

[57]Laboratory for Particle Physics and Cosmology, Harvard University, Cambridge MA; United States of America.

[58](a)Department of Modern Physics and State Key Laboratory of Particle Detection and Electronics, University of Science and Technology of China, Hefei;(b)Institute of Frontier and Interdisciplinary Science and Key Laboratory of Particle Physics and Particle Irradiation (MOE), Shandong University, Qingdao;(c)School of Physics and Astronomy, Shanghai Jiao Tong University, KLPPAC-MoE, SKLPPC, Shanghai;(d)Tsung-Dao Lee Institute, Shanghai; China.

[59](a)Kirchhoff-Institut für Physik, Ruprecht-Karls-Universität Heidelberg, Heidelberg;(b)Physikalisches Institut, Ruprecht-Karls-Universität Heidelberg, Heidelberg; Germany.

[60]Faculty of Applied Information Science, Hiroshima Institute of Technology, Hiroshima; Japan.

[61](a)Department of Physics, Chinese University of Hong Kong, Shatin, N.T., Hong Kong;(b)Department of Physics, University of Hong Kong, Hong Kong;(c)Department of Physics and Institute for Advanced Study, Hong Kong University of Science and Technology, Clear Water Bay, Kowloon, Hong Kong; China.

[62]Department of Physics, National Tsing Hua University, Hsinchu; Taiwan.

[63]Department of Physics, Indiana University, Bloomington IN; United States of America.

[64](a)INFN Gruppo Collegato di Udine, Sezione di Trieste, Udine;(b)ICTP, Trieste;(c)Dipartimento di Chimica, Fisica e Ambiente, Università di Udine, Udine; Italy.

[65](a)INFN Sezione di Lecce;(b)Dipartimento di Matematica e Fisica, Università del Salento, Lecce; Italy.

[66](a)INFN Sezione di Milano;(b)Dipartimento di Fisica, Università di Milano, Milano; Italy.

[67](a)INFN Sezione di Napoli;(b)Dipartimento di Fisica, Università di Napoli, Napoli; Italy.

[68](a)INFN Sezione di Pavia;(b)Dipartimento di Fisica, Università di Pavia, Pavia; Italy.

[69](a)INFN Sezione di Pisa;(b)Dipartimento di Fisica E. Fermi, Università di Pisa, Pisa; Italy.

[70](a)INFN Sezione di Roma;(b)Dipartimento di Fisica, Sapienza Università di Roma, Roma; Italy.

[71](a)INFN Sezione di Roma Tor Vergata;(b)Dipartimento di Fisica, Università di Roma Tor Vergata, Roma; Italy.

[72](a)INFN Sezione di Roma Tre;(b)Dipartimento di Matematica e Fisica, Università Roma Tre, Roma; Italy.

[73](a)INFN-TIFPA;(b)Università degli Studi di Trento, Trento; Italy.

[74]Institut für Astro- und Teilchenphysik, Leopold-Franzens-Universität, Innsbruck; Austria.

[75]University of Iowa, Iowa City IA; United States of America.

[76]Department of Physics and Astronomy, Iowa State University, Ames IA; United States of America.

[77]Joint Institute for Nuclear Research, Dubna; Russia.

[78](a)Departamento de Engenharia Elétrica, Universidade Federal de Juiz de Fora (UFJF), Juiz de Fora;(b)Universidade Federal do Rio De Janeiro COPPE/EE/IF, Rio de Janeiro;(c)Universidade Federal de São João del Rei (UFSJ), São João del Rei;(d)Instituto de Física, Universidade de São Paulo, São Paulo; Brazil.

[79]KEK, High Energy Accelerator Research Organization, Tsukuba; Japan.

[80]Graduate School of Science, Kobe University, Kobe; Japan.

[81](a)AGH University of Science and Technology, Faculty of Physics and Applied Computer Science, Krakow;(b)Marian Smoluchowski Institute of Physics, Jagiellonian University, Krakow; Poland.

[82]Institute of Nuclear Physics Polish Academy of Sciences, Krakow; Poland.

[83]Faculty of Science, Kyoto University, Kyoto; Japan.

[84]Kyoto University of Education, Kyoto; Japan.

[85]Research Center for Advanced Particle Physics and Department of Physics, Kyushu University, Fukuoka ; Japan.

[86]Instituto de Física La Plata, Universidad Nacional de La Plata and CONICET, La Plata; Argentina.

[87]Physics Department, Lancaster University, Lancaster; United Kingdom.

[88]Oliver Lodge Laboratory, University of Liverpool, Liverpool; United Kingdom.

[89]Department of Experimental Particle Physics, Jožef Stefan Institute and Department of Physics, University of Ljubljana, Ljubljana; Slovenia.

[90]School of Physics and Astronomy, Queen Mary University of London, London; United Kingdom.

[91]Department of Physics, Royal Holloway University of London, Egham; United Kingdom.

[92]Department of Physics and Astronomy, University College London, London; United Kingdom.

[93]Louisiana Tech University, Ruston LA; United States of America.

[94]Fysiska institutionen, Lunds universitet, Lund; Sweden.

[95]Centre de Calcul de l'Institut National de Physique Nucléaire et de Physique des Particules (IN2P3),

Villeurbanne; France.

[96]Departamento de Física Teorica C-15 and CIAFF, Universidad Autónoma de Madrid, Madrid; Spain.

[97]Institut für Physik, Universität Mainz, Mainz; Germany.

[98]School of Physics and Astronomy, University of Manchester, Manchester; United Kingdom.

[99]CPPM, Aix-Marseille Université, CNRS/IN2P3, Marseille; France.

[100]Department of Physics, University of Massachusetts, Amherst MA; United States of America.

[101]Department of Physics, McGill University, Montreal QC; Canada.

[102]School of Physics, University of Melbourne, Victoria; Australia.

[103]Department of Physics, University of Michigan, Ann Arbor MI; United States of America.

[104]Department of Physics and Astronomy, Michigan State University, East Lansing MI; United States of America.

[105]B.I. Stepanov Institute of Physics, National Academy of Sciences of Belarus, Minsk; Belarus.

[106]Research Institute for Nuclear Problems of Byelorussian State University, Minsk; Belarus.

[107]Group of Particle Physics, University of Montreal, Montreal QC; Canada.

[108]P.N. Lebedev Physical Institute of the Russian Academy of Sciences, Moscow; Russia.

[109]Institute for Theoretical and Experimental Physics (ITEP), Moscow; Russia.

[110]National Research Nuclear University MEPhI, Moscow; Russia.

[111]D.V. Skobeltsyn Institute of Nuclear Physics, M.V. Lomonosov Moscow State University, Moscow; Russia.

[112]Fakultät für Physik, Ludwig-Maximilians-Universität München, München; Germany.

[113]Max-Planck-Institut für Physik (Werner-Heisenberg-Institut), München; Germany.

[114]Nagasaki Institute of Applied Science, Nagasaki; Japan.

[115]Graduate School of Science and Kobayashi-Maskawa Institute, Nagoya University, Nagoya; Japan.

[116]Department of Physics and Astronomy, University of New Mexico, Albuquerque NM; United States of America.

[117]Institute for Mathematics, Astrophysics and Particle Physics, Radboud University Nijmegen/Nikhef, Nijmegen; Netherlands.

[118]Nikhef National Institute for Subatomic Physics and University of Amsterdam, Amsterdam; Netherlands.

[119]Department of Physics, Northern Illinois University, DeKalb IL; United States of America.

[120][(a)]Budker Institute of Nuclear Physics, SB RAS, Novosibirsk;[(b)]Novosibirsk State University Novosibirsk; Russia.

[121]Department of Physics, New York University, New York NY; United States of America.

[122]Ohio State University, Columbus OH; United States of America.

[123]Faculty of Science, Okayama University, Okayama; Japan.

[124]Homer L. Dodge Department of Physics and Astronomy, University of Oklahoma, Norman OK; United States of America.

[125]Department of Physics, Oklahoma State University, Stillwater OK; United States of America.

[126]Palacký University, RCPTM, Joint Laboratory of Optics, Olomouc; Czech Republic.

[127]Center for High Energy Physics, University of Oregon, Eugene OR; United States of America.

[128]LAL, Université Paris-Sud, CNRS/IN2P3, Université Paris-Saclay, Orsay; France.

[129]Graduate School of Science, Osaka University, Osaka; Japan.

[130]Department of Physics, University of Oslo, Oslo; Norway.

[131]Department of Physics, Oxford University, Oxford; United Kingdom.

[132]LPNHE, Sorbonne Université, Paris Diderot Sorbonne Paris Cité, CNRS/IN2P3, Paris; France.

[133]Department of Physics, University of Pennsylvania, Philadelphia PA; United States of America.

[134]Konstantinov Nuclear Physics Institute of National Research Centre "Kurchatov Institute", PNPI, St.

Petersburg; Russia.

[135]Department of Physics and Astronomy, University of Pittsburgh, Pittsburgh PA; United States of America.

[136][(a)]Laboratório de Instrumentação e Física Experimental de Partículas - LIP;[(b)]Departamento de Física, Faculdade de Ciências, Universidade de Lisboa, Lisboa;[(c)]Departamento de Física, Universidade de Coimbra, Coimbra;[(d)]Centro de Física Nuclear da Universidade de Lisboa, Lisboa;[(e)]Departamento de Física, Universidade do Minho, Braga;[(f)]Departamento de Física Teorica y del Cosmos, Universidad de Granada, Granada (Spain);[(g)]Dep Física and CEFITEC of Faculdade de Ciências e Tecnologia, Universidade Nova de Lisboa, Caparica; Portugal.

[137]Institute of Physics, Academy of Sciences of the Czech Republic, Prague; Czech Republic.

[138]Czech Technical University in Prague, Prague; Czech Republic.

[139]Charles University, Faculty of Mathematics and Physics, Prague; Czech Republic.

[140]State Research Center Institute for High Energy Physics, NRC KI, Protvino; Russia.

[141]Particle Physics Department, Rutherford Appleton Laboratory, Didcot; United Kingdom.

[142]IRFU, CEA, Université Paris-Saclay, Gif-sur-Yvette; France.

[143]Santa Cruz Institute for Particle Physics, University of California Santa Cruz, Santa Cruz CA; United States of America.

[144][(a)]Departamento de Física, Pontificia Universidad Católica de Chile, Santiago;[(b)]Departamento de Física, Universidad Técnica Federico Santa María, Valparaíso; Chile.

[145]Department of Physics, University of Washington, Seattle WA; United States of America.

[146]Department of Physics and Astronomy, University of Sheffield, Sheffield; United Kingdom.

[147]Department of Physics, Shinshu University, Nagano; Japan.

[148]Department Physik, Universität Siegen, Siegen; Germany.

[149]Department of Physics, Simon Fraser University, Burnaby BC; Canada.

[150]SLAC National Accelerator Laboratory, Stanford CA; United States of America.

[151]Physics Department, Royal Institute of Technology, Stockholm; Sweden.

[152]Departments of Physics and Astronomy, Stony Brook University, Stony Brook NY; United States of America.

[153]Department of Physics and Astronomy, University of Sussex, Brighton; United Kingdom.

[154]School of Physics, University of Sydney, Sydney; Australia.

[155]Institute of Physics, Academia Sinica, Taipei; Taiwan.

[156][(a)]E. Andronikashvili Institute of Physics, Iv. Javakhishvili Tbilisi State University, Tbilisi;[(b)]High Energy Physics Institute, Tbilisi State University, Tbilisi; Georgia.

[157]Department of Physics, Technion, Israel Institute of Technology, Haifa; Israel.

[158]Raymond and Beverly Sackler School of Physics and Astronomy, Tel Aviv University, Tel Aviv; Israel.

[159]Department of Physics, Aristotle University of Thessaloniki, Thessaloniki; Greece.

[160]International Center for Elementary Particle Physics and Department of Physics, University of Tokyo, Tokyo; Japan.

[161]Graduate School of Science and Technology, Tokyo Metropolitan University, Tokyo; Japan.

[162]Department of Physics, Tokyo Institute of Technology, Tokyo; Japan.

[163]Tomsk State University, Tomsk; Russia.

[164]Department of Physics, University of Toronto, Toronto ON; Canada.

[165][(a)]TRIUMF, Vancouver BC;[(b)]Department of Physics and Astronomy, York University, Toronto ON; Canada.

[166]Division of Physics and Tomonaga Center for the History of the Universe, Faculty of Pure and Applied Sciences, University of Tsukuba, Tsukuba; Japan.

[167]Department of Physics and Astronomy, Tufts University, Medford MA; United States of America.

[168]Department of Physics and Astronomy, University of California Irvine, Irvine CA; United States of America.

[169]Department of Physics and Astronomy, University of Uppsala, Uppsala; Sweden.

[170]Department of Physics, University of Illinois, Urbana IL; United States of America.

[171]Instituto de Física Corpuscular (IFIC), Centro Mixto Universidad de Valencia - CSIC, Valencia; Spain.

[172]Department of Physics, University of British Columbia, Vancouver BC; Canada.

[173]Department of Physics and Astronomy, University of Victoria, Victoria BC; Canada.

[174]Fakultät für Physik und Astronomie, Julius-Maximilians-Universität Würzburg, Würzburg; Germany.

[175]Department of Physics, University of Warwick, Coventry; United Kingdom.

[176]Waseda University, Tokyo; Japan.

[177]Department of Particle Physics, Weizmann Institute of Science, Rehovot; Israel.

[178]Department of Physics, University of Wisconsin, Madison WI; United States of America.

[179]Fakultät für Mathematik und Naturwissenschaften, Fachgruppe Physik, Bergische Universität Wuppertal, Wuppertal; Germany.

[180]Department of Physics, Yale University, New Haven CT; United States of America.

[181]Yerevan Physics Institute, Yerevan; Armenia.

[a] Also at Borough of Manhattan Community College, City University of New York, NY; United States of America.

[b] Also at California State University, East Bay; United States of America.

[c] Also at Centre for High Performance Computing, CSIR Campus, Rosebank, Cape Town; South Africa.

[d] Also at CERN, Geneva; Switzerland.

[e] Also at CPPM, Aix-Marseille Université, CNRS/IN2P3, Marseille; France.

[f] Also at Département de Physique Nucléaire et Corpusculaire, Université de Genève, Genève; Switzerland.

[g] Also at Departament de Fisica de la Universitat Autonoma de Barcelona, Barcelona; Spain.

[h] Also at Departamento de Física Teorica y del Cosmos, Universidad de Granada, Granada (Spain); Spain.

[i] Also at Department of Applied Physics and Astronomy, University of Sharjah, Sharjah; United Arab Emirates.

[j] Also at Department of Financial and Management Engineering, University of the Aegean, Chios; Greece.

[k] Also at Department of Physics and Astronomy, University of Louisville, Louisville, KY; United States of America.

[l] Also at Department of Physics and Astronomy, University of Sheffield, Sheffield; United Kingdom.

[m] Also at Department of Physics, California State University, Fresno CA; United States of America.

[n] Also at Department of Physics, California State University, Sacramento CA; United States of America.

[o] Also at Department of Physics, King's College London, London; United Kingdom.

[p] Also at Department of Physics, St. Petersburg State Polytechnical University, St. Petersburg; Russia.

[q] Also at Department of Physics, Stanford University; United States of America.

[r] Also at Department of Physics, University of Fribourg, Fribourg; Switzerland.

[s] Also at Department of Physics, University of Michigan, Ann Arbor MI; United States of America.

[t] Also at Dipartimento di Fisica E. Fermi, Università di Pisa, Pisa; Italy.

[u] Also at Giresun University, Faculty of Engineering, Giresun; Turkey.

[v] Also at Graduate School of Science, Osaka University, Osaka; Japan.

[w] Also at Hellenic Open University, Patras; Greece.

[x] Also at Horia Hulubei National Institute of Physics and Nuclear Engineering, Bucharest; Romania.

[y] Also at II. Physikalisches Institut, Georg-August-Universität Göttingen, Göttingen; Germany.

[z] Also at Institucio Catalana de Recerca i Estudis Avancats, ICREA, Barcelona; Spain.

[aa] Also at Institut für Experimentalphysik, Universität Hamburg, Hamburg; Germany.

[ab] Also at Institute for Mathematics, Astrophysics and Particle Physics, Radboud University Nijmegen/Nikhef, Nijmegen; Netherlands.

[ac] Also at Institute for Particle and Nuclear Physics, Wigner Research Centre for Physics, Budapest; Hungary.

[ad] Also at Institute of Particle Physics (IPP); Canada.

[ae] Also at Institute of Physics, Academia Sinica, Taipei; Taiwan.

[af] Also at Institute of Physics, Azerbaijan Academy of Sciences, Baku; Azerbaijan.

[ag] Also at Institute of Theoretical Physics, Ilia State University, Tbilisi; Georgia.

[ah] Also at Istanbul University, Dept. of Physics, Istanbul; Turkey.

[ai] Also at LAL, Université Paris-Sud, CNRS/IN2P3, Université Paris-Saclay, Orsay; France.

[aj] Also at Louisiana Tech University, Ruston LA; United States of America.

[ak] Also at LPNHE, Sorbonne Université, Paris Diderot Sorbonne Paris Cité, CNRS/IN2P3, Paris; France.

[al] Also at Manhattan College, New York NY; United States of America.

[am] Also at Moscow Institute of Physics and Technology State University, Dolgoprudny; Russia.

[an] Also at National Research Nuclear University MEPhI, Moscow; Russia.

[ao] Also at Physikalisches Institut, Albert-Ludwigs-Universität Freiburg, Freiburg; Germany.

[ap] Also at School of Physics, Sun Yat-sen University, Guangzhou; China.

[aq] Also at The City College of New York, New York NY; United States of America.

[ar] Also at The Collaborative Innovation Center of Quantum Matter (CICQM), Beijing; China.

[as] Also at Tomsk State University, Tomsk, and Moscow Institute of Physics and Technology State University, Dolgoprudny; Russia.

[at] Also at TRIUMF, Vancouver BC; Canada.

[au] Also at Universita di Napoli Parthenope, Napoli; Italy.

* Deceased